國立交通大學

機械工程學系

博 士 論 文

可攜式和固定式細水霧系統滅火性能之實驗評估

Experimental Evaluations of Portable and Fixed Water Mist Systems

研 究 生：張文耀

指導教授：陳俊勳　教授

中 華 民 國 九十七 年 九 月

可攜式和固定式細水霧系統滅火性能之實驗評估

Experimental Evaluations of Portable and Fixed Water Mist Systems

研 究 生：張文耀　　Student：Wen-Yao Chang

指導教授：陳俊勳　　Advisor：Prof. Chiun-Hsun Chen

國 立 交 通 大 學

機械工程 學 系

博 士 論 文

A Dissertation

Submitted to Department of Mechanical Engineering

College of Engineering

National Chiao Tung University

in partial Fulfillment of the Requirements

for the Degree of

Doctor of Philosophy

In Mechanical Engineering

September 2008

Hsinchu, Taiwan, Republic of China

中華民國九十七年九月

可攜式和固定式細水霧系統滅火性能之實驗評估

學 生：張 文 耀　　指導教授：陳俊勳

國立交通大學機械工程學系

摘要

本論文主要分為兩部份來評估細水霧的滅火性能及其應用，第一部份為可攜式細水霧系統及添加劑的滅火性能評估，第二部份則為在高科技廠房濕式清洗槽中，細水霧系統的應用及效能評估。

在可攜式含添加劑細水霧滅火系統的實驗中，主要針對噴灑方法對池火的滅火性能及其相對應滅火機制的影響進行一系列的研究。不同的油料種類、噴頭噴灑角度、添加劑溶液的體積濃度為主要實驗參數。使用油料分別為庚烷、汽油、柴油；噴頭噴灑角度分別為與水平夾角 30 度、45 度、60 度；添加劑溶液的體積濃度分別為 0%、3%、6%、10%。高噴灑角度時的主要滅火機制為火焰冷卻和氧氣置換；低噴灑角度時為油氣的阻隔與稀釋。本實驗使用的可攜式細水霧滅火系統擁有良好的熱輻射稀釋與降溫能力，對使用者能供良好的保護。細水霧加入添加劑後可使滅火性能極明顯提升，但過多的添加劑反而會造成滅火性能下降。滅火效率不僅受到水霧效應影響,亦同時受添加劑效應影響。因此對滅火效能而言，必然存在某個細水霧與添加劑間最理想的混合比率。

在評估細水霧系統對濕式清洗槽的火災實驗中，實驗參數為工作壓力、油盆大小、噴頭位置、障礙物及門的開度。適當的工作壓力及噴頭位置設計能有效的撲滅早期火災。細水霧噴頭則建議裝設在油盆正上方或油盆兩側，確保水霧能涵蓋住火燄並有足夠動能來撲滅火場，如此就能避免火勢延燒到整個溼式清洗槽。

在 PIV 影像量測中以三種不同之實驗參數，噴灑壓力，添加劑體積濃度以及噴頭種類，討論對 SMD 以及細水霧密度分佈造成之變動。透過使用 PIV 系統拍攝在三個不同量測點， 23cm，40 cm 及 52

處，所有的實驗照片。

研究結果發現當噴灑壓力上昇時，水霧的 SMD 值會隨之減少。因不同濃度的添加劑造成 SMD 分佈呈現 W 形狀的曲線，此一現象給予先前的論文中關於火焰撲滅時間的結果適當的解釋。研究結果發現對於含有添加劑的細水霧，其滅火效能主要取決於 SMD 之值，其次則是添加劑的化學反應。

關鍵字: 細水霧、PIV、添加劑、SMD

Experimental Evaluations of Portable and Fixed Water Mist Systems

Student: Wen-Yao Chang Advisor: Prof. Chiun-Hsun Chen

Department of Mechanical Engineering

National Chiao Tung University

ABSTRACT

This thesis consists of two parts. In the first part, a series of tests subjected to various discharge methodologies and fire scenarios were carried out based on a portable water mist fire extinguishing system with additive on pool fires. Different fuel types, nozzle discharge angles, additive solution volumes, amount of fuels and cross-section area of pans were selected as the major experimental parameters. The fuels used were heptane, gasoline, and diesel, the nozzle discharge angles are 30°, 45°, and 60° with respect to the horizon, and the additive solution volumes were 0%, 3%, 6% and 10%. The dominant mechanisms of restraining fire in the higher nozzle discharge angle regime (>45°) are flame cooling and oxygen-displacement, and in the lower one (<45°) are fuel vapors blocking and dilution. The portable water mist fire extinguishing system used has a good ability for radiation attenuation and temperature reduction that can provide a good protection for the operators. By using water mist with additive, the fire extinguishing efficiencies are significantly improved. However, if too much additive is

provided, the fire extinguishment efficiency will decrease. The tendencies of the fire extinction times for different amount of fuel in a size-fixed pan are similar. Although the situation of non-uniform fuel surface resulted from water mist impingement slightly reduces the burning rate, it can be ameliorated as the height of liquid fuel attains at 1cm. The fire extinguishing efficiency is not only influenced by mist effects but also by additive ones. Therefore, there must be an optimal mixing ration between the mist and additive for fire suppression.

In the second part of the thesis for assessing the fire protection performance in wet bench fires, several field tests were performed using a water mist system installed in the wet bench. The test parameters were operational pressure, pan size, nozzle location, cylinder obstruction and degree of door closure. An appropriate design for operating pressure and the location of water mist nozzles extinguished wet bench fires effectively in the early fire stages. The nozzles are suggested to be fixed above or on the each side of the pan, ensuring that mist can completely cover a pan surface with sufficient momentum. With this suggested design, fires can be extinguished in the pan and do not spread over the wet bench.

In the particle image processing, SMD and water mist density distribution were investigated with three parameters, discharge pressure, volumetric additive concentration and nozzle type. By using PIV, all experimental pictures were caught in three acquisition locations, 23 cm, 40cm and 52cm away from the nozzle respectively.

The study indicated that SMD shrunk as discharged pressure increased. With different concentration of additive, the “W” shape curve

for SMD variation gave explanations for the extinction time mentioned in the previous thesis. The result showed that the major factor for the performance of fire extinguishing was SMD and the minor one was chemical reaction by organic metal compound.

Key Word: Water Mist, PIV, Additive, SMD

ACKNOWLEDGEMENTS

此論文得以順利完成，首要感謝指導教授 陳俊勳老師五年來的諄諄教誨與協助，不論於學業上或生活上皆使學生受益良多，師恩浩蕩，銘感五內。此外，還要感謝沈子勝老師、 王鵬智老師、徐一量老師、雷明遠老師以及陳慶要老師於計劃口試與論文口試時的教導，使此論文得以更臻完善。論文能順利付梓，特別要感謝這五年來幸賴許多實驗室成員與朋友們各方面的協助，使得研究工作得以順利完成，如有挂一漏萬，在此均一併致謝。

最後要感謝父母親的辛勤培育協助與陪伴，感謝他們當初的堅持，使文耀能夠順利完成學業，謝謝他們一直以來的鼓勵與，並包容文耀在外求學的這幾年無法時常陪伴在他們身旁，而造就今日的我。

Contents

ABSTRACT(Chinese) I

ABSTRACT(English) III

ACKNOWLEDGEMENTS VI

Contents VII

List of Tables X

List of Figures XI

CHAPTER 1 INTRODUCTION 1

1.1 Motivation 1
1.2 Literature Review 5
1.3 Scope of Present Study 10

CHAPTER 2 EXPERIMENTAL DESIGN AND APPARATUS 13

2.1 Experiment Design 13
2.2 Portable-Water-Mist-System Experiment 13
2.2.1 Parameters of Tests 14
2.2.2 Fire Source 15
2.2.3 Water Mist System 16
2.2.4 Water Mist Additive Property 17
2.2.5 Temperature Measurement 17
2.2.6 Radiation Heat Flux Measurement 18
2.3 Wet-Bench Fire Experiments 18
2.3.1 Parameter of Tests 19
2.3.2 Fire source 19
2.3.3 Temperature Measurement 19
2.4 Measurement Instrumentations 20
2.4.1 Hydraulic Pressure Measurement 20
2.4.2 Oxygen Concentration Measurement 20
2.4.3 Data Acquisition 21
2.4.4 Digital Video 21
2.5 Particle Image Velocimetry 21
2.5.1 Imaging Subsystem 22
2.5.1.1 Laser 22
2.5.1.2 Optic Lens 22

2.5.2 Image Capture Subsystem 22
2.5.3 Analysis Subsystem 22
2.5.4 Procedure of the Experimental Operation 23
CHAPTER 3 UNCERTAINTY ANALYSIS AND PIV IMAGE PROCESSING 24
3.1 Uncertainty Analysis 25
3.1.1 Analyses of the Propagation of Uncertainty in Calculations 25
3.1.2 Uncertainty Level Analysis in the Experiment 26
3.1.3 The Asymmetric Uncertainties of Thermocouple 26
3.1.4 The Uncertainties of Radiometer 27
3.1.5 The Experimental Repeatability 28
3.2 PIV IMAGE PROCESSING 29
3.2.1 Image Transform 29
3.2.1.1 Convolution Theorem 29
3.2.1.2 Fast Fourier Transform (FFT) 30
3.2.2 Image Enhancement 32
3.2.3 Image Restoration 32
3.2.4 Image Processing Procedure for Experimental Data 33
3.2.5 Measurement for Water Mist Density Distribution 33
3.2.5.1 Measurement by Tubes 34
3.2.5.2 Measurement by Image Processing 34
CHAPTER 4 RESULTS AND DISCUSSION 35
4.1 Portable-Water-Mist-System Experiments 35
4.1.1 Qualitative Fire Tests 35
4.1.1.1 Class A fire tests—wood slabs 35
4.1.1.2 Class B fire tests—gasoline pan fire 36
4.1.1.3 Motorcycle fire tests 36
4.1.1.4 Car fire tests 36
4.1.2 Quantitative Fire Tests 37
4.1.2.1 Fire Tests with Different Fuel Types 37
4.1.2.2 Pure Water Mist 37
4.1.2.3 Water Mist with Additive on Diesel Pan Fires 40
4.1.2.4 Water Mist with Additive on Heptane Pan Fires 41
4.1.2.5 Water Mist with Additive on Gasoline Pan Fires 43
4.2 Wet-Bench Fire Experiments 44
4.2.1 Single nozzle tests with different pan sizes and operating pressures 44
4.2.2 Tests for nozzle distribution 45

4.2.3 Obstruction tests 47
4.2.4 Tests for degree of closure of the wet bench door 47
4.2.5 Fire spreading in a wet bench 48
4.3 PIV Analysis 49
4.3.1 Experimental Apparatus Settings 49
4.3.2 SMD with Different Pressures 50
4.3.2.1 Diameter measurements with Location X=23cm 51
4.3.2.2 Diameter Detection with Location X=40cm 52
4.3.2.3 Diameter Detection with Location X=52cm 52
4.3.3 SMD with Different Volumetric Additive 53
4.3.4 Water Mist Density Distribution 55
4.3.4.1 Density Distribution by Experiment 56
4.3.4.2 Density Distribution by Measuring Grey Level 56
4.3.4.3 FP-25 Nozzle 57
CHAPTER 5 CONCLUSIONS 58
REFERENCE 61

List of Tables

Table 2.1 The properties of fuels 65
Table 2.2 The volume flow rates in different additive volumes(L/min) ..66
Table 3.1 (a) Pure water tests with different fuel types in 25cm pan 67
(b) Water mist with additive in 50cm pan with heptane fires ..67
Table 4.1 The summary of parametric studies.....69
Table 4.2 Nozzle discharge angle and extinction time without additive..70
Table 4.3 Corresponding extinction time(sec) of diesel fires.....71
Table 4.4 Corresponding extinction time(sec) of heptane fires.....71
Table 4.5 Corresponding extinction time(sec) of gasoline fires.....71
Table 4.6 Fuel Pan Size and extinction time(sec) under different pressure.....72
Table 4.7 Extinction time(sec) under different pressure and location.....73
Table 4.8 Distruibution tests and extinction time under different pressure74
Table 4.9 Extinguishing time of obstruction tests under different pressure.....75
Table 4.10 Door closure degree and extinction time(sec) under different pressure.....76
Table 4.11 Values for experimental apparatus.....77
Table 4.12 $\overline{D}$ and SMD distribution for Fp-25 nozzle.....78
Table4.13 $\overline{D}$ and SMD distributions with different additive concentrations.....79
Table 4.14 Effects for different additive concentration.....80

List of Figures

Fig. 1.1. Operational units of water mist system.....81
Fig. 1.2. Spectrum of droplet diameters, reproduced from Ref. [7].....82
Fig. 1.3. Droplet diameters, reproduced from Ref. [8].....82
Fig. 1.4. Schematic of the Thesis 83
Fig.2.1 The schematic of experiment 84
Fig. 2.2 The picture and schematic configuration of the circular stainless pan (a) small-scale (b) middle-scale 85
Fig. 2.3 The picture of high pressure pump 86
Fig. 2.4 The picture of high pressure system nozzle (a) Front view....87
(b) Side view (c) Spray angle 87
Fig. 2.5. The picture of thermocouple tree 88
Fig. 2.6. The schematic configuration of the thermocouple tree.....89
Whole view and (b) Local view 89
Fig. 2.7. The radiometer (a) The picture and (b) The schematic.....90
configuration.....90
Fig. 2.8. The schematic configuration of the water-cooling system 91
Fig. 2.9. Experiment layout of wet bench fire tests.....92
Fig. 2.10. The picture of pressure gauge 93
Fig. 2.11. The picture of Gaseous Oxygen Analyzer 94
Fig. 2.12. Schematic configuration of preliminary handling system 94
Fig. 2.13. The picture of datalog (a) Front view and (b) Back view.....95
Fig. 2.14 .The schematic configuration of the experimental apparatus ..96
(a)Side View and (b) Up View 96
Fig. 2.15. The Nd:YVO 4 laser 97
Fig. 2.16. The picture of optic lens.....98
Fig. 2.17. The image capture device-Olympus E330 99
Fig. 2.18. SIGMA Long-Distance Macro Lens 99
Fig. 2.19. The experimental flow chart 100
Fig. 3.1. The relationship of temperature and error.....101
Fig. 3.2. The procedure for digital image processing with NI Version Assistant software.....102
Fig. 4. Wooden slabs of CNS1387 103
Fig. 4.2 Pictures of Class B (pan fire) fire test 103
Fig. 4.3 Pictures of motorcycles fire tes 104
Fig. 4.4 Pictures of car fire test (1) 104
Fig. 4.5 Pictures of car fire test (2) 104

Fig. 4.6. The relationship between nozzle discharge angles and extinction time in different fuel types without addtive 105
Fig. 4.7. The temperature history of fires with pure water at the nozzle discharge angle of 30° (a) Heptane (b) Gasoline (c) Diesel....107
Fig. 4.8. The radiation heat flux history of fires with pure water at the nozzle discharge angle of 30° (a) Heptane (b) Gasoline (c) Diesel 109
Fig. 4.9. Oxygen concentration variation history.....110
Fig. 4.10. Extinguishing time for diesel fire with different nozzle discharge angles and additive solution volumes 111
Fig. 4.11. Extinguishing time for heptanel fire with different nozzle discharge angles and additive solution volumes 112
Fig. 4.12. Extinguishing time for gasoline fire with different nozzle discharge angles and additive solution volumes 113
Fig. 4.13 Temperature history of totally open door tests.....114
Fig. 4.14 Temperature history of half closed door tests 115
Fig. 4.15 Temperature history of totally closed door tests 116
Fig. 4.16 Oxygen concentration history for different door closure degree.....117
Fig 4.17 The relation between average diameter and pressure for different position.....118
Fig 4.18 The relation between SMD and pressure for different position.119
Fig. 4.19 The NFPA750 standard form for droplet diameter v.s. cumulative % volume at x=23cm.....120
Fig. 4.20 The NFPA750 standard form for droplet diameter v.s. cumulative % volume at x=40cm.....121
Fig. 4.21 The NFPA750 standard form for droplet diameter v.s. cumulative % volume at x=52cm.....122
Fig 4.22 The relation between volume % addition and droplet diameter123
Fig. 4.23 Extinguishing time for heptanel fire with different nozzle....124
discharge angles and additive solution volumes 124
Fig. 4.24 Extinguishing time for gasoline fire with different nozzle discharge angles and additive solution volumes 125
Fig. 4.25 Water mist density distribution measured by experiment.....126
Fig. 4.26 Water mist distribution picture for P=10 Kg/cm2.....127
Fig. 4.27 Grey level for image captured at P=10 Kg/cm2. 127
Fig. 4.28 Water mist distribution picture for P=20 Kg/cm2.....128
Fig. 4.29 Grey level for image captured at P=20 Kg/cm2 128

Fig. 4.30 Water mist distribution picture for P=30 Kg/cm2.....129
Fig. 4.31 Grey level for image captured at P=30 Kg/cm2. 129
Fig. 4.32 Water mist distribution picture for P=40 Kg/cm2.....130
Fig. 4.33 Grey level for image captured at P=40 Kg/cm2 130
Fig. 4.34 Water mist distribution picture for P=50 Kg/cm2.....131
Fig. 4.35 Grey level for image captured at P=50 Kg/cm2. 131
Fig. 4.36 Spray angle for P=10 Kg/cm2.....132
Fig. 4.37 Spray angle for P=20 Kg/cm2.....132
Fig. 4.38 Spray angle for P=30 Kg/cm2.....133
Fig. 4.39 Spray angle for P=40 Kg/cm2.....133
Fig. 4.40 Spray angle for P=50 Kg/cm2.....134

CHAPTER 1
INTRODUCTION

1.1 Motivation

Since 1960, Halon becomes a common-used fire suppression agent in computer rooms and communication equipments because of its non-electric conduction, quick extinguishing of fire and harmless on protection objects, etc. However, such agents are being phased out due to their destructive effects of halogen atoms on the atmospheric ozone layer and were banned on the Montreal protocol in 1987.

The extensive efforts have been carried out to search for the replacements, such as water mist, compressed-air-foam, carbon dioxide and so on. Among which, the water mist used for fire suppression and control is taken as one of the potential alternative agents.

In general, water-related fire protections or sprinkler system are not suggested to use for Class B fires since most of liquid will splash over the water. Therefore, it is difficult to cool down the fuel surface with water evaporation and possible to encounter with a ‘running liquid fire’. However, for water mist system the momentum is insufficient to cause the liquid fuel to float over, since its water amount is only 1/10 of that used in the traditional sprinkler system. Besides, with a much lager surface to volume ratio, water mist can greatly enhance both evaporation rate and suspension time for cooling down the liquid fuel surface. It has been proved that water mist system can suppress ClassA, Class B,

Motorcycle, Car and Wet Bench fires effectively with proper design and operation.

According to NFPA 750[1], water mist has been defined as sprays that have 99% of the volume of water droplets less than 1000 microns in diameter. Because of the large surface to volume ratio, water mist shows effective in fire quenching. Besides, small droplets have the capability of reaching obstructed areas by following the gas flow [2]. The study and description of the fundamental principles of extinguishment of solid fuel fires by water mist can be traced back to the mid-1950s in the work of Braidech et al. [3]. They identified flame cooling and oxygen displacement as the dominant mechanisms in water mist fire suppression. Recent investigations by Mawhinney et al. [4] , they found that the mechanisms also include the radiation attenuation, dilution of flammable vapors, and direct impingement and cooling of the combustibles.

Water mist fire suppression systems have demonstrated a number of advantages, such as good fire suppression capability, no environmental impact, and non-toxicity [5]. For these reasons, water mist had been considered as an ideal alternative for halon agents. However, water mist dose not behave like a total flooding agent, thus the fire suppression effectiveness of water mist depends on the potential size of the fire, properties of the combustibles, and the degree of obstruction, as well as the water mist characteristics.

The operation units of water mist system are shown in Fig.1.1. Since water mist system is operated in a high-pressure condition, the corresponding pipes, pumps, and valves should have the capabilities to

sustain the high pressure, sometimes to 150bar for high pressure system. According to Fig.1.1, the fixed water mist system could be transformed into portable or moveable one, if we redesign the water supply system, power source and pump.

For the operating pressure, the water mist system can be divided into three categories: the high-, medium- and low- pressure water mist systems. When the operational pressure is greater than 34.5bar (500psi), it's called high-pressure system. When the operation pressure is lower than 12.1bar (175psi), it is called low-pressure system. The one in between is medium-pressure system.

Therefore, it motivates this dissertation to evaluate the performance and the applications of water mist system. The fixed fire extinguishing systems have already demonstrated their capability in providing the fire protection in a wide range of applications. However, their performances are generally limited by the distribution and allocation of spray nozzles.

Fixed fire extinguishing systems have demonstrated their capability in providing the fire protection in a wide range of applications. However, their performance is generally limited by spray nozzle distribution and allocation. Portable fire extinguishers, whose spray nozzles are designed as movable that can be aimed at a fire generally utilized for early stage of fire control. For portability, the weight of such extinguishers should not be too heavy to carry and, consequently, extinguisher content should be limited. Thus, portable fire extinguishers can only be operated for a short time, and are unfavorable control for the larger fire. However, water damage is unacceptable, particularly in contexts where collateral damage by water is undesirable, such as in high-tech facilities, on

aircraft, in shipboard engine rooms and museums. Consequently, identifying a fire control system that can be operated for a long time and with reduced amounts of water to reduce water damage is necessary.

In the first part of the dissertation, a series of tests subjected to various discharge methodologies and fire scenarios are carried out base on a portable water mist fire extinguishing system with additive on pool fires. Different fuel types, nozzle discharge angles, additive solution volumes, amount of fuels and cross-section area of pans are selected as the major experimental parameters.

Taiwan has roughly 1,000 semiconductor facilities, with a total output value of approximately US$23 billion in 2006, ranking the Taiwanese industry as third largest worldwide. A polypropylene (PP)/polyvinyl chloride (PVC) wet bench is typically utilized in clean room environments. Hundreds of chemicals are used during manufacturing, some of which evaporate easily and have a wide flammability range. FM Global has estimated that 1 in 10 manufacturing plants experience a fire loss annually. Fires involving wet benches have caused significant losses in the semiconductor industry in past years. At the start of the 1990s, FM focused on replacing materials or protecting existing plastic wet benches in the semiconductor industry. Numerous companies simply accepted the recommendations, following the FM7-7 guidelines and installed carbon dioxide or fine water mist fire suppression systems in wet benches [6]. This study analyzes the performance of water mist fire suppression systems utilized for wet bench protection.

In the second part of the dissertation, it analyzes the performance

of water mist fire suppression systems utilized for wet bench protection. The test parameters were operational pressure, pan size, nozzle location, cylinder obstruction and degree of door closure. An appropriate design for operating pressure and the location of water mist nozzles extinguished wet bench fires effectively in the early fire stages.

Drop sizes of the various water mist generated by pump are measured by a Particle Image Velocimetry (PIV) machine. PIV converts laser into light sheet by shooting laser through a cylindrical lens. The small particles in within the light sheet will scatter the light and then be detected by the digital camera. These data are stored in the computer and analyzed with specialized software to observe the change of the fluid. Unlike the traditional intrusive techniques, such as Pitot tube, Hot Wire Anemometer (HWA), using PIV has the advantage that it is a non-intrusive technique.

1.2 Literature Review

Water mist is defined as sprays in which 99% of spray droplets, for flow-weighted cumulative distribution, have diameters <1000 microns as the minimum design operating pressure of water mist nozzle.

Grant et al. [7] reported the spectrum of droplet sizes, as shown in Fig. 1.2, where the most interesting ‘average’ size range for fire fighting is deemed to be from 100 to 1000 μm. Afterward, a mist classification system based on a ‘cumulative percent volume’ distribution plot was proposed by Mawhinney and Solomon [8], which make distinguishment between ‘coarser’ and ‘finer’ water sprays, as shown in Fig. 1.3. The

more drops of ‘fine’ sizes contain in sprays, the more rapidly sprays evaporate in the fire environment and facilitate the characteristic extinguishment mechanisms of water mist. However, in practice, sprays for which the Dv90 (90% volume diameter) is less than or equal to 400 μm, are suitable to the suppression of liquid pool fires or where ‘splashing’ of the fuel is to be avoided.

Mawhinney [9] used a twin-fluid nozzle to produce a fine spray to extinguish liquid pool fire. It was found that spraying down directly onto the flame is the most effective means of extinction. Any obstructions placed in the path of the spray lower both the spray’s momentum and the amount of water suspended in the air as mist, and result in a reduction of its capacity to extinguish the fire.

Yao et al. [10] investigated the interaction of water mists with a diffusion flame in a confined space with proper ventilation control. It was shown that the poorer is the ventilation, the easier the suppression. The water mists can affect the smoke release rate and its movement, and have a more complex effect on the solid sample than on the liquid one.

Previous researches have shown that it is very difficult for water mist to extinguish flammable liquid fires with flash points below normal ambient temperature, such as n-heptane (C7H16, FP = -4oC), because the fuel temperature cannot be cooled down enough to reduce the vapor/air mixture above the fuel surface below its lean flammability limit [11].

Liu et al. [11-13] carried out a series of full-scale fire tests by using portable water mist extinguishers to suppress various types of fires, including cooking oils, n-heptanes, diesel fuels, wood cribs and

energized targets. For the diesel fire, comparing to the heptane one with the same size of fuel pan, it is much easier to extinguish, because the diesel fuel has a higher flash point (FP = 60oC) and a lower heat release rate. Besides, the surface temperature of diesel fuel is higher than that of heptane fuel and the burning rate of diesel is affected by the fuel cooling owing to the presence of water mist. The diesel flame is also enlarged is much smaller than the one caused by heptane fuel, because it generates less volatile fuel vapor.

In order to further improve the fire-extinguishment performance of water mist, many kinds of additives have been developed in the past year. Zhou et al. [14] conducted a phenomenological study for the effect of MC (multi-composition) additive on water mist's fire-extinguishing efficiency through the base of the ethanol, diesel and wood crib fires. With MC additive presented, the oxygen is isolated and the radiative feedback from the fire to the fuel is mitigated by fluorocarbon surfactant, which forms a thin film layer over the pool or wood surfaces. It was found that adding a small quantity of MC additive into the water mist significantly improves the performance of the water mist system in suppressing fires. However, if too much MC additive is applied, the fire extinguishment efficiency will decrease.

Cong et al. [15] added sodium chloride into water mist system to test the performance when used in pool fire. They varied the sodium chloride mass concentration, discharge pressure and fuel types to seek the best performances. The experiment results showed that raising the discharge pressure can shorten the quenching time period. Usually, sodium chloride mass concentration has positive effect on fire

suppression, but there is a limiting value about 5% of weight. Exceeding that value, the performance curve shows a reverse trend. An important issue should be addressed is that water mist with sodium chloride provides a positive effect on coal oil fire, but it becomes worse for alcohol fire. Liao et al. took the same experiment setting and parameters to determine the extinguishing performance for water mist with iron compounds additives. They draw the same conclusion that iron compounds additives have a limiting value of 0.83% of the total mass and positive performance for coal oil fire, but negative for alcohol fire.

Another study of the application of composite additives used for water mist system was investigated by Cong et al. [16]. The additives contain hydrocarbon surface activator and fluorine surface activator. These two activators can weaken the water surface tension to raise the mist effect. They found that the suppression efficiencies of water mist system with additives for liquid pool fires (ethanol and diesel fuels) and wood crib fires are different. The amount of surface activator does not affect the extinguishing time for liquid pool fires, but has a positive effect on wood crib fires.

Shu et al. [17] evaluated the performance of a water mist system in the fume exhaust pipes used in semiconductor facilities by comparing with that of a standard sprinkler system. The parameters were the amount of water that the mist nozzles used, air flow velocity, fire intensity and operating pressure. It was found that the droplet size in a water-related fire protection system plays a critical role. Water mist system can produce a better performance than that of a standard sprinkler one, and furthermore a higher operating pressure of water mist

system can achieve a better performance.

Previous studies indicated that wet bench fires should be suppressed in the early fire stage [18, 19]. Wu, Taylor and Harriman experimentally analyzed simulated wet bench fires using fine water spray [20]. A polypropylene pool fire was placed in the middle of working surface with two seven inch cylinders on each side to block direct impingement with water mist. Two nozzles on the each end wall extinguished all polypropylene pool fires in 10 seconds. Mawhinney [21] utilized a twin-fluid nozzle to generate a fine spray to extinguish liquid pool fires. Mawhinney demonstrated that spraying downward directly at the flames is the most effective means of extinguishing a fire. Obstructions in the spray path reduce spray momentum and the amount of water suspended in air as mist, resulting in reduced ability to extinguish a fire.

The relative studies of particle image techniques are arranged by Adrian [22]. He made detailed comments for the performances of different image analysis technique with different experimental apparatuses.

The images taken by the camera are analyzed by special software. According to the purpose, the images have to be enhanced, filtered, compressed or calibrated. Gonzalez and Woods [23] demonstrated the development of digital image processing and all kinds of technique used to deal with the image.

To obtain a complete physical process involved in liquid suppressant transport in a cluttered space, Cary et al. [24] uses PIV measurements to catch the turbulent flow over both an unheated and heated cylinder, and

a body-centered cube (BCC) arrangement of spheres. It is observed that the droplet dispersion around an obstacle is dependent on the droplet size and velocity. Larger droplets move ballistically and smaller droplets are entrained into the surrounding aerodynamic flow field. Therefore, the design strategy to control and optimize the spatial dispersion of droplet should be developed carefully for the fire suppression environment.

Brain et al. [25] investigated the flow behavior on the suppression effectiveness of sub-10-μm water droplet in non-premixed flame with PIV. This study compared the performance of suppression in nitrogen/water vapor with water mist system. The mass concentrations required to extinct flame for nitrogen/water vapor and water mist are 28.6% and 10.0% individually. The traces of the droplets are observed by the PIV system. The picture showed that there is a clear void space between the water drop and the flame front. The absence of scattering particles indicated that the water drops are fully evaporated. These researchers finally concluded that the suppression effectiveness of water mist is directly to the proximity of the drops to the flame and the flow dynamics

1.3 Scope of Present Study

The structure of schematic diagram of the thesis is shown in Fig. 1.4. In the first part of dissertation, the effects of high pressure portable water mist system discharge methodologies on the performance and the corresponding mechanisms of restraining fire are studied. This study

conducted qualitative and quantitative fire tests in a test field. Qualitative fire tests utilized Class A and Class B, motorcycle and car fires. For quantitative study of a portable system, several fire scenarios and discharging methodologies were designed to evaluate fire suppression performance of portable water-mist systems with additives to identify the key fire protection parameters. The effects of high-pressure water-mist system discharge methodologies on performance and the corresponding mechanisms of restraining fire are evaluated. The fire source is a pool-fire burner. Fine water-spray is injected from a portable device in an open environment. The additive is neither toxic nor corrosive. Different nozzle discharge angles, fuels, and concentrations of water-mist additives are selected as the primary experimental parameters. The aim of this study is to investigate the effects of directions of water-mist injected and resulting fire-extinguishment performance. Moreover, a phenomenological study investigates the effects of the additive on water-mist and different fuels.

In the second part of the dissertation, it analyzes the performance of water mist fire suppression systems utilized for wet bench protection. Wet benches are typically utilized in semiconductor facilities for wafer and parts cleaning. Heaters and some flammable liquids, such as acetone and isopropyl alcohol (IPA), are employed during the cleaning process. Wet bench fires have caused serious losses in the semiconductor industry. To assess the fire protection performance, several field tests were performed using a water mist system installed in the wet bench. In this study, test parameters were operational pressure, pan size, nozzle location, cylinder obstruction and degree of door closure. An appropriate

design for operating pressure and the location of water mist nozzles extinguished wet bench fires effectively in the early fire stages.

Finally, this study set up a PIV system to shoot the dispersion of the droplet and use software to analyze the variation of diameters in different conditions such as pressure and additive concentrations. These data acquired from the experiments will be the reference book for future design of water mist system.

The whole PIV experimental apparatus are divided into two systems, the water mist system and the PIV system. The water mist system contain pump, water tank, nozzle and pressure gage. It makes droplet to be detected. PIV system has the properties of non-intrusiveness and whole-field investigation, which provides more information of fluid visualization. PIV system includes four subsystems, the imaging subsystem, image capture system, timing hub and analysis subsystem. The information of each facility is described later in detail.

CHAPTER 2
EXPERIMENTAL DESIGN AND APPARATUS

All of the experimental apparatus are set up in a test field, whose dimensions are 25-meter long, 9-meter wide and 7-meter high. All tests were considered open-air tests; that is, air was supplied naturally. The test facility consists of a test compartment, water mist systems and instruments for data collection.

2.1 Experiment Design

In the first part of dissertation, the effects of high pressure portable water mist system discharge methodologies on the performance and the corresponding mechanisms of restraining fire are studied. In the second part of the dissertation, it analyzes the performance of water mist fire suppression systems utilized for wet bench protection.

2.2 Portable-Water-Mist-System Experiment

This Experiment conducted qualitative and quantitative fire tests in a test field. Qualitative fire tests utilized Class A and Class B, motorcycle and car fires. For quantitative study of a portable system, several fire scenarios and discharging methodologies were designed to evaluate fire suppression performance of portable water-mist systems

with additives to identify the key fire protection parameters.

The schematic configuration of the quantitative experimental apparatuses is shown in Fig. 2.1. The nozzle was not hand-held during the experiments. The discharge angle and the distance between the nozzle and the pan were preciously measured before the tests. The K factor of the nozzle was 1.42 L/min/bar1/2. The volume mean diameter of droplet is about 100 μm at 100bar. The spray angle is 60 degree. There are 21 jet holes in the nozzle, 3 holes in the inner ring and 18 holes in the outer ring . The mist discharge nozzle angle could be adjusted from 0 to 90 degree measured from the horizon for different test scenarios. The mist nozzle was connected to high-pressure pump through a soft hose. The release pressure could be adjusted by the pressure valve in the pump and was indicated on the pressure gauge attached behind the nozzle. The fire temperatures were measured by a thermocouple tree set up in the center of the pan. A radiometer was employed to observe the radiant attenuation effect of mist. All measured data were transferred to the disk storage using a PC-controlled data acquisition system.

2.2.1 Parameters of Tests

The parameters of fire tests included fuel type, nozzle discharge angle, additive solution volume, amount of fuel. The fuels used were heptane, gasoline, and diesel. Nozzle discharge angles were 30°, 45°, and 60° with respect to the horizon, and the additive solution volumes were 0% (pure water), 3%, 6% and 10%. The amounts of fuel used were 250ml, 500ml and 1000ml respectively, and the diameters of pan are 25cm and 50cm. For each pool fire, the tests used three different nozzle

discharge angles and four different additive solution volumes. Each fire test was carried out at lease three times for data consistence.

2.2.2 Fire Source

In the qualitative fire tests, the pan is 1x1m square and 0.2m high. This is conducted according to CNS1387 test protocol in Taiwan.

In the quantitative fire tests, the pan is 25cm in diameter and 15cm high to simulate a small pool fire. The pan was mounted onto a steel stand 15cm above ground to minimize the effects of surrounding ground surfaces on fire behavior. The small-scale pool fires were generated by using heptane, gasoline or diesel as the fuel, which were contained in a circular stainless pan with a diameter of 25cm and a height of 15cm, as shown in Fig. 2.2(a). In the middle-scale one, the pool fire was generated by using heptane, which was contained in a circular stainless pan with a diameter of 50cm and a height of 15cm, as shown in Fig. 2.2(b). The pans were mounted on a steel stand 15cm above the ground to minimize the effects of surrounding ground surfaces on the behaviors of the fire.

The properties of these fuels are shown in Table 2.1. Heptane was chosen as one of the test fuels because it has the advantage of a fixed boiling point (98°C) below that of water. As a consequence, it does not experience any serious splashing effect caused by water droplets. Besides, its low flash point temperature (-4°C) and high vapor pressure could extend the experimental time since it was not easy to reduce the vapor/air mixture ratio below its lean flammability limit. On the other hand, gasoline and diesel were chosen as the contrast reason because of their different characteristics in fire suppression as comparing to that of

heptane.

For the tests of heptane and gasoline, the pan was filled with 750ml of water and 250ml of fuel, that is, total height is 2cm. The fuel was above the water and they were not mixed. The fuel was allowed to pre-burn for 60s to ensure to reach the quasi-steady burning before the mist system activated. For the test of diesel, an extra of 50ml gasoline, served as the accelerator, was given, because diesel is hard to ignite due to its high flash point temperature (>52°C). Then, the fuel was allowed to pre-burn for 120s to ensure the burnout of gasoline and the quasi-steady burning was reached before the mist system released.

2.2.3 Water Mist System

The high pressure water mist system was made up of two major components, the high pressure pump and nozzle. The high pressure pump, shown in Fig. 2.3, could produce 130-bar of pressure and the corresponding flow rate is up to 13 liters per minute. However, it was not easy to observe the fire extinguishment process under such a high pressure because the complete extinguishment occurs immediately after the discharge of water mist. Therefore, a critical pressure 35 bars, a minimum water mist injection pressure required for fire extinction for a distance of 1m, was chosen for the purpose of having enough experimental duration. The high pressure water mist nozzle used was a commercial one, as shown in Fig. 2.4. It relies on hydraulic pressure to force water flowing through the small diameter orifices with a high velocity and to form the water mist. The spray angle of the nozzle is 60°, and the mean droplet size of the water mist is 200 microns in diameter. The K factor of the nozzle was 1.16 l/min/bar1/2, indicating that the

flow rate was 11.6 liter per minute at a pressure of 100 bars. Because orifices' diameter was so small that it was possible to be obstructed. Once the path of mist was obstructed, it would affect the effective water fluxes very much. Therefore, the water used in experiments was pre-filtered to remove its impurities beforehand.

2.2.4 Water Mist Additive Property

The water mist additive used was made of 97% fire-retardant chemical, 1.8% surfactant, 0.6% mint and 0.6% camphor and it was proofed non-toxic. The components of the fire-retardant chemical includes critic acid (molecular formula: HOC(COOH)(CH2COOH)2), borax (Na2B4O7·10H2O) and salt (molecular formula, NaCl). The additive is able to form a thin layer of foamy film on the fuel surface after being sprayed out from the nozzle. Such foamy film can isolate the oxygen, block the fuel vapors, and mitigate the radiative feedback from the fire to the burning fuel surface, so that it makes the fuel hard to re-burn.

2.2.5 Temperature Measurement

A thermocouple tree, shown in Fig. 2.5, was set up in the center of the pan to measure the temperatures. Four K-type thermocouples were installed on that. They were marked as #1, #2, #3 and #4, respectively, and their corresponding locations were given in Fig. 2.6. Thermocouple #1 was located at 0.5cm below the fuel surface and 12.5cm from the side wall of the pan to measure the fuel temperature. Thermocouple #2 was at the interface of fuel and air to measure the fuel and the subsequent flame temperatures. The last two thermocouples (#3 and #4) were located 15cm and 30cm, respectively, above the fuel surface to

measure flame and its plume temperatures.

2.2.6 Radiation Heat Flux Measurement

The radiometer (Type 64 SERIES, MEDTHERM) is shown in Fig. 2.7. It was installed beneath the nozzle, about 70.7cm from the pan, as shown in Fig. 2.1, to collect the radiation heat flux from flame. The radiation heat flux is absorbed at the sensor surface and is transferred to an integral heat sink that remains at a different temperature from the one of sensor surface. The temperature difference between two selected points along the path of the heat flow from the sensor to the sink is the functions of the heat being transferred and the net absorbed heat flux. The transducer has thermocouples or thermopiles to form a differential thermoelectric circuit, thus providing a self-generated emf at the output leads that is directly proportional to the heat transfer rate. No power supply or thermoelectric reference junction is needed. The full scale output level of the radiometer is $10.23\,mV$ at $10\,\mathrm{B}tu/(ft^2 \cdot s)$, and its responsivity is $1.023\,mV$ per $\mathrm{B}tu/(ft^2 \cdot s)$. Besides, a water-cooling system, shown in Fig. 2.8, is used in order to protect the transducer from being overheated. Cooling water, about 30°C in the flow rate of 10.7 ml/s, is provided from one of the water tube attached to an underwater pump, and then warm water is released from the other water tube. Water cooling system should be provided since un-cooled transducer might reach up to 400F (204.44°C).

2.3 Wet-Bench Fire Experiments

Figure 2.9 shows the schematic configuration of the experimental apparatuses. The wet bench is 2.3m long, 0.64m wide and 1.61m high, based on FM 5560 approval standard [11]. Five square pans were placed isometrically in the working surface. Mist nozzles were fixed on the top of the wet bench wall based on test scenarios. The mist nozzle was connected to an electric high-pressure pump via a soft hose. Mist operating pressure was adjusted via the pump pressure valve. The high-pressure pump produced 130 bar pressure and a flow rate up to 13 L/min. A commercially available high-pressure water mist nozzle was used. The nozzle K factor was 1.42 L/min/bar1/2 and flow rate was 11.65 L/min at 100 bar. Pressure was monitored using a pressure gauge attached behind the nozzle. Temperature was measured using a thermocouple tree, arranged at the pan center line. The radiometer was employed to measure the radiant attenuation effects of the mist. All measured data were transferred to a disk storage system using a PC-controlled data recording system.

2.3.1 Parameter of Tests

The fire tests parameters utilized were operating pressure, nozzle location, pan size, cylinder obstruction and degree of door closure. Each fire test was repeated at least three times to achieve data consistency.

2.3.2 Fire source

The wet bench fire source, using acetone as the fuel, was contained in a square iron pan 20cm×20cm or 30cm×30cm; both pans were 15cm deep. The water mist system was manually activated after a 60 second pre-burn to reach a steady state burning condition.

2.3.3 Temperature Measurement

Five k-type thermocouples were set in the pan center. The thermocouples were marked #1, #2, #3, #4, #5 and located at 15cm, 35cm, 55cm, 75cm and 95cm, respectively, arranged in the pan center line above the fuel surface to measure temperature history.

2.4 Measurement Instrumentations

2.4.1 Hydraulic Pressure Measurement

A pressure gauge, shown in Fig. 2.10, was installed in the pipe near the nozzle to monitor the discharge pressure of the water mist system. The applied hydraulic pressure of 35 bars was chosen in such a way that complete extinguishment did not occur immediately or even did not occur at all in order to earn enough time for experimental purposes. The volume flow rates of mist in different additive solution volumes are listed in Table 2.2. It shows that the volume flow rates are almost the same in the in different additive solution volumes so that the added additive does not significantly affect the run-off of water mist.

2.4.2 Oxygen Concentration Measurement

Part of burnt gas products are collected from the fire, and sucked into the Gaseous Oxygen Analyzer (Model 755A, Rosemount Analytical), shown in Fig 2.11 to measure the oxygen concentration within the fire. Before measuring and analyzing the gas samples in the instrument, a preconditioning process is carried out in advance. The preconditioning system includes two tandem connection sets of glass wool filters, a set of membrane filter, a gas cooler and a micro pump, which are indicated in Fig 2.12.

2.4.3 Data Acquisition

All experimental data were recorded by a data acquisition system (Type 5000, Jiehan) with 2s sampling interval. The picture of the datalog is shown in Fig. 2.13.

2.4.4 Digital Video

One digital video camera (Type DCR-TRV40, SONY), fixed at an appropriate position, was used to provide visual records of the fire, water mist discharge, and fire suppression process. The images from the video were transmitted to a PC by IEEE 1394 card, and they were processed by the CyberLink PowerDirector software to show a series of flame structures.

2.5 Particle Image Velocimetry

The PIV system used in this experiment is developed by IDT Company. It contains three subsystems, which are imaging, image capture and analysis subsystem. Imaging subsystem consists of two units, the Nd:YVO 4 laser generator and optic lens. The laser generator produces a green straight light that goes through the optic lens to produce the laser sheet. When the water mist droplets pass through the light sheet, they reflect the light that can be captured by camera. The second subsystem is image capture subsystem, consisting of camera and image capture software. The main function is to control the camera as well as gather and store the images. The last subsystem is analysis subsystem, including PC and digital software. The details are described below. The schematic is shown as Fig 2.14.

2.5.1 Imaging Subsystem

2.5.1.1 Laser

The laser adapted in the experiment is the Nd:YVO 4 laser produced by Spectra Physics corp. It is a visible, continuous wave of green light. Comparing to the original infrared laser produced by IDT Company, it has the advantage to improve the sensitivity of CCD (Charge-Coupled Device) and lower the difficulty of adjusting laser light. The laser operates with the power of 2W, the wavelength of 532 nm, the beam diameter of 2.3mm, the spray angle of 0.5 mrad and the laser sheet width of 3.4 mm. The picture is shown in Fig 2.15.

2.5.1.2 Optic Lens

The optic modules in Fig 2.16 include optic lens (BK7 Precision Cylindrical Lenses), optic platform, optic lens holder and fixer. The effective focal distance for lens is 6.4 mm.

2.5.2 Image Capture Subsystem

The digital camera Olympus E-330, shown in Fig. 2.17, is used to capture the image of droplets. Its effective pixel is approximately 7.5 million; the shutter varies from 1/4000 to 60 second; the resolution is 3136x2350 pixel in the x and y axis individually. The operation range of focus is 3.5~5.6 and the ISO value can reach the maximum value for 1600. SIGMA Apo Macro camera lens provides large magnification and takes picture clearly with long distance. The magnification varies from 1:1 to 1:10, while the shooting distance varies from 0.38 to 1.65m. With its large F value of 2.8, the object shot in the dark place also has good performance. The picture is presented in Fig. 2.18.

2.5.3 Analysis Subsystem

A high speed, large volume storage system is taken to collect the image data gathered by the PIV system. The storage system is a PC with Pentium 4 CPU and 1GB RAM. These images are processed with the NI Vision Assistant 8.5 software. After several post-processes, the water droplets in the image are calculated to get the pixels occupied by the particles. The detail operations are demonstrated in next chapter.

2.5.4 Procedure of the Experimental Operation

The flow chart is shown as Fig. 2.19. Here is the detail description.

(1) Make sure that sufficient water without additive (pure water) in the tank is ready.

(2) Check if any impurities block off the orifices of the nozzle.

(3) Turn on the laser power and set up the lens to transform the beam into light sheet

(4) Turn on the CCD and adjust appropriate diaphragm and shutter.

(5) Turn on the high pressure pump for 4 second and then capture the image of droplet. The interval between detections is 10 second.

(6) Turn off the pump.

(7) Take discharge pressure as an experimental parameter. Repeat the procedure (5)-(6) steps.

(8) Take detection location as an experimental parameter. Repeat the procedure (5)-(6) steps.

CHAPTER 3
UNCERTAINTY ANALYSIS AND PIV IMAGE PROCESSING

All of the data from experimental results may not be equally good to adopt. Their accuracy should be confirmed before the analyses of experimental results are carried out. Uncertainty analysis (or error analysis) is a procedure used to quantify data validity and accuracy [25]. Errors always are presented in experimental measuring. Experimental errors can be categorized into the fixed (systematic) error and random (non-repeatability) error, respectively [25]. Fixed error is the same for each reading and can be removed by proper calibration and correction. Random error is different for every reading and hence cannot be removed. The objective of uncertainty analysis is to estimate the probable random error in experimental results.

From the viewpoint of reliable estimation, it can be categorized into single-sample and multi-sample experiments. If experiments could be repeated enough times by enough observers and diverse instruments, then the reliability of the results could be assured by the use of statistics [26]. Like such, repetitive experiments would be called multi-sample ones. Experiments of the type, in which uncertainties are not found by repetition because of time and costs, would be called single-sample experiments.

3.1 Uncertainty Analysis

3.1.1 Analyses of the Propagation of Uncertainty in Calculations

Uncertainty analysis is carried out here to estimate the uncertainty levels in the experiment. Formulas for evaluating the uncertainty levels in the experiment can be found in many papers [26, 27] and textbooks [25, 28, 29]. They are presented as follows:

Suppose that there are n independent variables, $x_1, x_2, \ldots, x_n$, of experimental measurements, and the relative uncertainty of each independently measured quantity is estimated as ui. The measurements are used to calculate some experimental result, R, which is a function of independent variables, $x_1, x_2, \ldots, x_n$; $R = R(x_1, x_2, ..., x_n)$.

An individual xi, which affects error of R, can be estimated by the deviation of a function. A variation, δx_i, in x_i would cause R to vary according to

$$\delta R_i = \frac{\partial R}{\partial x_i}\delta x_i \tag{3.1}$$

Normalize above equation by dividing R to obtain

$$\frac{\delta R_i}{R} = \frac{1}{R}\frac{\partial R}{\partial x_i}\delta x_i = \frac{x_i}{R}\frac{\partial R}{\partial x_i}\frac{\delta x_i}{x_i} \tag{3.2}$$

Eq. (3.2) can be used to estimate the uncertainty interval in the result due to the variation in xi. Substitute the uncertainty interval for xi,

$$u_{R_i} = \frac{x_i}{R}\frac{\partial R}{\partial x_i}u_{x_i} \tag{3.3}$$

To estimate the uncertainty in R due to the combined effects of

uncertainty intervals in all the xi's, it can be shown that the best representation for the uncertainty interval of the result is [27]

$$u_R = \pm\left[\left(\frac{x_1}{R}\frac{\partial R}{\partial x_1}u_1\right)^2 + \left(\frac{x_2}{R}\frac{\partial R}{\partial x_2}u_2\right)^2 + \ldots + \left(\frac{x_n}{R}\frac{\partial R}{\partial x_n}u_n\right)^2\right]^{1/2} \quad (3.4)$$

3.1.2 Uncertainty Level Analysis in the Experiment

The surface area of pool is selected to demonstrate the process of uncertainty level analyses as follows.

The surface area of pool, A_{Pool}, is

$$A = \frac{\pi}{4} \times a^2, \quad a = 250 \pm 0.5mm$$

$$A = A(a)$$

$$u_A = \pm\left[\left(\frac{a}{A}\frac{\partial A}{\partial a}u_a\right)^2\right]^{1/2} = \pm\left[(u_a)^2\right]^{1/2} = \pm 0.002$$

$$\left(u_a = \frac{0.5}{250} = 0.002\right)$$

3.1.3 The Asymmetric Uncertainties of Thermocouple

Room temperatures are measured by a 1mm diameter K-typed thermocouple, whose signals are sent to a PC-record (Ethernet). The accuracy of the thermocouple itself without coating is ±0.2%. Due to the effects of conduction, convection, and radiation, it is worthwhile to check the correctness of gas temperature measured by such K-typed thermocouple. Via an application of energy balance, i.e.,

Energy in = Energy out, or

Convection to the junction of thermocouple = Radiation from the junction of thermocouple + Conduction loss from the probe

Because of the fine thermocouple (1mm), the conduction term can

be neglected. Then, the steady-state energy equation can be rewritten as follows.

$$A_w h(T_g - T_t) - A_w \sigma(\varepsilon T_t^4 - \alpha T_w^4) = 0 \tag{3.5}$$

In practice, the flame temperature is much higher than the wall temperature of thermocouple, so the absorption term, αT_w^4, from the relatively low wall temperature of thermocouple can be removed from Eq. (3.5). According to Eq. (3.5), the expression of correlation is given as:

$$T_g = T_t + \frac{\varepsilon \sigma T_t^4}{h} \tag{3.6}$$

where T_g = the true gas temperature

T_t = the temperature measured by thermocouple probe

ε = emissivity of the thermocouple

σ = Stefan Boltzmann constant

h = convection heat transfer coefficient at wire surface

Now, the analysis method of uncertainty can be utilized to obtain the uncertainty in the flame temperature from the correlation associated with h, T_t, and ε. The relationship between temperature and error is shown in Fig. 3.1.

3.1.4 The Uncertainties of Radiometer

The radiometer (Type 64 SERIES, MEDTHERM) is provided with the certified calibrations, compiled with ISO/IEC 17025, ANSI/NCSL Z540-1 and MIL-STD-45662A. Calibrations, shown in Fig. 2.8, are corrected by the National Institute of Standards and Technology through temperature standards and electrical standards. The uncertainty of its

performance is 3%, shown in the report as well.

3.1.5 The Experimental Repeatability

In order to confirm the accuracy and coincidence of experimental data, each fire test under the specified fuel, discharge angle and additive volume rate was carried at least three times to ensure the repeatability. The following examples are use to illustrate the creditability in the previous statement. There are two cases selected to demonstrate the experimental repeatability. Firstly, pure water tests with different fuel types in 25cm diameter of the pan is selected. Secondly, water mist with additive in 50cm-diameter of pan with heptane fires is selected as well. It recorded three measured data of extinction time and made an average value for each fire test. The three measured data, their averaged value, and the coefficient of variation are listed in Table 3.1. The coefficient of variation (C.V.) is defined as the ratio of the standard deviation s to the mean $\overline{X}$, where the standard deviation s is calculated as:

$$s = \sqrt{\frac{1}{N}\sum_{i=1}^{N}(X_i - \overline{X})^2} \qquad (3.7)$$

The coefficient of variation is a dimensionless number that allows comparison of the variation of data points in a data series around the mean. Figure 3.2 graphically shows the presentation of Table 3.1. The averaged values formed a dashed curve. It can be seen that in general the coefficients of variation are within the acceptable range since the maximum is below 10%, consequently, the experimental repeatability is quite good. The fire extinguishment processes and their corresponding characteristics will be discussed in details in next chapter.

3.2 PIV IMAGE PROCESSING

The fundamental theories of PIV detecting technique and digital image processing will be illustrated. In the image detecting technique, a simple introduction of PIV system and its relative mathematical equations are provided. In the field of digital image processing, two major methods, the image enhancement and image restoration, are described. All of the methods have the same purpose: to get clear, non-interfering image. For different scenarios, the corresponding processing methods also change.

3.2.1 Image Transform

In the digital image processing, no matter the image enhancement or image restoration the basic methods are deal with spatial domain and frequency domain. In the spatial domain, the image processing procedure is based on direct manipulation of pixels in an image. In the frequency domain, the procedure is based on modifying the Fourier transform of an image. These two domains are connected by a Fourier transform theorem, the convolution theorem. Most transformations in frequency domain are Discrete Fourier Transform (DFT). To accelerate the calculation, the technique of Fast Fourier Transform (FFT) is adapted. The details are described below.

3.2.1.1 Convolution Theorem

Assume the convolution, consisting of two continuous functions p(x) and q(x), is presented as p(x)*q(x), the integral form is

$$p(x)*q(x)=\int_{-\infty}^{+\infty} p(\propto)q(x-\propto)d\propto \qquad (3.8)$$

where x represents a continuous variable, α the dummy variable, and * the operator.

In the frequency domain, the Fourier transform pair consists of p(x)*q(x) and p(u)q(u). In other words, if the Fourier transform of p(x) and q(x) are P(u) and Q(u) individual, then the Fourier transform of p(x)*q(x) is P(u)Q(u):

$$p(x)*q(x) \Leftrightarrow P(u)\,Q(u) \tag{3.9}$$

Equation (3.9) shows that the convolution in x domain can be acquired through the inverse Fourier transform of P(u) Q(u). The similar conclusion is that the convolution in the frequency domain by the inverse Fourier transform of the product in x domain,

$$p(x)q(x) \Leftrightarrow P(u)*\,Q(u) \tag{3.10}$$

Usually Eqs. (3.9) and (3.10) are called convolution theorem.

3.2.1.2 Fast Fourier Transform (FFT)

In the frequency domain, the Fourier transform pair are showed as

$$F(u) = \frac{1}{M}\sum_{x=0}^{M-1} f(x)e^{-j2\pi ux/M} \tag{3.11}$$

where u=0, 1, 2,…, M-1, and

$$f(x) = \sum_{u=0}^{M-1} F(u)e^{-j2\pi ux/M} \tag{3.12}$$

where x=0, 1, 2,…, M-1

If there are M points to be transformed by 1D DFT, the plus/multiply procedures will repeat M^2 times. It costs a lot of operational time. The FFT method, based on the successive doubling method, is invented to raise the calculation efficiency. The basic concept is described below. Rewire Eq. (3.11) as

$$F(u) = \frac{1}{M}\sum_{x=0}^{M-1} f(x) W_M^{ux} \tag{3.13}$$

$$W_M = e^{-j2\pi ux/M} \tag{3.14}$$

Assume that M has the form of $M=2^n$, where n is a positive integral. Then M is presented as

$$M=2k \tag{3.15}$$

Substitutes Eq.(3.14) into Eq.(3.13)

$$F(u) = \frac{1}{2K}\sum_{x=0}^{2K-1} f(x) W_{2K}^{ux}$$

$$= \frac{1}{2}\left[\frac{1}{K}\sum_{x=0}^{K-1} f(x) W_{2K}^{u(2x)} + \frac{1}{K}\sum_{x=0}^{K-1} f(2x+1) W_{2K}^{u(2x+1)}\right] \tag{3.16}$$

Because $W_{2K}^{2ux} = W_K^{ux}$ (proved by Eq.(3.14)), Eq. (3.16) is rewritten as

$$F(u) = \frac{1}{2}\left[\frac{1}{K}\sum_{x=0}^{k-1} f(2x) W_K^{ux} + \frac{1}{K}\sum_{x=0}^{k-1} f(2x+1) W_K^{ux} W_{2K}^{u}\right] \tag{3.17}$$

Define

$$F_{even}(u) = \frac{1}{K}\sum_{x=0}^{K-1} f(2x) W_K^{ux} \tag{3.18}$$

where u= 0, 1, 2,…,K-1, and

$$F_{odd}(u) = \frac{1}{K}\sum_{x=0}^{K-1} f(2x+1) W_K^{ux} \tag{3.19}$$

where u= 0, 1, 2,…,K-1

Substitute these two equations into Eq. (3.17) to get

$$F(u) = \frac{1}{2}[F_{even}(u) + F_{odd}(u) W_{2K}^{u}] \tag{3.20}$$

Because $W_M^{u+M} = W_M^u$ and $W_{2M}^{u+M} = -W_{2M}^u$, Eq.(3.20) can be transformed into

$$F(u+k) = \frac{1}{2}[F_{even}(u) - F_{odd}(u) W_{2K}^{u}] \tag{3.21}$$

Therefore, if the values of M_{even} and M_{odd} in the M position are calculated, the DFT for M and M+1 can acquire at the same time. This transform process saves a lot of time. For a positive integral M, the

number of times for calculation varies from M^2 to $M/\log_2 M$. Take $M=2^{15}$ for example, the operation time in the computer for FFT is only 1/2200 compared to that of DFT.

3.2.2 Image Enhancement

The major purpose of image enhancement technique is to process an image to fit “specific” application. The word “specific” is very important, because image enhancement process is subjective and question-guiding. The methods for image enhancement are divided into two groups: spatial domain and frequency domain. For spatial domain method, the digital image is fixed by dealing with the pixels of the image directly. The mostly used filters are low-pass filter and median filter. For frequency domain method, the image is transformed into the form of Fourier series then modified. Homo-morphic filtering is commonly used.

3.2.3 Image Restoration

Like image enhancement process, image restoration process has the same purpose to improve the quality of the image. The difference between image enhancement and restoration is that image enhancement is to provide clear image to the observer; image restoration is to eliminate the noise to establish the original image. Image restoration is an objective process. It first sets up degradation model and reverses the process to get the initial image, such as Wiener filtering and adaptive filter. Like image enhancement, image recover also has spatial and frequency domain methods. When the only degradation is additive noise, it is easy to deal with it in spatial domain. If degeneration like

image-blur exists, it is better to work in frequency domain.

3.2.4 Image Processing Procedure for Experimental Data

In these experiments, all data acquired by the CCD camera are deal with NI Version Assistant software. The procedures for image processing include (I) Brightness and Contrast (II) RGB Green Plane, (III) Gaussian Smoothing Filter, (IV) Threshold and (V) Particle Analysis, and they are shown in Fig. 3.2. In step one, there are two parameters, brightness and contrast, adjusted to enhance the images of droplets. Then the multi-color image is processed with color plane extraction to isolate the green color image. To eliminate the noise and circularize the droplet image, Gaussian smoothing filter is adapted. Threshold is used to create a high contrast black-white image with an adjustable value K. There is no best value for K, but exists the appropriate one. With these procedures above, a black-white droplet image is acquired. The Particle Analysis procedure can calculate the pixels occupied by each particle. Knowing the resolution of the camera and the real size of appearance of picture, it is not hard to find the ratio of pixel/cm. With the relationship, the pixel of image can be transformed into diameter for droplet. Once the data of diameters are collected, they are calculated by following the ASTM 799-72 regulation.

3.2.5 Measurement for Water Mist Density Distribution

In addition to droplet diameter, water mist density distribution is another major factor for nozzle. For a nozzle with specific k value, the water mist distribution varies with different pressure. Not only the density distribution but also the spray coverage are varied. Therefore, the relation between them and pressure must be assured. The measuring methods are presented below.

3.2.5.1 Measurement by Tubes

In this experiment, the first measuring method adapted is to collect water by plastic tubes. These tubes are distributed within the area 60 x 60 cm which is only a quarter of total spray coverage. The number of tubes used in the region is 225. The experiment must repeat four times in different positions to get the full phenomena. It takes three minutes for each procedure, and the data is converted to flow rate per minute.

3.2.5.2 Measurement by Image Processing

When the PIV system is activated, a horizontal laser sheet is produced 1m under the nozzle. Water mist droplet reflects light while going through the laser sheet. If some location contains more water droplets, the reflective light is stronger. The brightness of reflective light is highly related to the grayscale which is used to measure the intensity of light at each pixel in a single band of electromagnetic spectrum. According to this concept, this study analyzes the grayscale distribution of the detected lines along the transverse direction. Each line is separated from the neighbor ones by 50 pixels along the longitude direction. After gaining the distribution of grayscale in the image, the contour lines can be drawn. These contour lines are regarded as the water mist density distributions.

CHAPTER 4

RESULTS AND DISCUSSION

This thesis consists of two parts. In the first part, a series of tests subjected to various discharge methodologies and fire scenarios were carried out based on a portable water mist fire extinguishing system with additive on pool fires. In the second part of the thesis for assessing the fire protection performance in wet bench fires, several field tests were performed using a water mist system installed in the wet bench. The corresponding experimental results are discussed as follows.

4.1 Portable-Water-Mist-System Experiments

4.1.1 Qualitative Fire Tests

4.1.1.1 Class A fire tests—wood slabs

The Class A fire test was conducted according to CNS1387 test protocol. The test object (Fig. 4) comprises wood slabs (0.9×0.9×0.9m) on a rack and a pan with 1.5 liters gasoline located under the rack. During the test, the gasoline is ignited first. The portable water-mist system then starts 3 minutes later. Figure.4.1 presents a series of photographs of the fire test. The fire was extinguished in 10 seconds. During the test, portable water-mist was very effective for extinguishing wood slab fire. The dark smoke generated by the fire changed to light-colored smoke after mist was released. The reason the smoke changed color may be that the water mist cooled the fire temperature

and decreased the combustion rate, thereby reducing the smoke production rate. Another reason is that the mist has large interaction surface with smoke and may have stifled the smoke.

4.1.1.2 Class B fire tests—gasoline pan fire

A gasoline pan fire was used as the Class B fire test scenario. The pan, 1×1m square and 0.2m high, was filled with 5 liters of gasoline. After 60 seconds of pre-burning, the portable water mist was released. Figure 4.2 presents a series of pictures of fire test. The fire was extinguished in 10 seconds. In the test series, operator skill had a significant affect on extinguish time. The mist had to cover the pan for good performance, and the mist angle is also important for when extinguishing fires.

4.1.1.3 Motorcycle fire tests

Motorcycles were used as fire source. Gasoline was sprinkled on three motorcycles and then ignited. After 30 seconds of pre-burning, the portable water-mist was released. As plastics are the primary motorcycle components, smoke production was high. Just as in the Class A fire test, after the water-mist was released, the smoke changed to a light color, it’s safe for an operator. The motorcycle fire was extinguished in approximately 20 seconds. However, operator skill has a significant affect on the time required to extinguish the fire. Figure 4.3 presents a series of photographs of the fire test.

4.1.1.4 Car fire tests

A car was utilized as the fire source. The gasoline was sprinkled into the sedan and then ignited. After 30 seconds of pre-burning, the portable water mist was released. As plastics are the primary

components of sedan, the smoke production rate remained high. Just as in the motorcycle fire test, after the water-mist was released, the smoke color became light. The car fire was extinguished in approximately 30 seconds. Operator skill critically affected the time required to extinguish the fire. Figures 4.4 and 4.5 present a series of photographs of the test fire.

4.1.2 Quantitative Fire Tests

In the first part of the dissertation, a series of fire tests using water mist as the extinguisher were conducted in a test field. Several fire scenarios and discharging features were designed to evaluate the fire suppression performance of a portable water mist system with additive in order to identify the controlling mechanisms of fire suppression. Table 4.1 shows the list of variables, which include fuel type, additive solution volume, nozzle discharge angle, amount of fuel and cross-section area of pan. The range for each variable are also listed in this table.

4.1.2.1 Fire Tests with Different Fuel Types

The tests were performed with diesel, heptane and gasoline fires respectively. The fuels were contained in a circular stainless pan, with a diameter of 25cm and a height of 15cm. For the tests of heptane and gasoline fires, 750ml of water and 250ml of fuel were used. For the tests of diesel one, an extra of 50ml gasoline, served as the accelerator, was given.

4.1.2.2 Pure Water Mist

In this section, pure water mist was used as the fire suppression agent and the corresponding results would be taken as the base data for

comparisons with those using additive. The extinction times for different fuel types under three nozzle discharge angles are shown in Table 4.2 and they are plotted in Fig. 4.6 as well.

The extinction time curves can be divided into two types: one is the monotonic decreasing curve for diesel, and the others are the convex curves for gasoline and heptane, respectively. For diesel fuel, its narrower combustion limits and higher flash point make the curve different from the ones of gasoline and heptane. The extinction time decreases as the nozzle discharge angle increase for diesel, whereas it shows the contrary behaviors in the tests of gasoline and heptane. The worst performance of fire suppression occurs at the nozzle discharge angle of 45° that the extinction time is lowered no matter how the nozzle discharge angles increases or decreases. In the higher nozzle discharge angle regime (>45°), water mist is possible to fully cover the pan fire, so that the flame cooling and oxygen-displacement play the important roles. On the other hand, in the lower nozzle discharge angle (<45°) regime the mist jet rebounds from the pan wall and forms a thin mist layer parallel to fuel surface, thus blocks and dilutes the fuel vapors. So, it makes the fire extinction easier in the low nozzle discharge angle than that at 45°.

Figure 4.7(a)-(c) show the temperature variation histories of heptane, gasoline and diesel fires at the nozzle discharge angle of 30°. For the three fuel fires, the temperatures measured at 15cm above the fuel surface (i.e. thermocouple #3) in the flame center are the highest ones, which can reach as high as 650 to 750°C. After water mist is released, the flame size reduces quickly and is pushed back toward the

side wall of the pan, which is close to the nozzle. The fluctuations of temperatures at 0.5cm below the fuel surface (i.e. thermocouple #1) are almost invariant, whereas the temperatures measured at the fuel surface (i.e. thermocouple #2) and at 15cm and 30cm above the fuel surface (i.e. thermocouple #3 and #4) all rapidly decrease as the water mist is reached.

The tendencies of temperature of gasoline and heptane fires measured at thermocouple #2 are different from the diesel one. The former ones rapidly increase as water mist is discharged since the flame is pushed toward the fuel surface, and furthermore fresh air entrained with water mist flow enhances the burning of fuels. However, the temperature of diesel fire measured at #2 does not increase after water mist is released. Because the low vapor pressure and high flash point make diesel fuel hard to re-ignite after the fuel surface cooled by water mist.

In the case of gasoline fire, it is remarkable that the highest temperature can only reach to 550°C during the free burning, but after water mist is released, it can rise to 750°C. When gasoline fuel is burning, it produces a lot of smoke and the available oxygen is not enough after a certain period. Once water mist is released, the fresh air is entrained with water mist flow to enhance the burning of gasoline fuel. Therefore, combustion enhancement may be resulted from an improper design of the water mist fire extinguishing system.

Figure 4.8(a)-(c) are the radiation heat flux histories of heptane, gasoline and diesel fires at the nozzle discharge angle of 30°. The highest radiation heat fluxes that different fuel fires can reach are

grouped into gasoline, heptane and diesel in descending order of their magnitudes. The result does correspond with their combustion heat. The radiation heat flux of fires rapidly reaches almost zero after the releasing of water mist. It shows that the water mist system has a good ability for radiation attenuation and can provide a good protection for the operators, who are using portable extinguishing equipment.

Figure 4.9 shows the oxygen concentration variation history in a gasoline fire for a demonstration. The oxygen mole concentration in air is about 20.9%, and after ignition, it gradually decreases to 14.4% since lots of smokes are produced during the initial burning. When the burning gradually reaches quasi-steady state, less smoke are produced. These result in a rise of oxygen concentration. When water mist is discharged, the fresh air is entrained with the flow so a large flare-up is generated in the moment. However, the measured oxygen concentration surge is not obvious. With continuous discharge of water, the evaporation of water mist brings a rapid clearance effect and reduces the oxygen concentration. Then the fire is pushed toward the fuel surface and its size becomes smaller so the oxygen concentration in the pan gradually rises again. After extinction, the oxygen concentration is back to 20.9%.

4.1.2.3 Water Mist with Additive on Diesel Pan Fires

Since diesel is hard to ignite due to its narrow combustion range and high flash point temperature (>52°C), an extra of 50ml gasoline, served as the accelerator, was provided. For ensuring the burnout of gasoline and reaching the quasi-steady burning, it took 120s of pre-burning before the water mist system activated. The extinction time

for different additive solution volumes at three nozzle discharge angles are listed in Table 4.3. In the cases of fire suppression by using pure water, the best fire extinguishing performance was occurred at the nozzle discharge angle of 60° because mist could fully cover the pan fire. By using the water mist with additive, the fire extinguishing efficiency is found to be improved. The best fire extinguishing efficiency occurs at 3% additive ones. However, if too much additive is provided, the fire extinguishment efficiency will decrease. Since the surfactant in additive not only has adverse effects on the atomization of water mist by increasing the surface tension but also can make the water mist more difficult to vaporize by increasing the boiling point. It does agree with the results of the experiments Zhou et al. [17] conducted. As shown in Fig. 4.10, the extinction time at three nozzle discharge angles were all significantly decreased comparing with those using pure water. There was an interesting phenomenon in these tests. When the nozzle discharge angle was at 30°, the more additive was added, the more time fire extinguishment needed. It shows that at the nozzle discharge angle of 30°, vaporizing effects of mist played a more important role in fire suppression than that of additive. However, the fire extinguishing time was still less than that using pure water.

4.1.2.4 Water Mist with Additive on Heptane Pan Fires

In the tests of heptane, its flame was turbulent but it didn’t produce a lot of smoke. At the beginning of the discharge, the flame height was reduced but the flame size became bigger than the initial one because the fresh air was entrained into the fire plume with water mist. Then, the flame expanded rapidly and stretched out concurrently with the

continuous discharge. It was not easy to extinguish the heptane pan fires in the present tests. The extinction times for different additive solution volumes at three nozzle discharge angles were listed in Table 4.4 and they also were plotted in Fig. 4.11. There were two types of curves existed in the extinction time relationships; one was convex curves for the 0% and 3% additive, and the other was monotonic decreasing curve for 6% and 10% additive.

For the case of using water mist of 3% additive for fire suppression, the fire extinguishing time at the nozzle discharge angle of 30° was less than that at 45°. Because in the low nozzle discharge angle tests, the entrained flow rebounded from the pan wall and blocked the fuel vapor. When 3% additive was used, the fire extinguishing time was substantially reduced compared with 0% additive. However, the performance of fire suppression with low additive solution volume is similar to that with pure water. For the cases of 6% and 10% additive ones used in fire suppression, the lower the nozzle discharge angle was, the more the extinguishing time took. It is because that at the lower nozzle discharge angle, there was less mist being able to reach the fuel pan.

Figure 4.11 shows that at the nozzle discharge angle of 30°, the best performance of fire suppression occurs in the additive solution of 3%. The more the additive solution volumes increases, the more the fire extinguishing time. That is because that the vaporizing effect of mist plays a more important role than that of the additive in fire suppression at the nozzle discharge angle of 30°. When the nozzle discharge angle was increased to 60°, the trend was different. Firstly, the fire

extinguishing time increased with the additive solution volume, which was less than 6%. When the additive solution volume was 6%, it took the longest time to extinguish the fire. After that, the fire extinguishing time decreased as the additive solution volume increased. This is because that the fire extinguishing efficiency is not only influenced by mist effects but also by additive ones. Therefore, there must exist an optimal zone between the mist and additive effects for fire suppression.

4.1.2.5 Water Mist with Additive on Gasoline Pan Fires

In the tests of gasoline, the turbulence of flame was quite intense and it produced a lot of smoke. The fire extinguishing behavior of gasoline was similar to that of heptane. The extinction time for different additive solution volumes at three nozzle discharge angles were listed in Table 4.5 and they were plotted in Fig. 4.12 as well. There were also two types of curves as a function of time existed, one was convex curves for 0% and 3% additive, and the other was monotonic decreasing curve for 6% and 10% of additive solution volume. The performance of fire suppression with low additive solution volume was similar to that with pure water. However, when additive was used, the fire extinguishing time were all obviously reduced as comparing with the one by using pure water. It was shown that the additive used in the present tests for fire suppression has a better performance for tackling gasoline fires than tackling heptane ones. Figure 4.12 shows that, at the nozzle discharge angle of 30°, the fire extinguishing time obviously decreases as the three additive solution volumes (3%, 6% and 10%) increases. It still reveals that vaporizing effects of mist are more important than additive ones at low nozzle discharge angle.

4.2 Wet-Bench Fire Experiments

Taiwan has roughly 1,000 semiconductor facilities, with a total output value of approximately US$23 billion in 2006, ranking the Taiwanese industry as third largest worldwide. A polypropylene (PP)/polyvinyl chloride (PVC) wet bench is typically utilized in clean room environments. Hundreds of chemicals are used during manufacturing, some of which evaporate easily and have a wide flammability range. FM Global has estimated that 1 in 10 manufacturing plants experience a fire loss annually. Fires involving wet benches have caused significant losses in the semiconductor industry in past years. This study analyzes the performance of water mist fire suppression systems utilized for wet bench protection.

4.2.1 Single nozzle tests with different pan sizes and operating pressures

The pan sizes used were 20cm×20cm square and 30cm×30cm, both pans were 15cm deep. In these tests, one water mist nozzle was fixed one meter above the pan center. Each pan was filled with 400c.c. or 900c.c. acetone such that the same fuel surface level (1cm high) was maintained. After 60 seconds of pre-burning, the water mist system was activated manually. The mist operating pressure was changed from 15bar to 55bar in series of tests to identify the critical pressure. Table 4.6 shows the time required to extinguish the fires in different pan sizes and at different operating pressures. When the nozzle was installed just above the pans, fires were extinguished in seconds at most operating pressures. The water mist system effectively extinguished the acetone

pan fires. During each pan size test, there was a critical pressure. Below the critical pressure, the mist took more than ten seconds to extinguish the fires or even did not extinguish the fires. For the 20cm and 30cm pan fires, the critical pressure was the same 15bar. Under that pressure, mist density (flux) and jet momentum was insufficient to extinguish the fires. According to Table 4.6, the time to extinguish a small pan fire was shorter than that for a large fire. For the 30cm×30cm pan, when operating pressure decreased, time to extinguish the fire increased; however, this phenomenon was not obvious for the 20cm pan. For different pan sizes, flux and momentum of water mist have significant roles in fire suppression. For the 20cm pan, the mist totally covered the pan during tests and fires were extinguished instantly. However, for the 30cm pan with larger fuel surface, additional mist and at an increased momentum was needed to extinguish the fires. That is, the 30cm pan fires needed additional time to be extinguished.

During the tests, the single nozzle fixed above the pool extinguished the wet bench fires in seconds with appropriate pressure. When pressure reached 15bar, the flame became unstable and started to tremble markedly. The fire even spread to other pans located beside the fire pan. At a low operating pressure, the fire had the potential to ignite fuel in another pan and spread over the wet bench.

4.2.2 Tests for nozzle distribution

These experiments addressed the effect of the following two parameters: location tests for a single nozzle; and, using two nozzles at the same time. In the first test, the water mist nozzles were placed at two different locations, 20cm and 40cm apart from the original position (pan

centerline), one meter above the pan center. Table 4.7 shows the times required to extinguish the fire with a single nozzle placed in different locations. For the 20cm distance, extinguishing times for the 30cm×30cm pan all were 3 seconds at operating pressures of 55bar, 45bar and 35bar. The extinguishing times for the 20cm×20cm pan were 2 s, 1 s and 1 s at pressures of 55bar, 45bar and 35bar, respectively. The water mist system effectively extinguished the pan fires. However, when the nozzle was placed 40cm away from the original position, the water mist could not extinguish the pan fires at all operating pressures. For the 40cm tests, the fire plume drifted to another side of the pan. This performance difference resulted from mist coverage. At 40cm, the mist did not cover all of the pan area, whereas at 20cm, the mist still covered the whole pan. Due to the low flash point of acetone, the mist needs sufficient momentum and totally covered to extinguish the fires. In 40cm case showed that the cooling effect of mist was insufficient to extinguish acetone fires.

The second test evaluated extinguishing efficiency of two nozzles on each side of the pan fixed symmetrically on the top of the wet bench. There were two distances, 40cm and 80cm used between each nozzle. It means 20cm and 40 cm from the pan center to each nozzle. The 20cm×20cm pan was utilized as the fire source for these nozzle distribution tests. Table 4.8 shows the times required to extinguish the wet bench fires with 40cm and 80cm between the two nozzles. In contrast to the single nozzle tests, the fire plume was suppressed in the pan and the fire did not tremble significantly. The extinguishing times indicated that using the two nozzles was slightly better than using a

single nozzle located the same distance from the pan center. When the two nozzles were utilized, density-to-pan-fire ratio was almost double; however, the mist momentum was still insufficient. This experimental finding indicates why the time difference between single nozzle and two nozzles was not obvious. The mist required adequate momentum to extinguish the fire, regardless of whether a single nozzle or two nozzles were used.

4.2.3 Obstruction tests

In real working process, tools or solvent tanks are sometimes located near the working surface of washing tanks (pan fire source). These tools or solvent tanks in this study were considered obstructions to a fire extinguishing system. In the following experiments, cylinders 30cm high and 18cm in diameter were utilized as obstructions to simulate tools or solvent tanks left on the bench. During the first test, one cylinder was placed 10 cm away from one side of a pan. In the second test, two cylinders were placed on each side of the pan, 10cm away. These obstructions may affect the direct flow of water mist to a fire, thereby changing the performance of the water mist system. However, tests results (Table 4.9), indicate little difference in extinguish capability with and without obstructions. In the 40cm tests, for the nozzles are fixed above the pan, the mist was partly blocked by one or two cylinders. Obstructions didn’t seriously affect the mist to fuel surface. However, for the 80cm tests, the impinging angle was changed and relatively more mist was blocked. In these scenarios, more time was needed to extinguish the fires than that without obstructions.

4.2.4 Tests for degree of closure of the wet bench door

During manufacturing, the wet bench door is closed and opened repeatedly. When a fire occurs, the door may be open, closed, or partially open. The degree of closure of the wet bench door is a factor that likely affects extinguishing performance. Degree of door closure affects the availability of oxygen in the wet bench. During this test, the door of the wet bench was half closed and totally closed. Table 6 presents the degree of door closure and the corresponding extinguishing times under different operating pressures. Figure 4.13-4.15 shows the temperature history during the extinguishing process for degrees of door closure. Figure 4.16 shows the oxygen consumption during the extinguishing process for degrees of door closure. When the door was closed completely, heat was stored on the upper layer of wet bench, making water mist evaporate rapidly and accelerating oxygen consumption, made the fire easy to be extinguished. However, according to Table 4.10, the extinguishing times for an open door and half-closed door were not significantly different because oxygen could still freely feed the fires in these situations. However, extinguishing times decreased markedly when the door was completely closed because oxygen consumption was near the combustion limit; thus, these fires were more easily extinguished than those when the door was half closed or opened.

4.2.5 Fire spreading in a wet bench

During the series of tests, several special phenomena should be discussed. The fire spread in some fire tests. In the distribution tests, a single nozzle fixed above the pan can destabilize the flame, making it tremble, jump to another pan and ignite when operating pressure was

insufficient. Additionally, when a single nozzle was fixed at the side of the wet bench or at a distance from the center above the pan, it stretched the flame to the other side and easily ignited other fuel pan. To prevent fire spread, nozzles should be fixed above pan fire and have sufficient operating pressure, or fixed on each side of the pan to prevent flame stretching. With proper nozzle locations, fires can be suppressed in the pan and not ignite other pans nearby.

4.3 PIV Analysis

The influences of the parameters, such as discharged pressure, volumetric additive concentration and nozzle type, on the distributions of water mist diameter are discussed. By using PIV system, the images of water mist particle were captured. With appropriate conversion, the pixel occupied by the droplet image could be transformed into real size, and SMD for three different detection points were calculated. In addition, the water mist density distribution and spray coverage were also investigated. By experimental measurements and digital image processing, the study provides the more detailed descriptions under different operating pressures.

4.3.1 Experimental Apparatus Settings

The key point to capture a well-shot picture is the corporation of fast speed shutter, sufficient light source and proper ISO value, whose specifications are listed in Table 4.11.

In order to capture the target in high speed motion, the interval between shutters on/off should be short enough to make it “frozen” in

the picture. Therefore the shutter is always locked on 1/4000 sec.. During photographing, the camera only can snap object with reflection light. In ideal condition, the laser generator operates with a power of 2KW. But in real operation, the machine shuts off automatically if the output power exceeds 1.4KW. In addition, the output power decreases while operating for a long time. Therefore, the operating power for laser from 1.0KW to 1.3KW is chosen in whole experiments. The ISO value offers the light sensibility of a negative in traditional camera, and corresponds to the exposure basis for digital camera. Generally speaking, high ISO value means that the camera operates with less exposure light and fast shutter during photographing. However, increasing ISO value enhances the noises, which produce RGB particles in whole picture. These noises seriously lower the image quality and make digital image hard to process. If photograph is in low ISO value, the image quality is quite well, but such operation condition is limited for shutter speed. Once the shutter speed is over-fast, the image cannot get sufficient exposure light to reveal itself. To compromise such dilemma, the ISO value is chosen for 800.

4.3.2 SMD with Different Pressures

The tests with nozzle FP-25 were performed at three specified locations away from the center axis of the water mist nozzle for 0.203D, 0.353D and 0.456D according to UL 2167, in which D means the spray coverage diameter at the horizontal surface 1-meter under the nozzle. The operation pressure varies from 10 (low pressure), 20, 30~40 (medium pressure) to 50 (high pressure) Kg/cm^2.

The resultant average diameters and SMDs as a function of

pressure at different locations are summarized in Table 4.12. In this table, average diameter $\overline{D}$, determined by arithematic average of all droplets' diameters in the image, provides rough information about the water mist diameter distribution. SMD for a given droplet distribution is presented as

$$\text{SMD}= D_{32} = \frac{D_{30}^3}{D_{20}^2} \tag{4.1}$$

where D_{30} is the volume mean diameter and D_{20} the surface area mean diameter. D_{30} is defined for a discrete distribution as

$$D_{30} = \left[\frac{\sum N_i D_i^3}{\sum N_i}\right]^{1/3} \tag{4.2}$$

where N_i is the number of droplets in a class and D_i is the middle diameter of its size range.

Analogous to D_{30}, D_{20} is defined as

$$D_{20} = \left[\frac{\sum N_i D_i^2}{\sum N_i}\right]^{1/2} \tag{4.3}$$

By combining volume mean diameter and surface area mean diameter, the SMD can be obtained. The calculation method was invented in the late 1920 by German scientist, J. Sauter. The related processes of calculation for SMD can be referred to ASTM 799 92 regulation.

4.3.2.1 Diameter measurements with Location X=23cm

The diameter measurements with Location X=23cm in Table 4.12 show that the measured mean diameter and SMD increase with an increase of pressure. The trends of diameter variation are also presented in Figs. 4.17 and 4.18.

In general, the droplet size (represented by $\overline{D}$ or SMD) should be decreased with an increase of working pressure in atomization. However, trend is reversed at this location. Due to fast velocity of

droplet, the images showed the phenomena of particle dragging in the air. So these particle images are not pure circular but closer to short line. From Table 4.12, it can imply that the increase SMD with pressure is due to the increasing amount of large dragging particles. In Fig 4.19, the cumulative % of volume curve shifts to right as pressure increases, meaning that the amount of large particles to total one's number ratio in the images became larger. The lack of data for pressure 40 and 50 kg/cm_2 is because the water mists are too thick to be sparked by laser sheet. Without sufficient light, the camera cannot catch clear image to analyze.

4.3.2.2 Diameter Detection with Location X=40cm

For pressure 10 kg/cm^2, the SMD is 614μm, and its value diminishes by a quantity of 20~30μm in each pressure interval. However, the SMD drops dramatically at P=50 kg/cm^2, whose SMD is half the one at P=10 kg/cm^2. The result shows that the degree of atomization is best at P=50 kg/cm^2.

All calculations for the measured data follows the ASTM 799-92 regulation, and they are presented in Appendix A. From P=10 to P=40 kg/cm^2, there exist few large particles, which are almost close to 1000μm. In the condition P=50 kg/cm^2, all particles are smaller than 450μm, and most of them are under 350μm. Looking at Fig. 4.20, the cumulative ratio curves show that the droplet sizes from P=10 to P=40 kg/cm^2 can be classified as Class 3 ($400\mu m<D_{v0.99}<1000\mu m$), and the one with P=50 kg/cm^2 is classified as Class 2 ($200\mu m<D_{v0.99}<400\mu m$).

4.3.2.3 Diameter Detection with Location X=52cm

In this location, average diameter diminishes with pressure, but

the variation of SMD shows a different trend. At first, SMD decreases from 695 to 685 μm as pressure increases from 10 to 20 kg/cm^2, then, it reaches a peak value, 729 μm, at p=30 kg/cm^2, and finally decreases from 688 to 677 μm from p= 40 to p=50 kg/cm^2. Following NFPA 750 standard form in Fig. 4.21, the cumulative curve shifts to the most right side at p=30 kg/cm^2, indicating that the ratio of larger droplet numbers at each level increases. In fact, even there exist few droplets greater than 1000 μm. These unusual patterns are because the camera cannot catch "frozen" pictures due to the fast moving droplets.

For the macroscopic viewpoint, the average diameter and SMD should be diminished with increasing pressure. Under the same operating pressure with different positions away from nozzle, SMD shows crescent trend toward outside. For example, SMD is 334 μm at the inner position X=23cm at p=20 kg/cm^2, while it is 689μm at outer position X=52cm. At the middle position X=40cm, SMD is 605μm, which is in-between the two values mentioned above. From above discussion, it can conclude that although all inner and outer orifices of FP-25 nozzle have the same diameters, they generate various SMDs for droplets at different locations. This means that the pressure distribution inside the nozzle is not uniform. The different pressures on the inner and outer orifices lead to the distinct SMD distributions for location X=23cm and X=52cm. The SMD value at location X=40 cm is between those at X=23 and 52cm. It is suggested that the water mist in this location is a combination of the ones from inner and outer orifices.

4.3.3 SMD with Different Volumetric Additive

The distributions of droplet diameters are presented in Table 4.13.

The data are collected at the position X=40cm under p=20 kg/cm^2. The influence of diferent volumetric concentration of addtion on droplet size distribution shows an interesting result. The curve appears as “W” shape, Fig.4.22. The droplet diameter (SMD) shrinks at 3% concentration of additives, then at 6% concentration it expands larger than the one in non-additive water mist, and shrinks again at 10% concentration. As mentioned before, the additive contains surfactant, mint, champor, citric acid, borax and salt. Surfactant and borax have positive effect on the atomization by decreasing the surface tension. On the other hand, organic metal compound (salt) has adverse effect for atomization by increasing the surface tension. In addition, the chemical reaction occurring between borax and citric acid and its products also influence the degree of atomization. These coupling effects lead to the variation of droplet diameter. The SMD changed from 614, 416, 666 to 428 μm for additive concentration of 0%,3%, 6% and 10%, relatively.

In the previous experiments, the fire extinction time for two organic fuels, heptane and gasoline were measured. Figs. 4.23 and 4.24 show the extinction time with different volumetric additive concentrations. For heptane, the extinction time is 18 seconds for 3% and 10% concentration additive, and the extinction time is 28 seconds for 6%. For gasoline, the extinction time for 3%, 6% and 10% concentration are 9, 15 and 9seconds, respectively. The trend of extinction time is highly agreed with the one of SMD in this study. In 3% and 10% additives, SMDs are smaller than that of non-additive water mist and they have similar size. The extinction times also have the same value. In 6% additive, the SMD becomes larger, but the extinction

time is decreased.

The related additive studies [26~28] investigated the fire extinguishing mechanisms, which included physical and chemical aspects. In the aspect of physics, organic metal compound and other decomposable materials increase the boiling point of water mist and make it hard to evaporate. On the other hand, the coupling effect made by Nacl and surfactant has a changing effect on the atomization of water mist. In the aspect of chemistry, Nacl produces active radicals, Na^+ and Cl^-, to capture the free radicals H, O, and OH to suppress the chain-reaction in the burning procedure. Once the chain-reaction is suppressed, the burning rate will decrease to weaken the flame. The surface tension for 3%, 6% and 10% concentration are 18, 17.2 and 17 dyne/cm, respectively.

Table 4.14 lists all the effects occurred after adding additives. For 6% additive, the SMD of water mist is larger than the non-additive one, and the BP (boiling point) is higher also. Therefore, water mist is hard to evaporate and it decreases the ability of extinguishing fire. However, the chemical reaction induced by Nacl decreases the burning rate. The influence by chemical reaction is greater than the ones by SMD and BP, therefore, the extinction time becomes shorter. For 3% and 10% concentration additives, they have similar extinction time. Despite it shows a better performance of chemical fire extinguishing in 10% additive, the extinction time is 8 seconds longer than that of 3% additive. Therefore, it can conclude that the main factor to control the extinction time is SMD.

4.3.4 Water Mist Density Distribution

Water mist momentum, coverage and flow rate are the three major factors for extinguishing fire. The first one is related to water mist velocity and size, and the last two are related to water mist density distribution. In this section, the study measured the variation of water mist density and spray coverage among in different pressures.

4.3.4.1 Density Distribution by Experiment

Fig. 4.14 is the density distribution of Fp-25 nozzle at p= 50Kg/cm^2. The location of nozzle is at (15, 15). Water mist density decreases as the acquisition point is moving away from the nozzle. It should be noticed that water amount around the nozzle is 4 times higher than those away from the center. In fact, the behavior of water mist is quite different from water droplets from sprinklers. Because it is a multi-phase fluid, the mist does not spray along a straight line like water droplets do. For the tubes away from the center (15, 15), water mist does not enter the tube directly but attach on the tube walls. When the globs attached on the wall become large, they fall down to the tube bottom. The mist can directly enter into the tubes near the center. In addition, some amount of water mists drift and evaporate in the air before they reach the tube. The cumulative amount of water in the tubes is 0.773ml/min, and the theoretical flow rate for FP-25 nozzle at p= 50Kg/cm^2 is 7.990ml/min. The tubes only collect less than 10 % of the total amount of water. Therefore, it is only to get a rough situation for water mist density distribution by experiment.

4.3.4.2 Density Distribution by Measuring Grey Level

Water mist has the ability of reflecting light automatically. And if there is more water mist gathered in some place, the reflection light

becomes stronger. In this aspect, the study analyzes the grey level distribution of images which are shut with different pressures.

4.3.4.3 FP-25 Nozzle

From Figs. 4.26 to 4.35, real pictures and their relative grey level distribution images are presented. For p=10 Kg/cm^2, spouts from 21 orifices can be distinguished, and the gray levels have high values for those 21 points. It means that water density is also high at these points. From p=20 to p=50 Kg/cm^2, spouts are spread out and the spray coverage of each spouts are overlapped. The shape of image seems to be an octopus stretching its tentacle. The degree of overlapping arises when the pressure increases. Comparing the grey level images from p=30 to p=50 Kg/cm^2, the total spray coverage shrinks and the total grey level value increases. The water mist droplets become smaller when the discharged pressure increases, therefore the ones suffer more air resistance during the way between nozzle and the detection plane. Some droplets could drift away because of the air flow field. These results find a dilemma when using water mist to extinguish fires. The higher water mist density promotes the performance of fire extinguishing, but if the spray coverage shrinks too much to cover the flame, it is hard to suppress the flame. Figs 4.36 to 4.40 are the pictures of the spray angles at respective pressure. All spray angles are almost 60 degree except the one at p=10 Kg/cm^2. Despite the spray angle fixed, the base width of the triangular shape decreases with pressure. The results fit the measurements for gray level distributions.

CHAPTER 5

CONCLUSIONS

In the experiments of portable water mist system, the effects of discharge methodologies on the pool fire extinguishment performance of portable high pressure water mist extinguishing system with additive and the corresponding mechanisms of restraining fire are studied. The additive added in water mist is neither toxic nor corrosive. All the tests are regarded as fuel-controlled. The test parameters include the fuel type, nozzle discharge angle, additive solution volume, amount of fuel, and cross-section area of pan. The fuels used are heptane, gasoline, and diesel, the nozzle discharge angles are 30°, 45°, and 60° with respect to the horizon, and the additive solution volumes are 0%, 3%, 6% and 10%. For all types of pool fires, the test results by using pure water mist show that the flame cooling and oxygen-displacement play the important roles in the higher nozzle discharge angle regime (>45°). In the lower one (<45°), the blocking and dilution of fuel vapors at interface are the dominant factors. Besides, the water mist system has a good ability for radiation attenuation and temperature reduction that can provide a good protection for the operators, who are using portable extinguishing equipment.

For the tests with different fuels, the fire extinguishing behaviors of diesel are different from the ones of heptane and gasoline. For diesel fires, the fire extinguishing efficiencies using the water mist with additive at three nozzle discharge angles are all significantly improved

comparing with those using pure water. However, if too much additive is provided, the fire extinguishment efficiency will decrease. For heptane and gasoline fires, the performance of fire suppression with 3% additive solution volume is similar to those with pure water, and for the 6% and 10% additive ones, the lower the nozzle discharge angle is, the more the extinguishing time spends since there is less mist being able to reach the fuel surface.

In this wet bench fire experiments, several parameters were examined in wet bench fires. In the single nozzle tests with different pan sizes, water mist extinguished the small pan fire easier than large pan fires. In the nozzle distribution tests, the area covered by the water mist and mist momentum played important roles. The closer the water mist to the center of pan (raised the coverage), the easier the fire can be extinguished. With sufficient coverage, a critical operating pressure exists. Above that pressure, fires were easily extinguished. The critical pressure should be used when designing a water mist system, as insufficient pressure can increase the opportunity of a fire spreading through fuel spread. In this study, the number of the nozzles used also affected the ability of water mist to extinguish a fire. When two nozzles were fixed on either side of the pan, efficiency extinguishing a fire was better than that with a single nozzle. During the obstruction test, there was little difference in extinction time when one cylinder was located on one side or two cylinders were placed on either side of the pan. Additionally, the degree to which the wet bench door was closed markedly affected extinguishing performance of the wet bench fire. We suggest that the door to a wet bench or ventilation should be closed

during a wet bench fire. This study identified several issues germane to preventing fire spreading out during wet bench fires. Low operating pressure, unsuitable location of nozzles and improper discharge angle can make fires to spread in a wet bench. An appropriate design with sufficient operating pressure and locations of water mist nozzles can extinguish wet bench fires effectively in early fire stages.

In the particle image processing, SMD and water mist density distribution were investigated with three parameters, discharge pressure, volumetric additive concentration and nozzle type. By using PIV, all experimental pictures were caught in three acquisition locations, 23 cm, 40cm and 52cm away from the nozzle respectively.

The study indicated that SMD shrunk as discharged pressure increased. With different concentration of additive, the “W” shape curve for SMD variation gave explanations for the extinction time mentioned in the previous thesis. The result showed that the major factor for the performance of fire extinguishing was SMD and the minor one was chemical reaction by organic metal compound.

REFERENCE

[1] NFPA 750, “Standard for the Installation of Water Mist Fire Protection Systems”, 2000 Edition, National Fire Protection Association, Quincy, MA, 2000.

[2] Teresa Parra, Francisco Castro, Cesar Mendez, Jose M. Villafruela and Miguel A. Rodriguez, “Extinction of Premixed Methane–Air Flames by Water Mist”, Fire Safety Journal, Vol. 39, pp. 581-600, 2004.

[3] Braidech, M.M., Neale, J.A., Matson, A.F. and Dufour, R.E. “The Mechanisms of Extinguishment of Fire by Finely Divided Water”, Underwriters Laboratories Inc. for the National Board of Fire Underwriters, NY, 73P, 1955.

[4] Mawhinney, J.R., Dlugogorski, B.Z. and Kim, A.K. “A Closer Look at the Fire Extinguishing Properties of Water Mist”, Fire Safety Science-Proceedings of Fourth International Symposium, Ottawa, ON, pp. 47,1994.

[5] Wighus, R., “Extinguishment of Enclosed Gas Fires with Water Spray”, Proceeding of the Third International Symposium of Fire Safety Science, 1991.

[6] FM Global Loss Prevention Data Sheet 7-7, 2003, Semiconductor Fabrication Facilities.

[7]G. Grant, J. Brenton, and D. Drysdale, “Fire Suppression by Water Sprays”, Progress in Energy and Combustion Science, Vol. 26, pp. 79-130, 2000.

[8] Mawhinney and Solomon, “Water Mist Fire Suppression Systems”,

Fire protection handbook, 18th ed., sect. 6, chap. 15, pp. 6/216-6/248, 1997.

[9] A. Jones and P. F. Nolan, “Discussion on the Use of Fine Water Sprays or Mists for Fire Suppression”, J. Loss Prev. Process Ind., Vol. 8 Number 1, pp. 17-22, 1995.

[10] Bin Yao, Weicheng Fan, and Guangxuan Liao, “Interaction of Water Mists with a Diffusion Flame in a Confined Space”, Fire Safety Journal, Vol. 33, pp. 129-139, 199.

[11] Zhigang Liu, Andrew K. Kim, and Don Carpenter, “Portable Water Mist Fire Extinguishers as an Alternative for Halon 1211”, Halon Options Technical Working Conference, pp. 435-439, April 24-26 2001.

[12] Zhigang Liu, Andrew K. Kim and Don Carpenter, “A Portable Water Mist Fire Extinguisher for Multi-Purpose Applications”, Workshop on Fire Suppression Technologies, Mobile, AL., pp. 1-3, Feb. 24-27 2003.

[13] Zhigang Liu, Andrew K. Kim and Don Carpenter, “A Study of Portable Water Mist Fire Extinguishers Used for Extinguishment of Multiple Fire Types”, Fire Safety Journal, Vol. 42, pp. 25-42, 2007.

[14] Zhou Xiaomeng, Liao Guangxuan, and Cai Bo, “Improvement of Water Mist’s Fire-Extinguishing Efficiency with MC Additive”, Fire Safety Journal, Vol. 41, pp. 39-45, 2006.

[15] Bei-Hua Cong, Tao Mao, Guang-Xuan Liao, “Experimental Investigation on Fire Suppression Effectiveness for Pool Fires by Water mist Containing Sodium Chloride Additive”, Journal of Thermal Science and Technology, Vol. 3 No.1, 2004.

[16] Guang-Xuan Liao, Bei-Hua Cong, Kai-Qian Kuang, “Experiment Study on The Fire Suppression Effectiveness of Water Mist with Iron Compounds Additives.”, Journal of Engineering Thermophysics, Vol. 26, 2005.

[17] Yi-Liang Shu, Wei-Jin Jeng, Chen-Wei Chiu, and Chiun-Hsun Chen, “Assessment of Fire Protection Performance of Water Mist Applied in Exhaust Ducts for Semiconductor Fabrication Process”, Fire Mater, Vol. 29, pp. 295-302, 2005.

[18] Fisher, L.F, Williamson, R.B, Toms, G.L, and Grinnion, D.M, Fire protection of flammable work stations in the cleanroom environment of a microelectronic fabrication facility. Fire Technology, Vol. 22, NO.2, May 1986.

[19] Wu, P.K, Chaffee, J, and Knaggs, B, 1995, A wet bench free-burn test under FMRC fire products collector, Factory Mutual Research Corporation, Norwood, MA.

[20] Wu, P.K, Taylor, J, and Harriman, R.B, 1996, Wet bench fire suppression with fine water sprays, Factory Mutual Research Corporation, Norwood, MA, October.

[21] Mawhinney and Solomon, Water Mist Fire Suppression Systems, Fire protection handbook, 18th ed, sect. 6, chap. 15, pp. 6/216-6/248, 1997.

[22] Adrian J. T., “Particle Imaging Techniques for Experimental Fluid Mechanics”, Annu. Rev. Fluid Mech, Vol. 23, pp. 261-304, 1991.

[23] Gonzalez, Woods, “Digital Image Processing”, Prentice Hall, 2002.

[24] Cary Presser, George Papadopoulos, John F. Widmann, “PIV Measurements of Water Mist Transport in a Homogeneous

Turbulent Flow past an Obstacle", Fire Safety Journal, Vol. 41, pp. 580-604, 2006.

[25] Brain T. Fisher, Andrew R. Awtry, Ronald . S. Sheinson, James W Fleming, "Flow Behavior Impact on The Suppression Effectiveness of Sub-10-μm Water Drops in Propane/air Co-flow Non-premixed Flames", Proceedings of The Combustion Institute, Vol. 31, pp 2731-2739, 2007.

[26] Beu-Hua Cong, Xiao-meng Zhou, Guang-xuan Liao, "Improment of Water Mist Fire Suppression Performance with Compositive Additives.", Journal of University of Science and Technology of China, Vil. 36 No. 1, 2006.

[27] "Kitchen Ventilation", ASHRAE Applications Handbook, Chapter 30, 1999.

[28] Adrian J. T., "Particle Imaging Techniques for Experimental Fluid Mechanics", Annu. Rev. Fluid Mech, Vol. 23, pp. 261-304, 1991.

Table 2.1 The properties of fuels

Properties	Fuel types		
	Heptane	Gasoline	Diesel
Boiling point (°C)	98	30~210	163~357
Density (kg/m^3)	675	720~760	876
Flash point (°C)	-4	-43~-38	>52
Auto-ignition point (°C)	104	280~456	103
Lower Explosive Limit (%)	1.07	1.2~1.4	1.3
Vapor Pressure (mmHg)	40	259~777	2
Heat of combustion (MJ/kg)	44.6	47	42.4

Table 2.2 The volume flow rates of mist in different additive solution volumes (L/min)

Additive solution volume	0%	3%	6%	10%
Volume flow rate	8.8	9.0	9.0	8.8

Table 3.1 The table of experimental repeatability (a) Pure water tests with different fuel types in 25cm diameter of the pan (b) Water mist with additive in 50cm diameter of the pan with heptane fires

(a)

Nozzle discharge angle	The extinction time for Heptane (s)				
	1st	2nd	3rd	Average	C.V.
60°	76	88	80	81	6.13%
45°	111	100	105	105	4.33%
30°	79	79	77	78	1.20%

Nozzle discharge angle	The extinction time for Gasoline (s)				
	1st	2nd	3rd	Average	C.V.
60°	90	87	91	89	1.90%
45°	156*	152*	152*	153*	1.23%
30°	97	113	112	107	6.82%

Nozzle discharge angle	The extinction time for Diesel (s)				
	1st	2nd	3rd	Average	C.V.
60°	8	7	7	7	6.43%
45°	56	52	55	54	3.13%
30°	64	64	58	62	4.56%

(b)

Nozzle discharge angle	The extinction time for water mist with 0% additive (s)				
	1st	2nd	3rd	Average	C.V.
60°	114	108	110	111	2.25%
45°	84	74	78	78	3.69%
30°	47	47	55	50	7.54%

Nozzle discharge angle	The extinction time for water mist with 3% additive (s)				
	1st	2nd	3rd	Average	C.V.
60°	18	18	17	18	2.67%
45°	35	37	35	36	2.64%
30°	50	47	51	49	3.45%

Nozzle discharge angle	The extinction time for water mist with 6% additive (s)				
	1st	2nd	3rd	Average	C.V.
60°	25	25	23	24	3.87%
45°	43	39	42	41	4.11%
30°	23	27	23	24	7.75%

Nozzle discharge angle	The extinction time for water mist with 10% additive (s)				
	1st	2nd	3rd	Average	C.V.
60°	23	22	24	23	3.55%
45°	45	47	50	47	4.34%
30°	25	22	24	24	5.27%

Table 4.1 The summary of parametric studies

Variables	Range
Fuel types	Heptane, Gasoline, Diesel
Additive solution volume	0%, 3%, 6% and 10%
Nozzle discharge angle	30°, 45° and 30°
Amount of fuel (*ml*)	250, 500 and 1000
Diameter of the pan (*cm*)	25 and 50

Table 4.2 Nozzle discharge angle and corresponding extinction time(sec) without additive

Pure Water without Additive			
Fuel type / Discharge angle	Diesel	Gasoline	Heptane
60°	8	89	82
45°	54	154	106
30°	59	106	79

(Diameter of pan: 25*cm*, Amount of fuel: 250*ml*)

Table 4.3 Corresponding extinction time(sec) of diesel fires

Diesel				
Additive / Discharge angle	0%	3%	6%	10%
60°	8	3	5	8
45°	54	9	19	10
30°	59	3	25	38

(Diameter of pan: 25*cm*, Amount of fuel: 250*ml*)

Table 4.4 Corresponding extinction time(sec) of heptane fires

Heptane				
Additive / Discharge angle	0%	3%	6%	10%
60°	81	18	28	18
45°	105	58	36	37
30°	78	17	77	79

(Diameter of pan: 25*cm*, Amount of fuel: 250*ml*)

Table 4.5 Corresponding extinction time(sec) of gasoline fires

Gasoline				
Additive / Discharge angle	0%	3%	6%	10%
60°	89	9	15	9
45°	154	26	15	14
30°	106	9	34	54

(Diameter of pan: 25*cm*, Amount of fuel: 250*ml*)

Table 4.6 Fuel Pan Size and corresponding extinction time(sec) under different operating pressure

Fuel Size Test		
Fuel Pan Size / Pressure(bar)	30×30 cm	20×20 cm
55	2	1
45	3	1
35	3	1
25	5	1
15	Fail	Fail

Fail: can not be extinguished

Table 4.7 Fuel Pan Size and corresponding extinction time(sec) under different operationing pressure and location

Fuel Size and nozzle location Test						
Fuel Pan Size	30×30 cm			20×20 cm		
nozzle location / Pressure(bar)	center	20cm	40cm	center	20cm	40cm
55	2	3	Fail	1	2	Fail
45	3	3	----	1	1	----
35	3	3	----	1	1	----
25	5	us	----	1	us	----
15	Fail	----	----	Fail		----

us: unstable condition

Fail: can not be extinguished

Table 4.8 Distruibution tests and corresponding extinction time(sec) under different operating pressure

Nozzle Distribution Tests (Two nozzles)		
Nozzle Distance / Pressure(bar)	40cm (20cm to pan center)	80cm (40cm to pan center)
55	1	1
45	1	Fail
35	3	----
25	5	----

Fail: can not be extinguished

Table 4.9 Extinguishing time of obstruction tests under different operating pressure

Obstruction Tests (Two nozzles)						
Nozzle distance	40cm			80cm		
Obstruction number / Pressure(bar)	0	1	2	0	1	2
55	1	1	1	1	3	3
45	1	1	1	Fail	Fail	Fail
35	3	3	2	----	----	----
25	5	3	**2**	----	----	----

Fail: can not be extinguished

Table 4.10 Door closure degree and corresponding extinction time(sec) under different operating pressure

Door Closure Test												
Nozzle Distance	20cm						40cm					
Closure Degree	open		Half closed		Totally closed		open		Half closed		Totally closed	
Nozzle No. / Pressure (bar)	1	2	1	2	1	2	1	2	1	2	1	2
55	2	1	2	1	1	1	Fail	1	Fail	1	2	1
45	1	1	4	1	1	1		Fail	----	3	2	1
35	1	3	9	1	2	1			----	3	6	1
25	us	**5**	us	1	2.6	1			----	us	us	1

*us: unstable condition

Fail: can not be extinguished

Table 4.11 Values for experimental apparatus

Shutter	1/4000 sec.
Power of source	1.0~1.3 KW
ISO value	800

Table 4.12 $\bar{D}$ and SMD distribution for Fp-25 nozzle.

Location / Pressure	23cm		40cm		52cm	
	$\bar{D}$	SMD	$\bar{D}$	SMD	$\bar{D}$	SMD
10 Kg/cm^2	183.428	293.712	310.450	614.253	403.665	695.733
20 Kg/cm^2	193.425	334.469	283.934	605.630	389.831	689.577
30 Kg/cm^2	226.669	415.258	259.687	561.322	357.293	729.633
40 Kg/cm^2			261.613	528.015	346.185	688.038
50 Kg/cm^2			144.061	277.919	328.867	677.699

Unit: μm

Table4.13 $\overline{D}$ and SMD distributions with different additive concentrations

Diameter / Concentration	$\overline{D}$ (μm)	SMD(μm)
0 %	310.4506	614.2528
3 %	206.3024	416.3930
6 %	331.5068	666.7141
10 %[2]	258.1685	428.1706

Unit: μm

Table 4.14 Effects for different additive concentration

Additive Concentration	SMD (μm)	Boiling Point	The ability to capture free radicals
3%	416	Low	Low
6%	666	Middle	Middle
10%	428	High	High

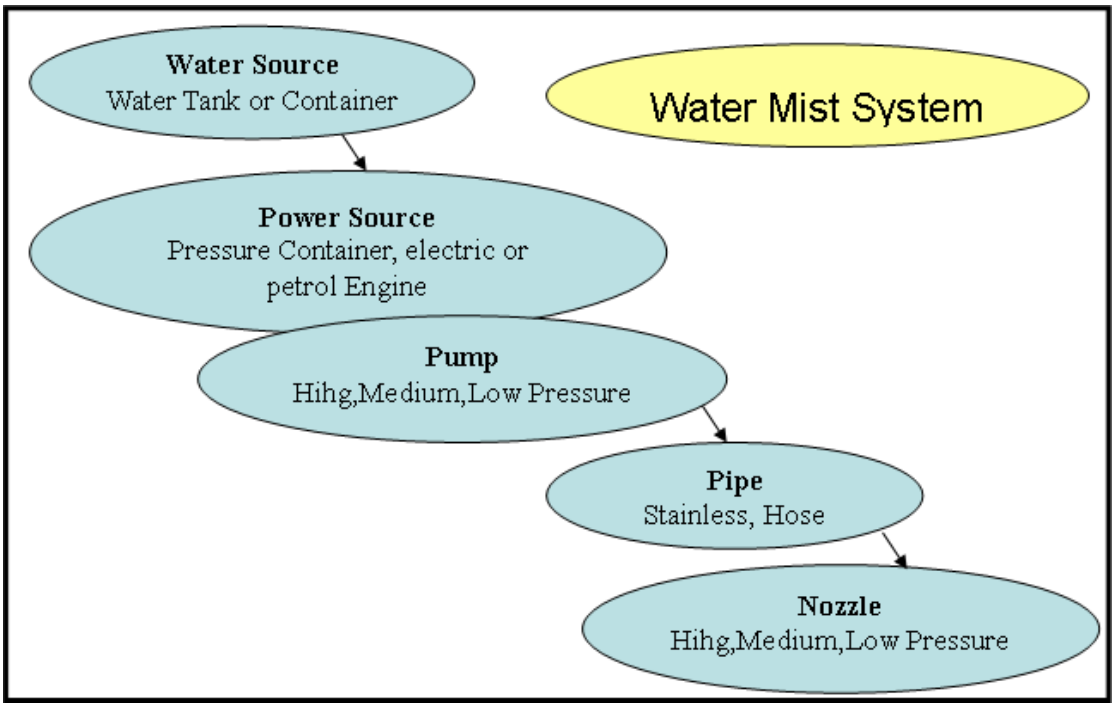

Fig. 1.1. Operational units of water mist system

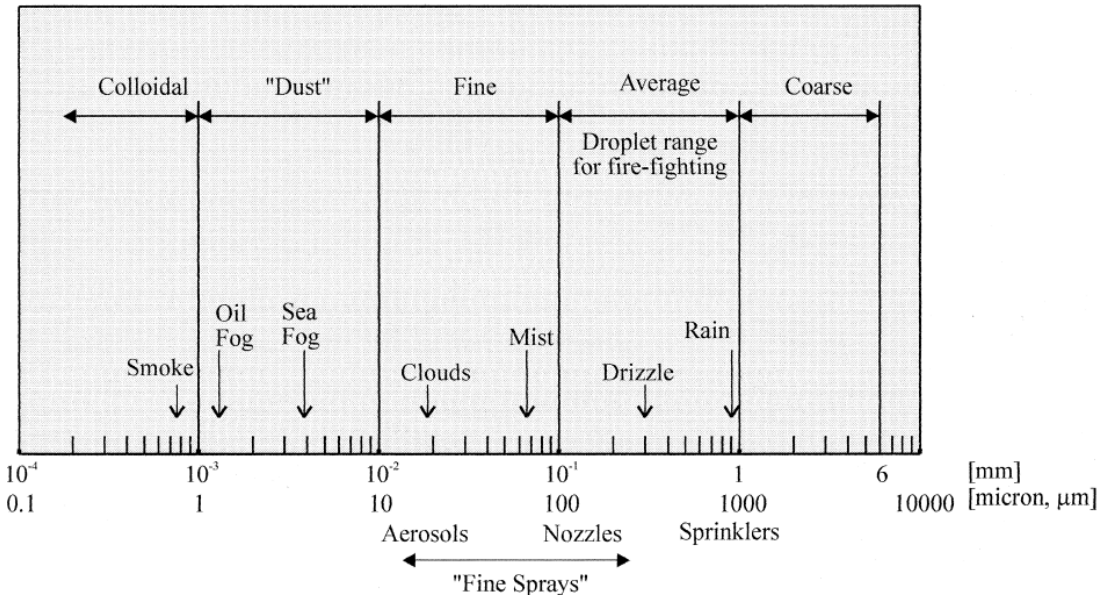

Fig. 1.2. Spectrum of droplet diameters, reproduced from Ref. [7]

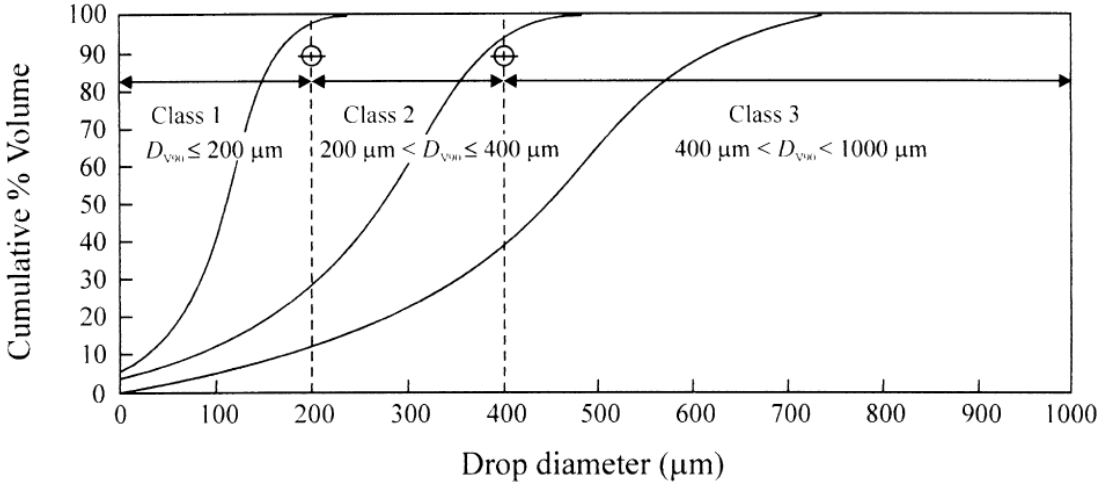

Fig. 1.3. Droplet diameters, reproduced from Ref. [8]

Fig. 1.4. Schematic of the Thesis

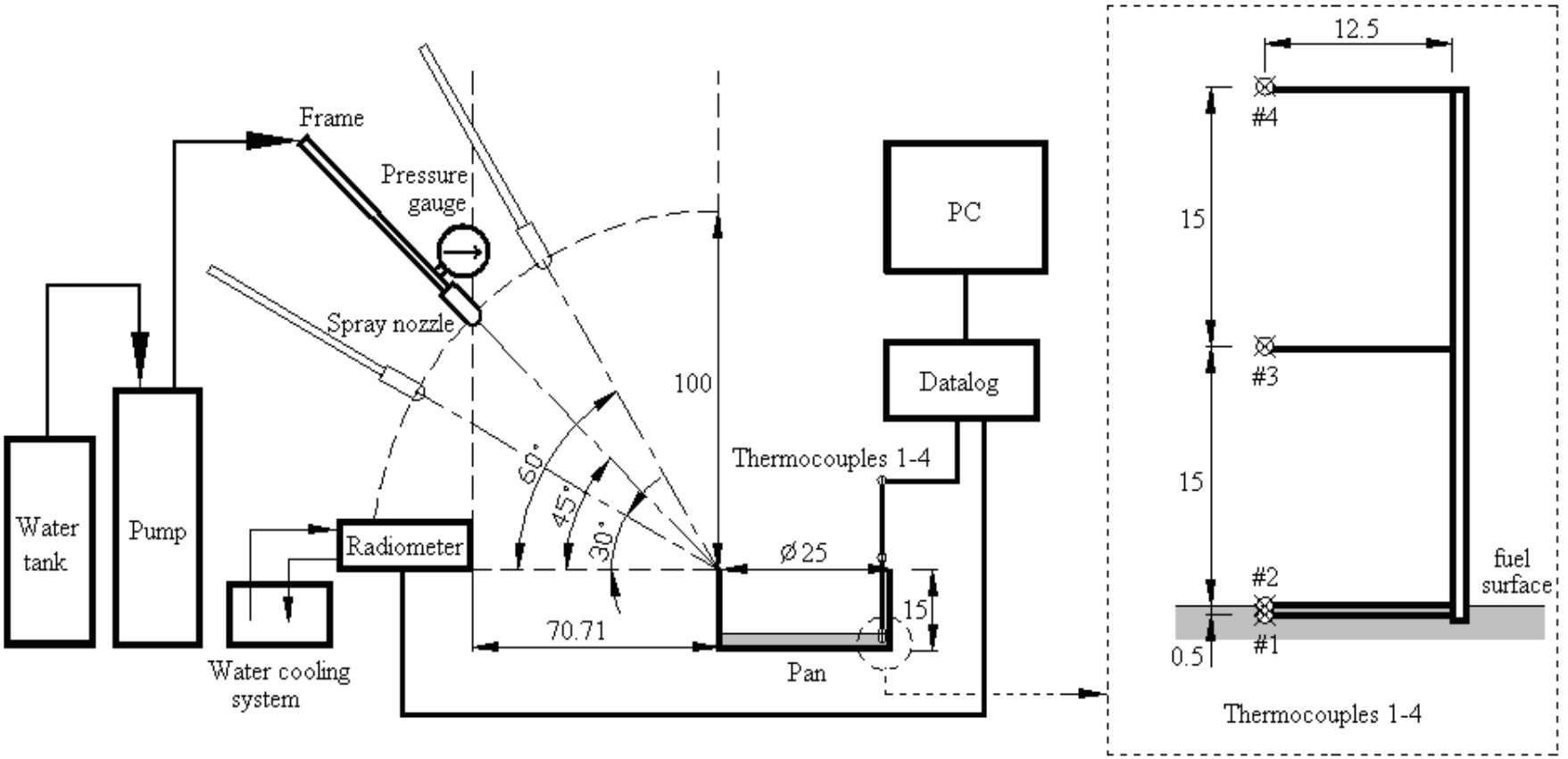

Fig. 2.1 The schematic configuration of the experimental apparatus (dimensions are in centimeters)

Fig.2.1The schematic of experiment

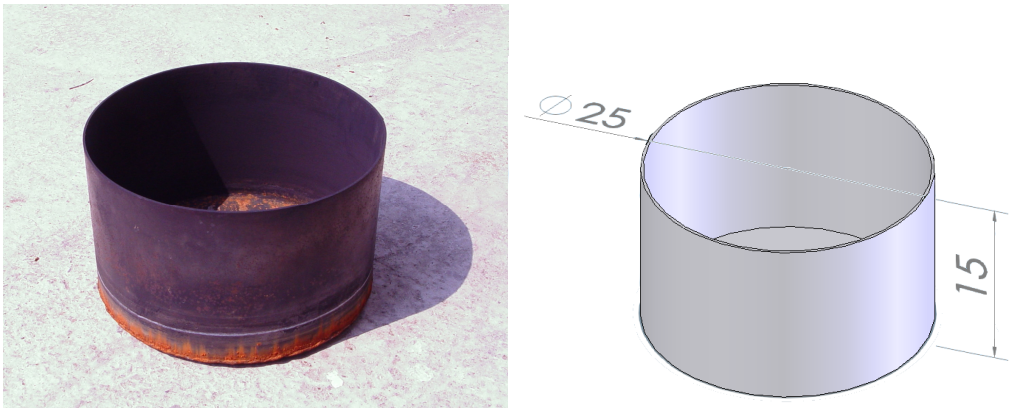

(a)

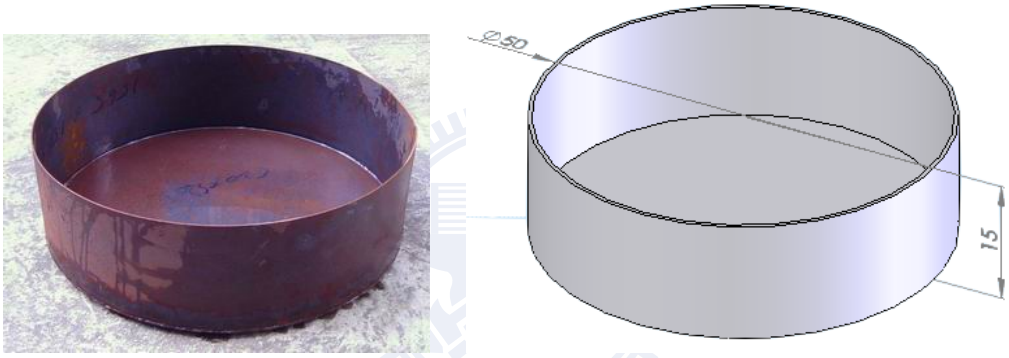

(b)

Fig. 2.2 The picture and schematic configuration of the circular stainless pan (a) small-scale (b) middle-scale (dimensions are in centimeters)

Fig. 2.3 The picture of high pressure pump

(a)

(b)

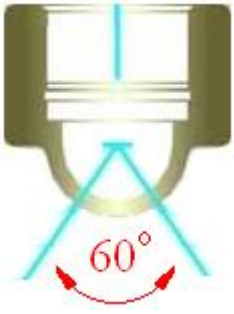

(c)

Fig. 2.4 The picture of high pressure system nozzle (a) Front view (b) Side view (c) Spray angle

Fig. 2.5. The picture of thermocouple tree

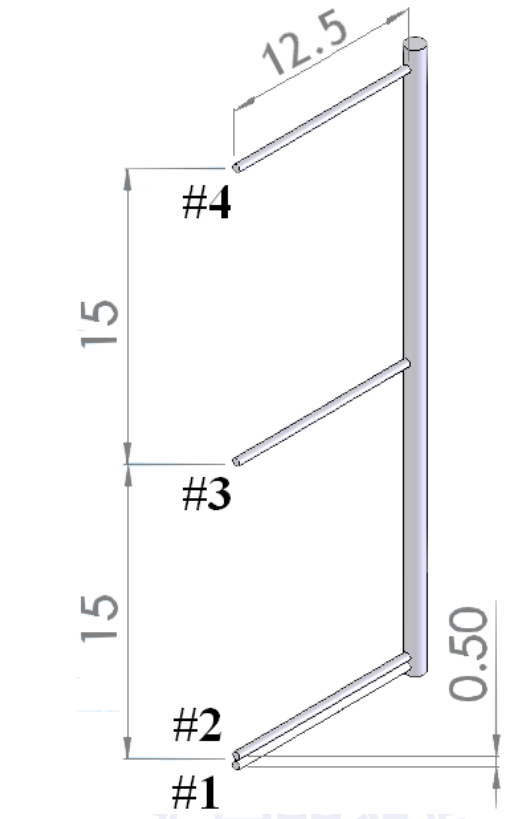

(a)

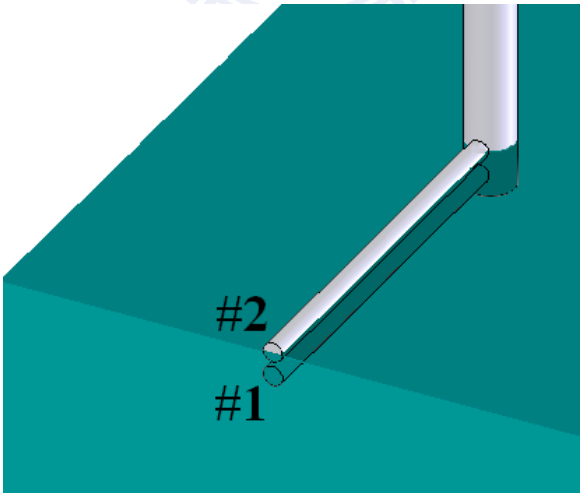

(b)

Fig. 2.6 The schematic configuration of the thermocouple tree Whole view and (b) Local view (dimensions are in centimeters)

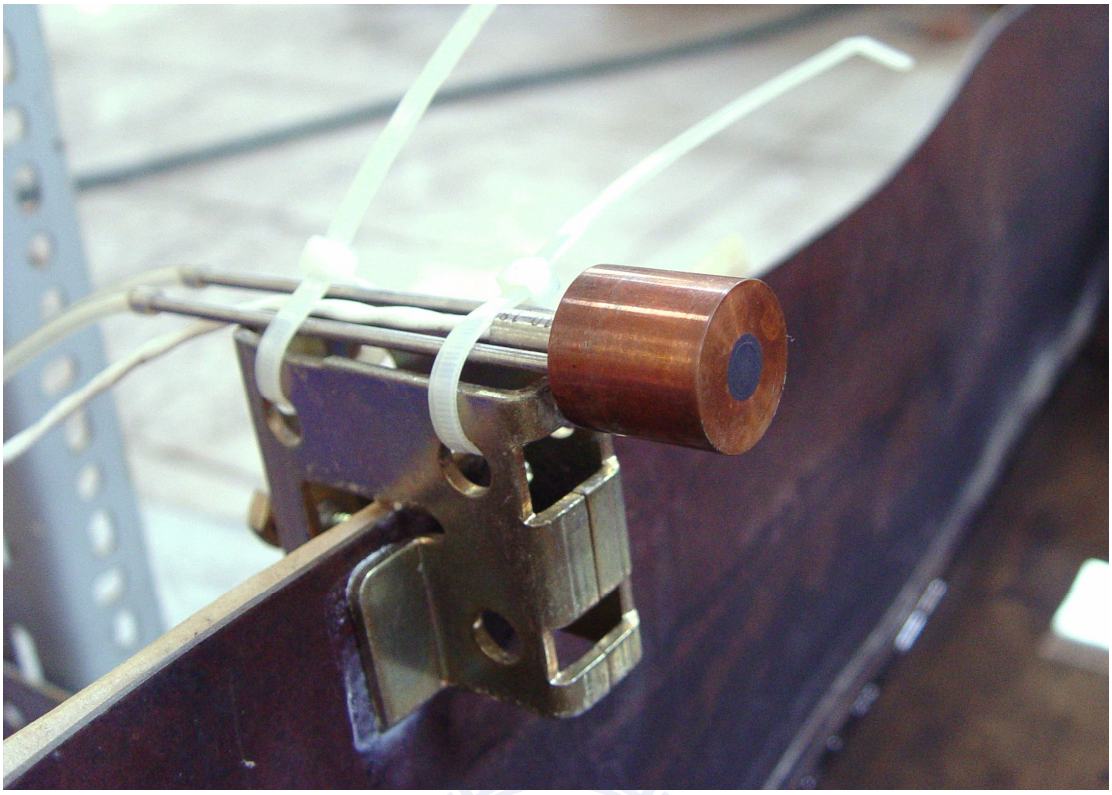

(a)

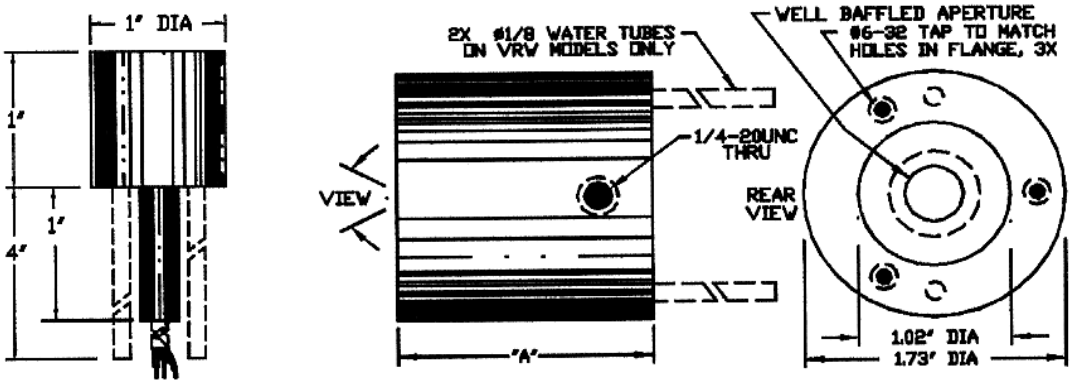

(b)

Fig. 2.7 The radiometer (a) The picture and (b) The schematic configuration

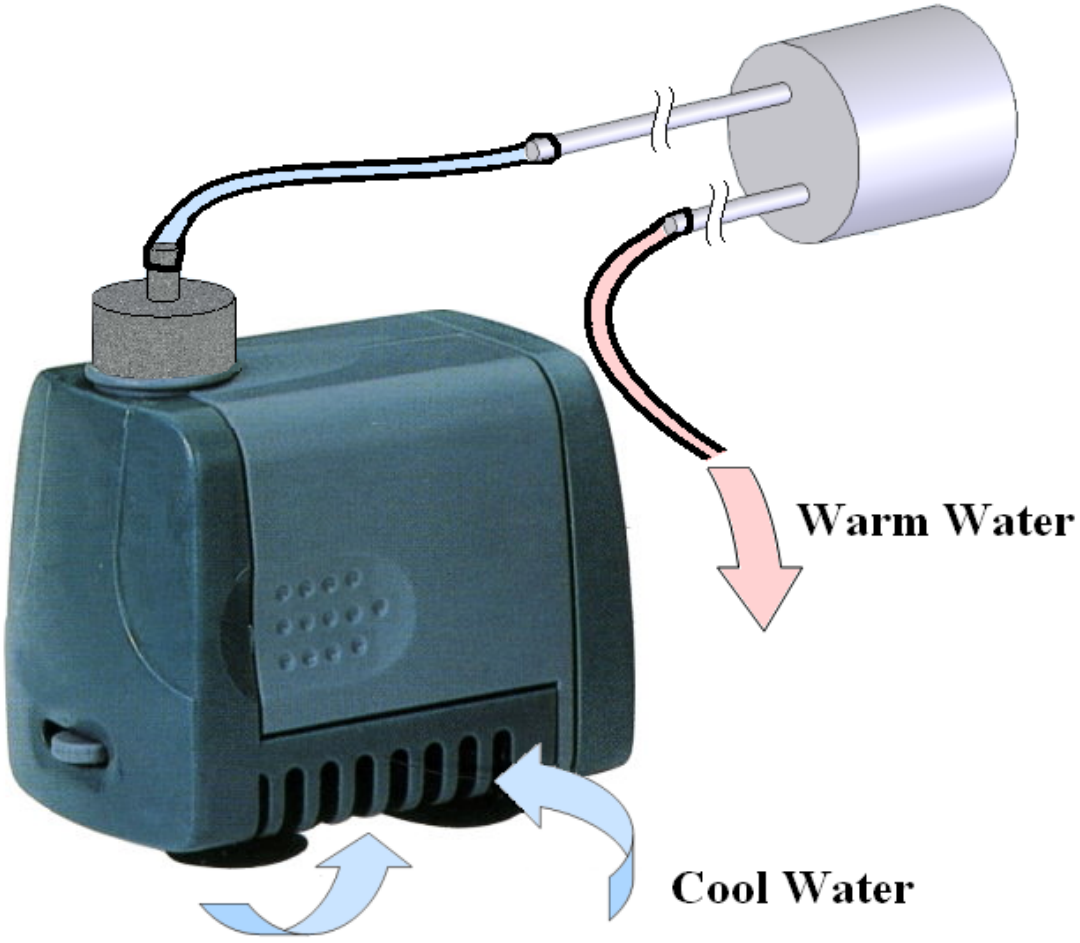

Fig. 2.8 The schematic configuration of the water-cooling system

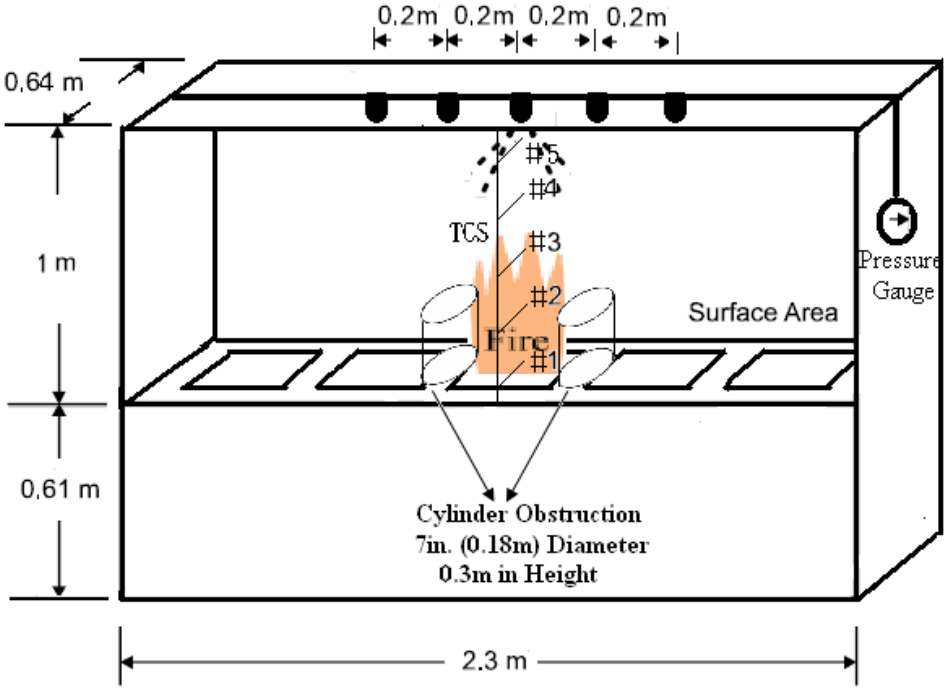

Fig. 2.9. Experiment layout of wet bench fire tests

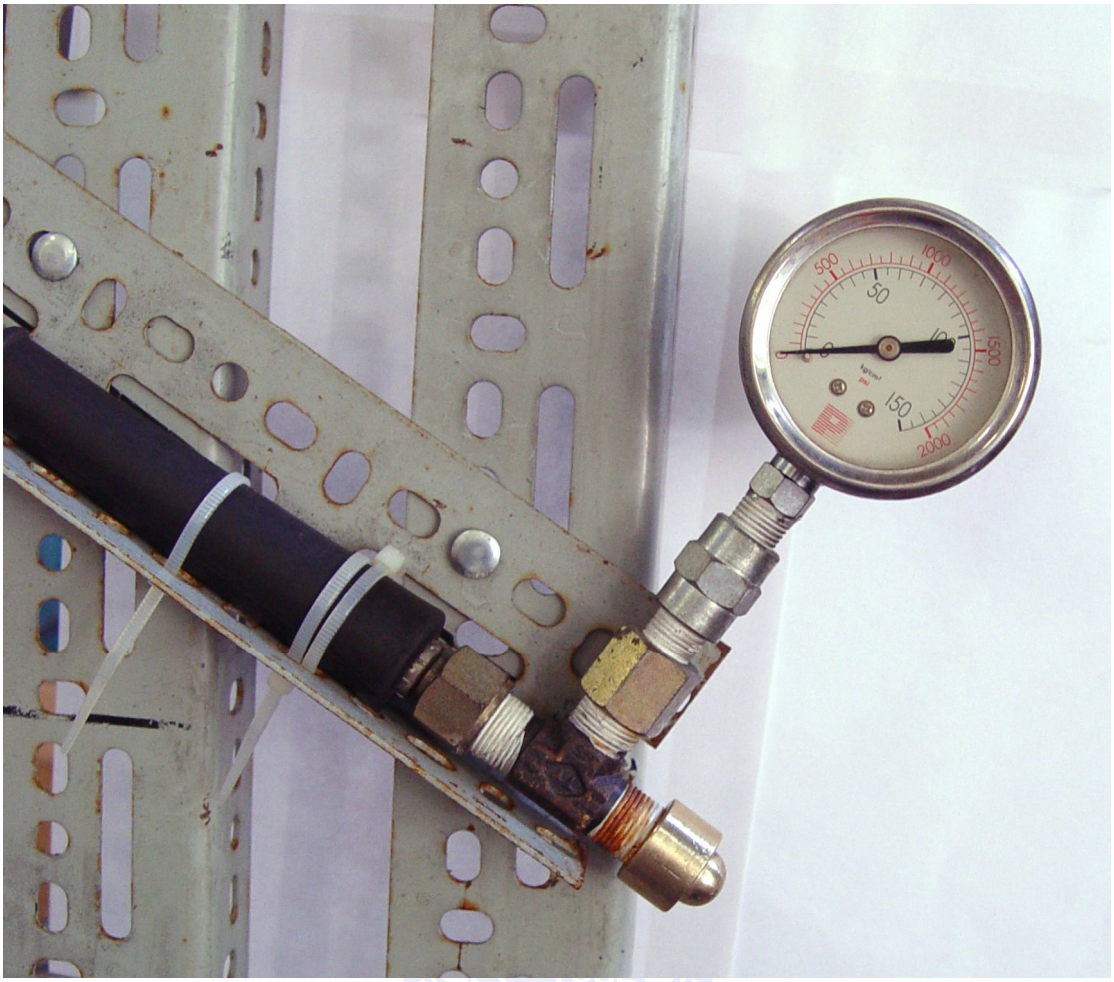

Fig. 2.10 The picture of pressure gauge

Fig. 2.11 The picture of Gaseous Oxygen Analyzer

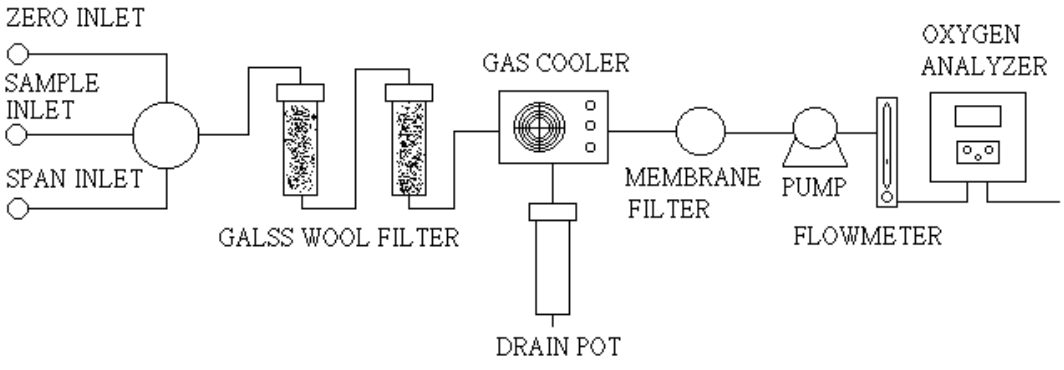

Fig. 2.12 Schematic configuration of preliminary handling system

(a)

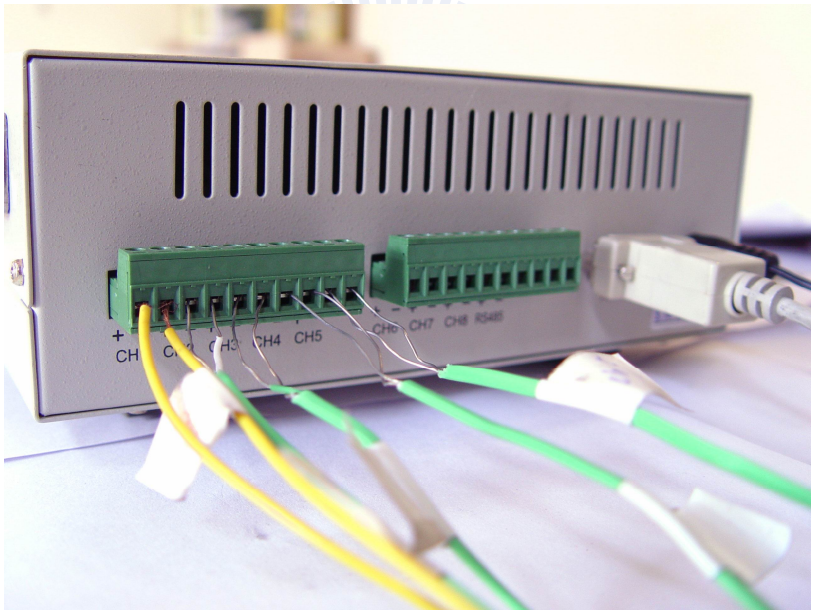

(b)

Fig. 2.13 The picture of datalog (a) Front view and (b) Back view

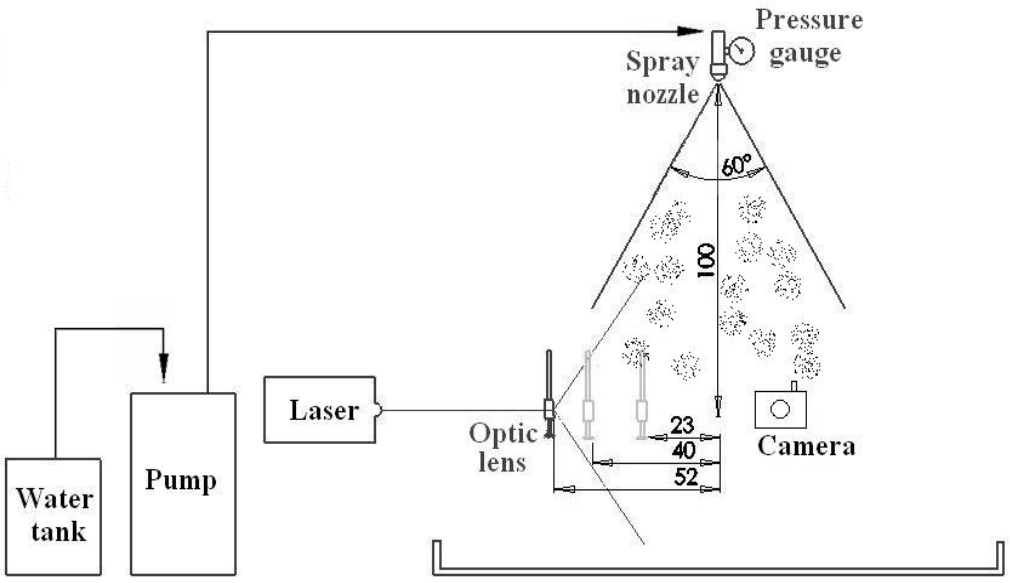

(a)

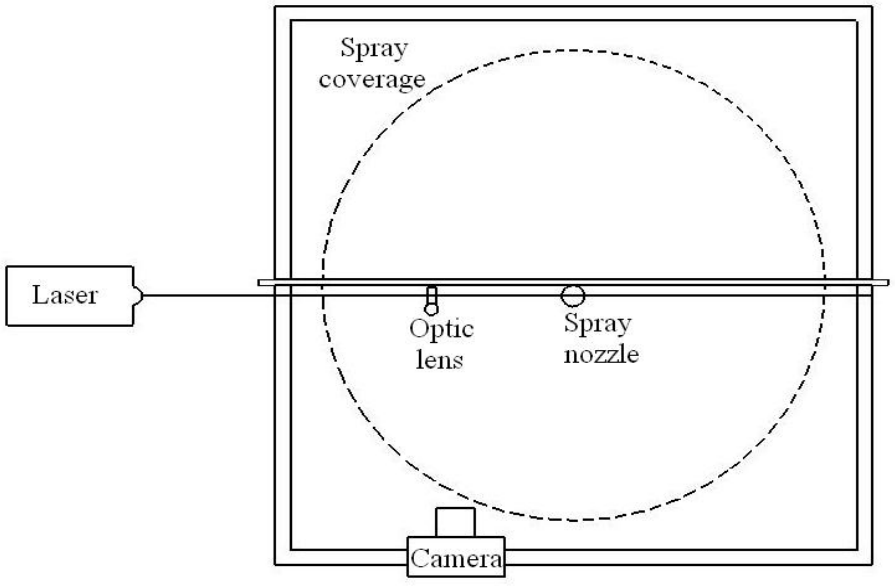

(b)

Fig. 2.14 The schematic configuration of the experimental apparatus

(a)Side View and (b) Up View

Fig. 2.15 The Nd:YVO 4 laser

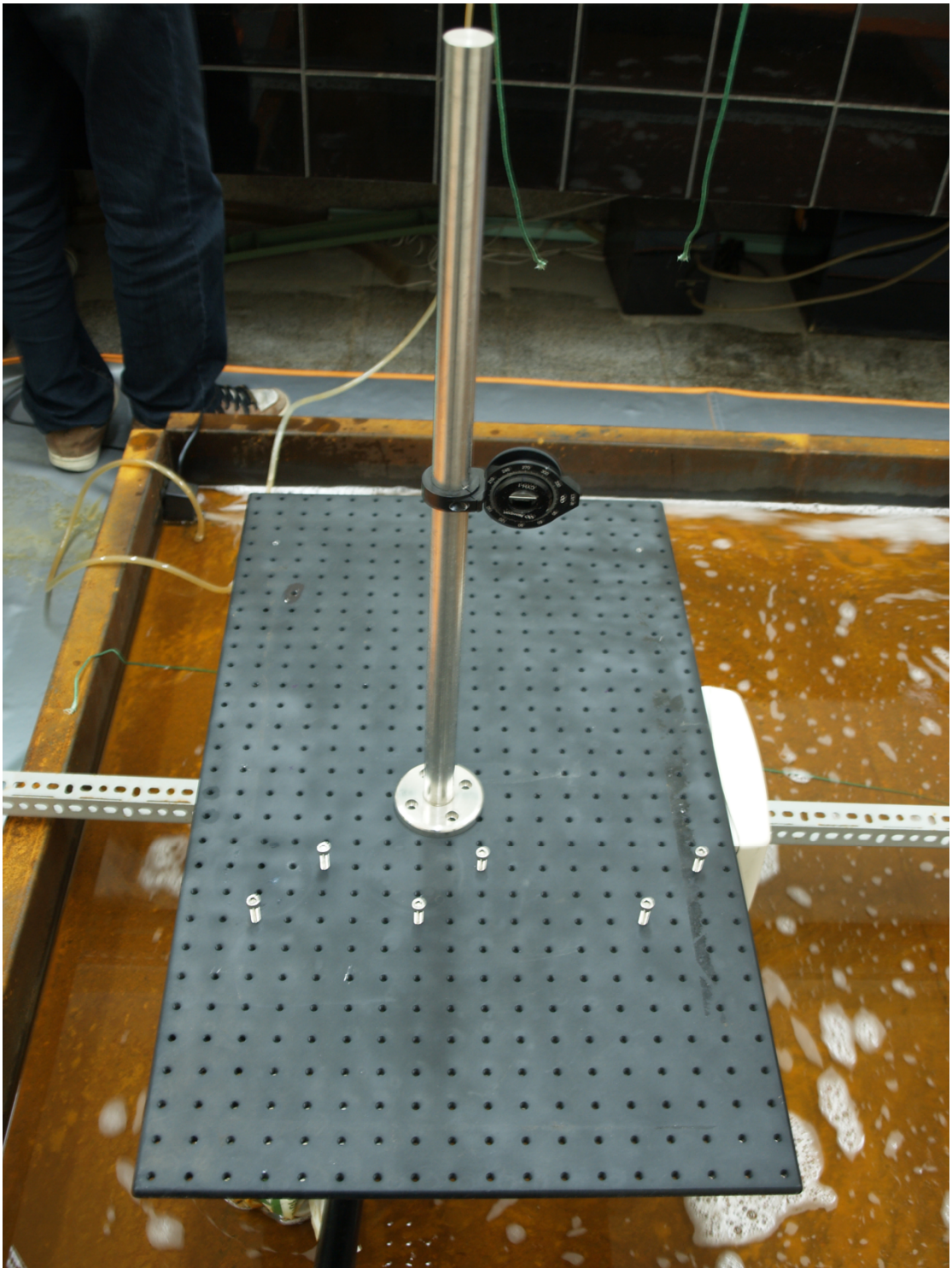

Fig. 2.16 The picture of optic lens

Fig. 2.17 The image capture device-Olympus E330

Fig. 2.18 SIGMA Long-Distance Macro Lens

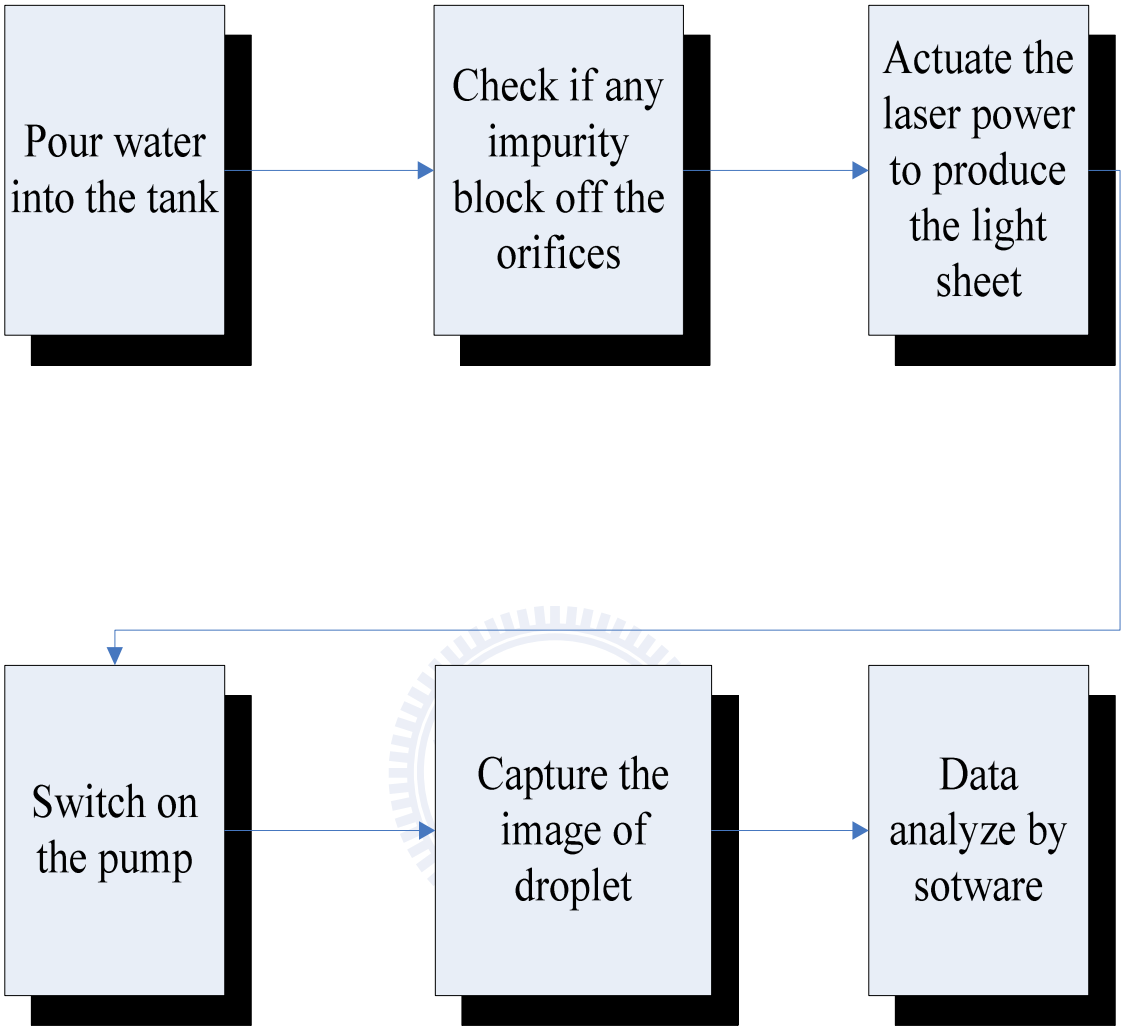

Fig. 2.19 The experimental flow chart

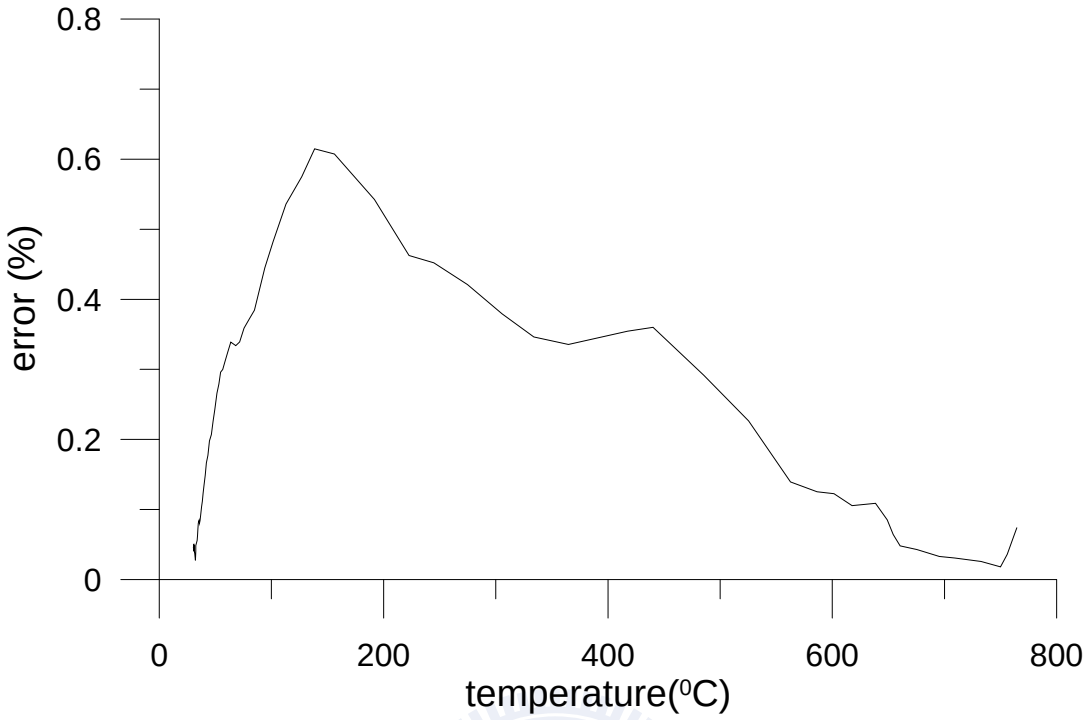

Fig. 3.1 The relationship of temperature and error

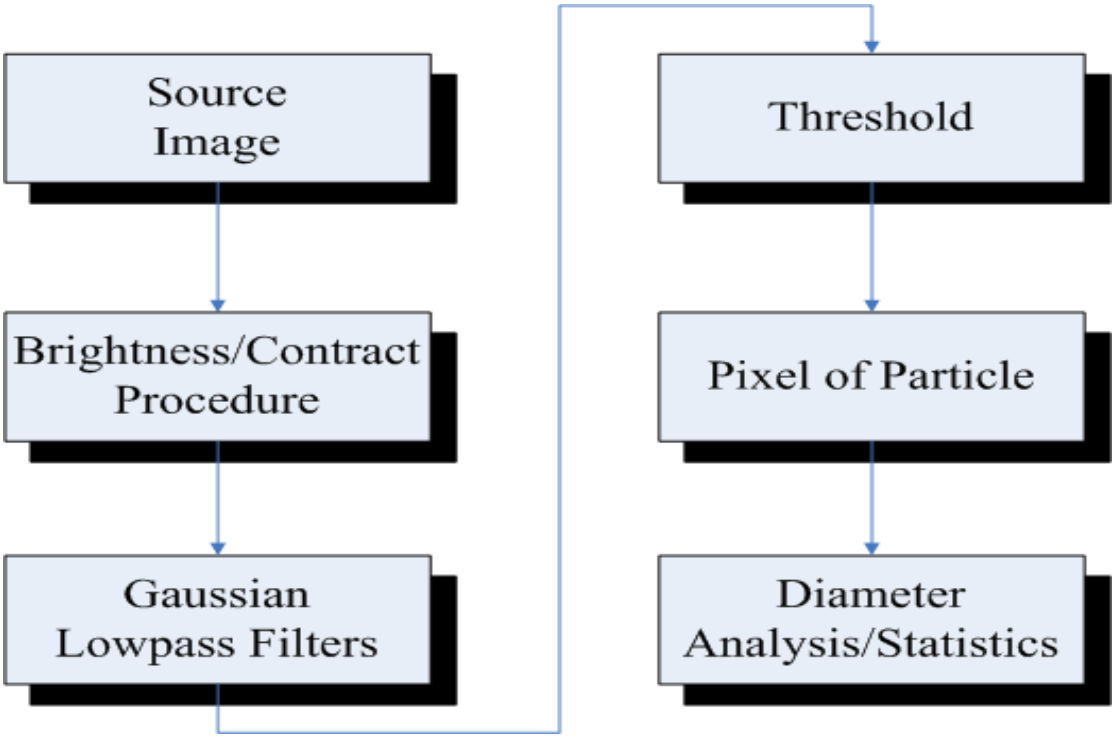

Fig. 3.2 The procedure for digital image processing with NI Version Assistant software.

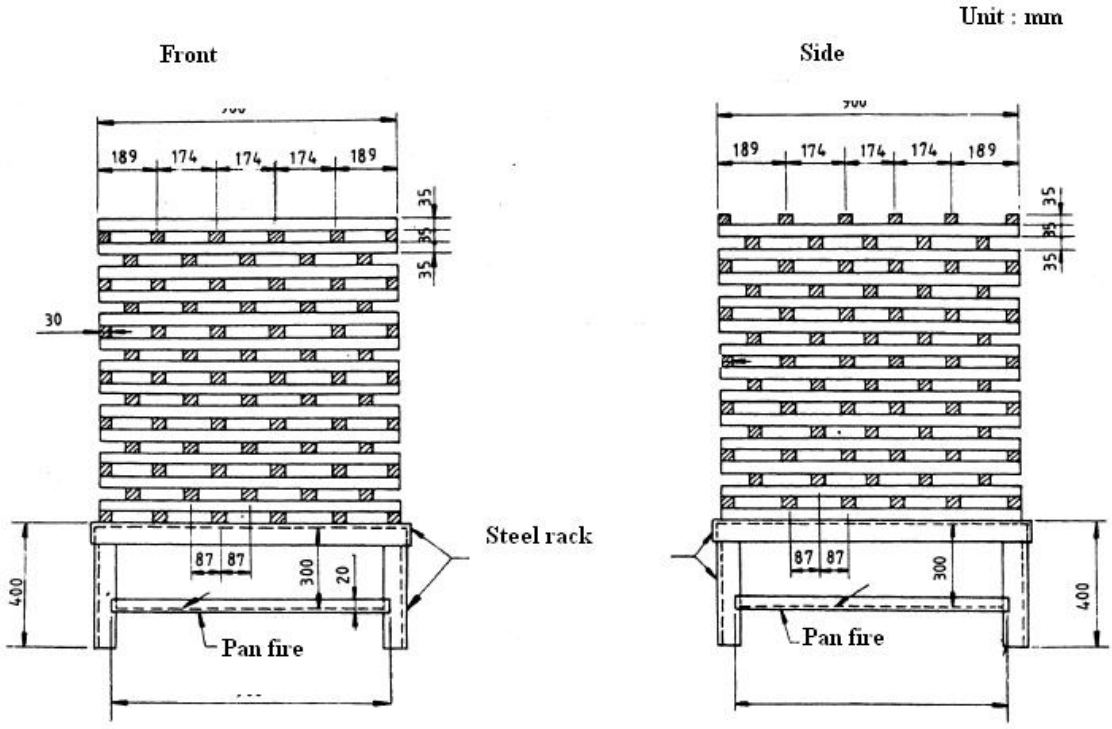

Fig. 4. Wooden slabs of CNS1387

Fig. 4.1 Pictures of Class A fire test

Fig. 4.2 Pictures of Class B (pan fire) fire test

Fig. 4.3 Pictures of motorcycles fire test

Fig. 4.4 Pictures of car fire test (1)

Fig. 4.5 Pictures of car fire test (2)

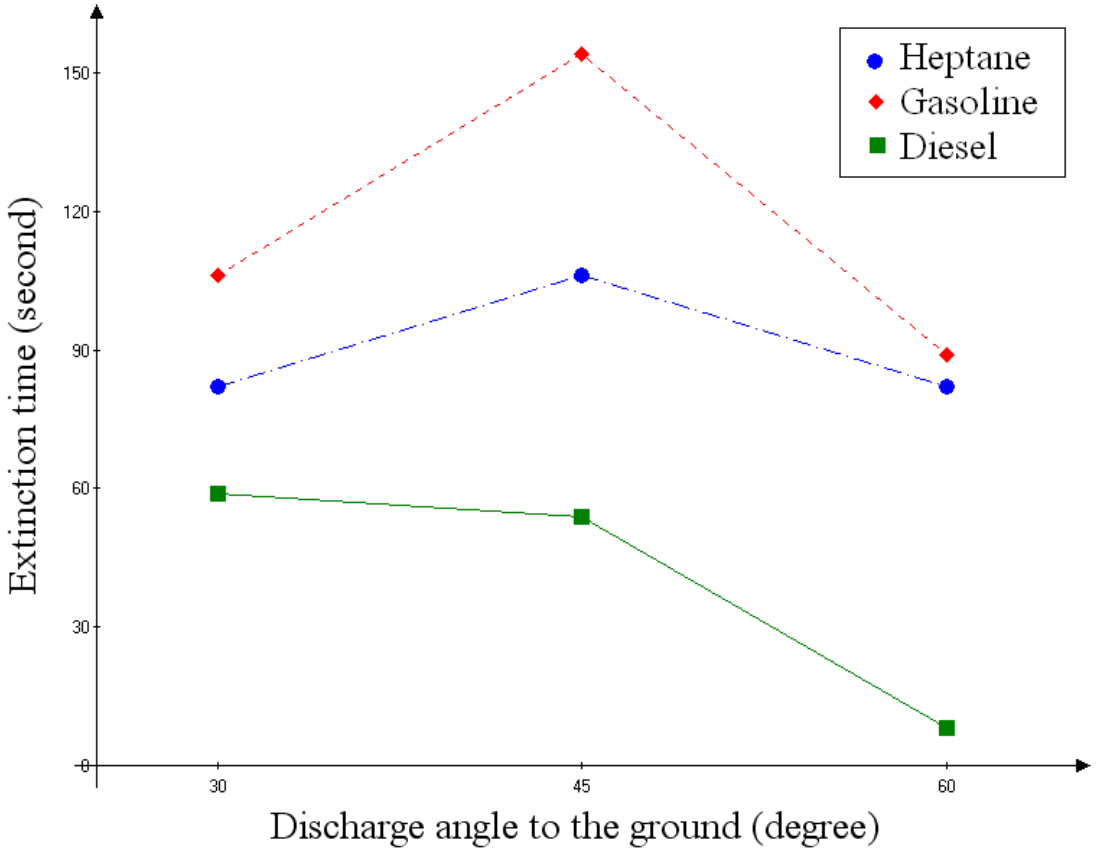

Fig. 4.6 The relationship between nozzle discharge angles and extinction time in different fuel types without addtive (Diameter of pan: 25*cm*, Amount of fuel: 250*ml*)

(a) Heptane

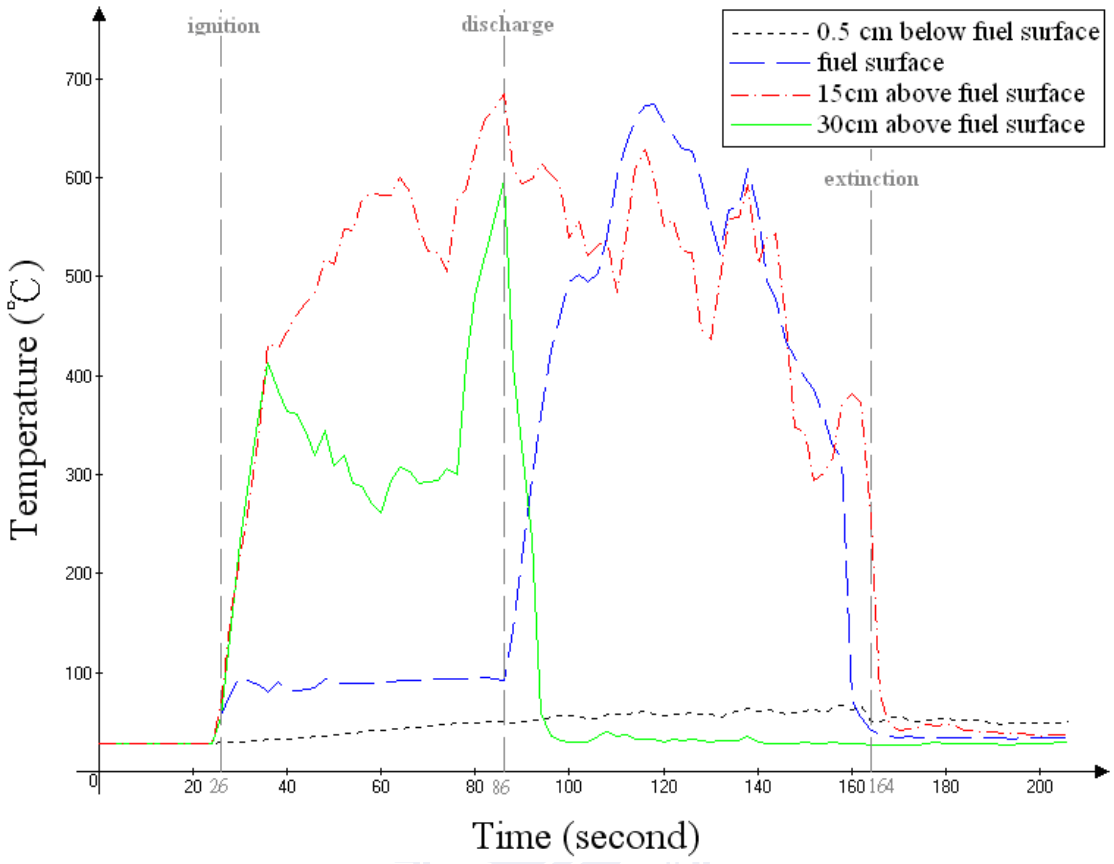

(b) Gasoline

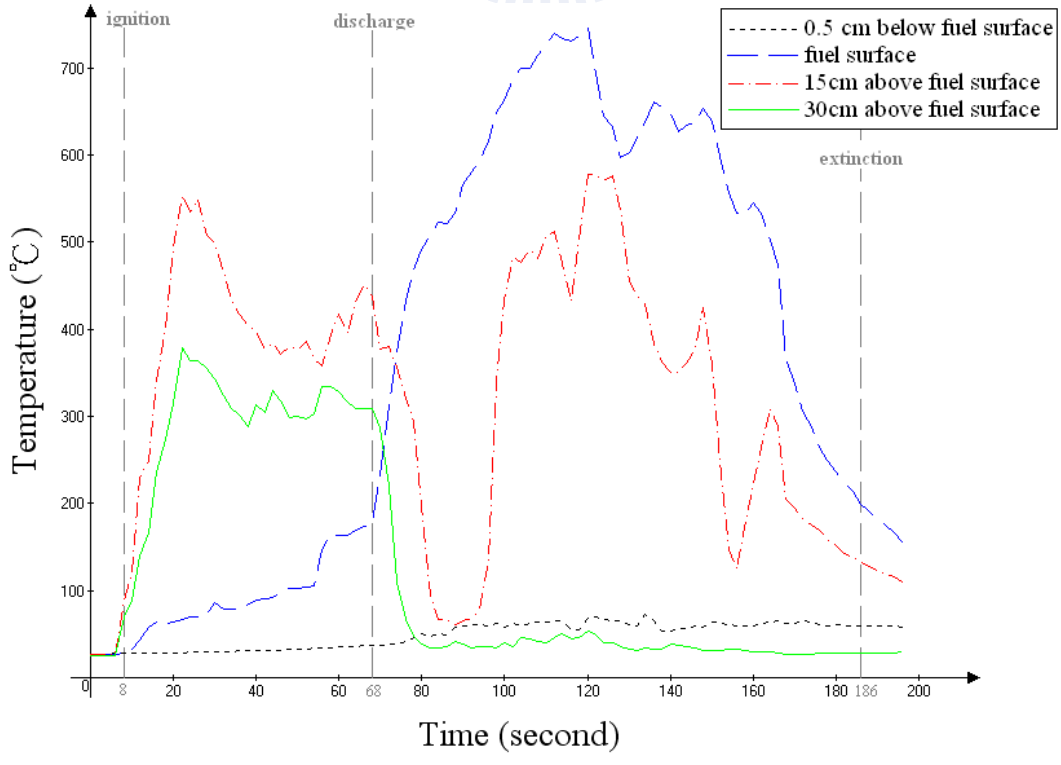

(c) Diesel

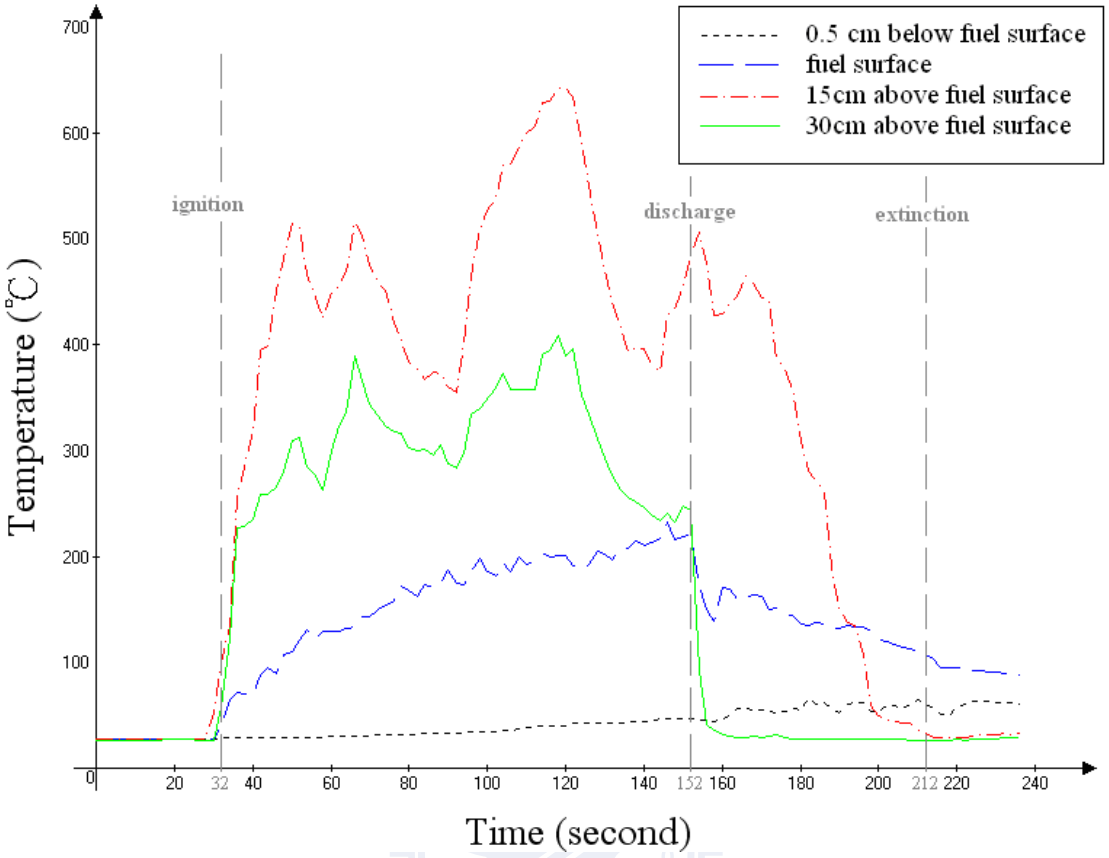

Fig. 4.7 The temperature history of fires with pure water at the nozzle discharge angle of 30° (a) Heptane (b) Gasoline (c) Diesel (Diameter of pan: 25*cm*, Amount of fuel: 250*ml*)

(a) Heptane

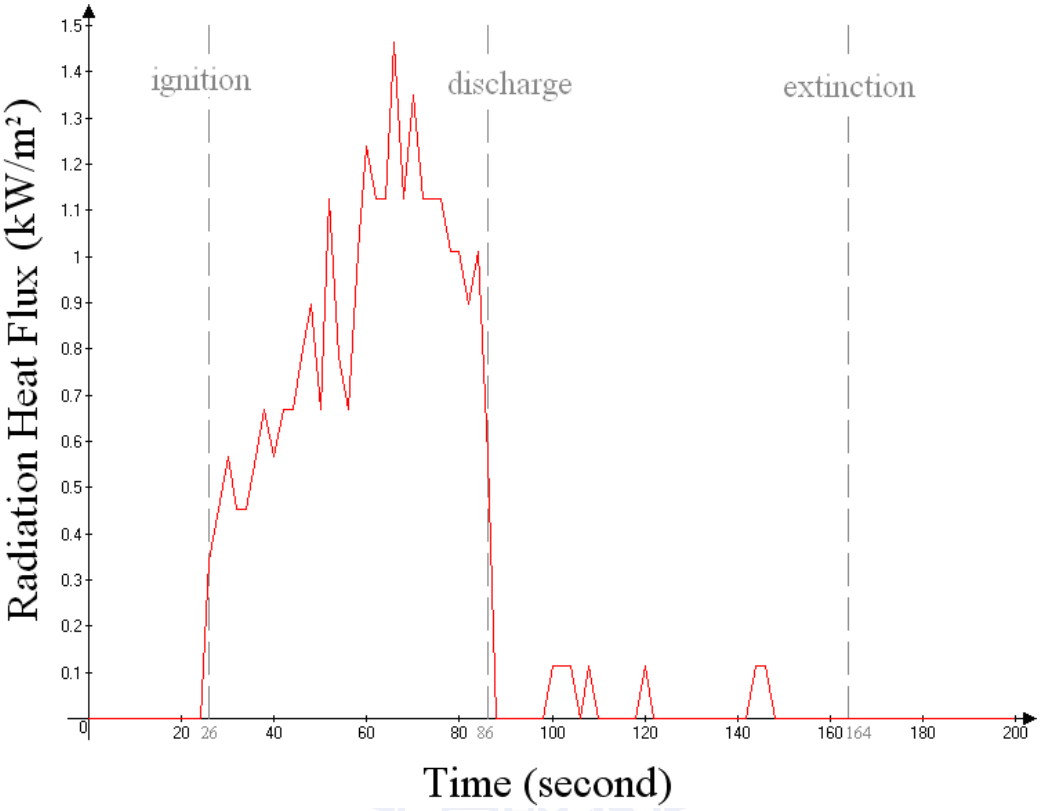

(b) Gasoline

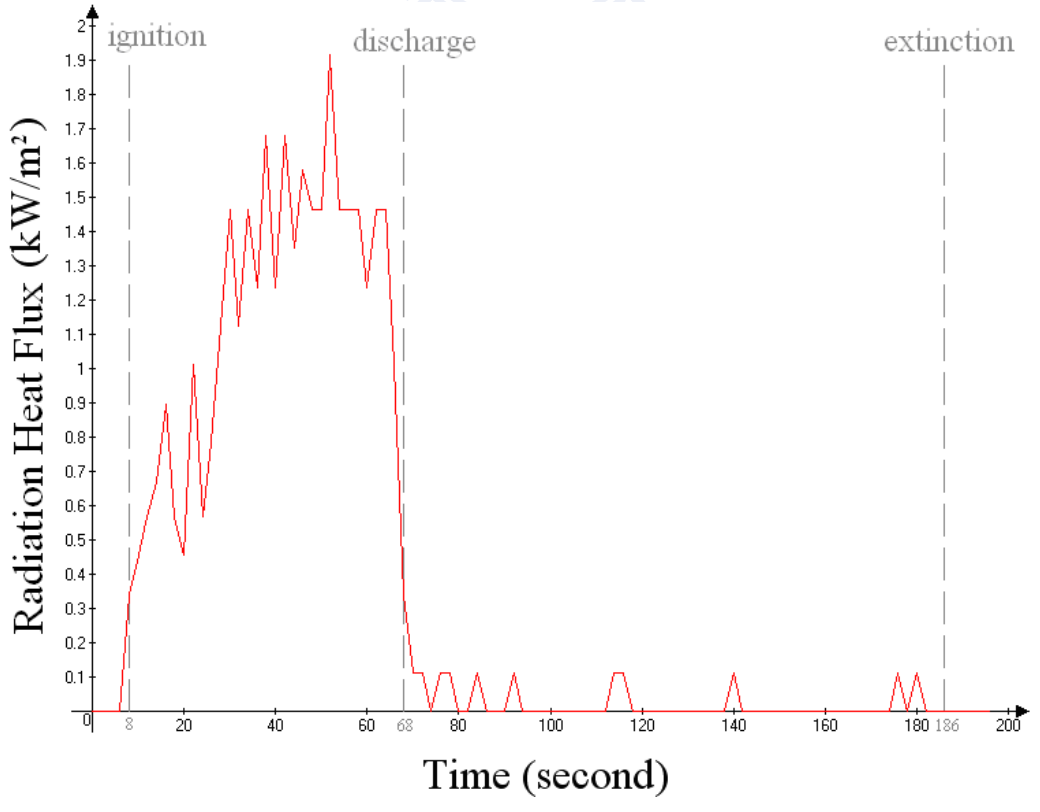

(c) Diesel

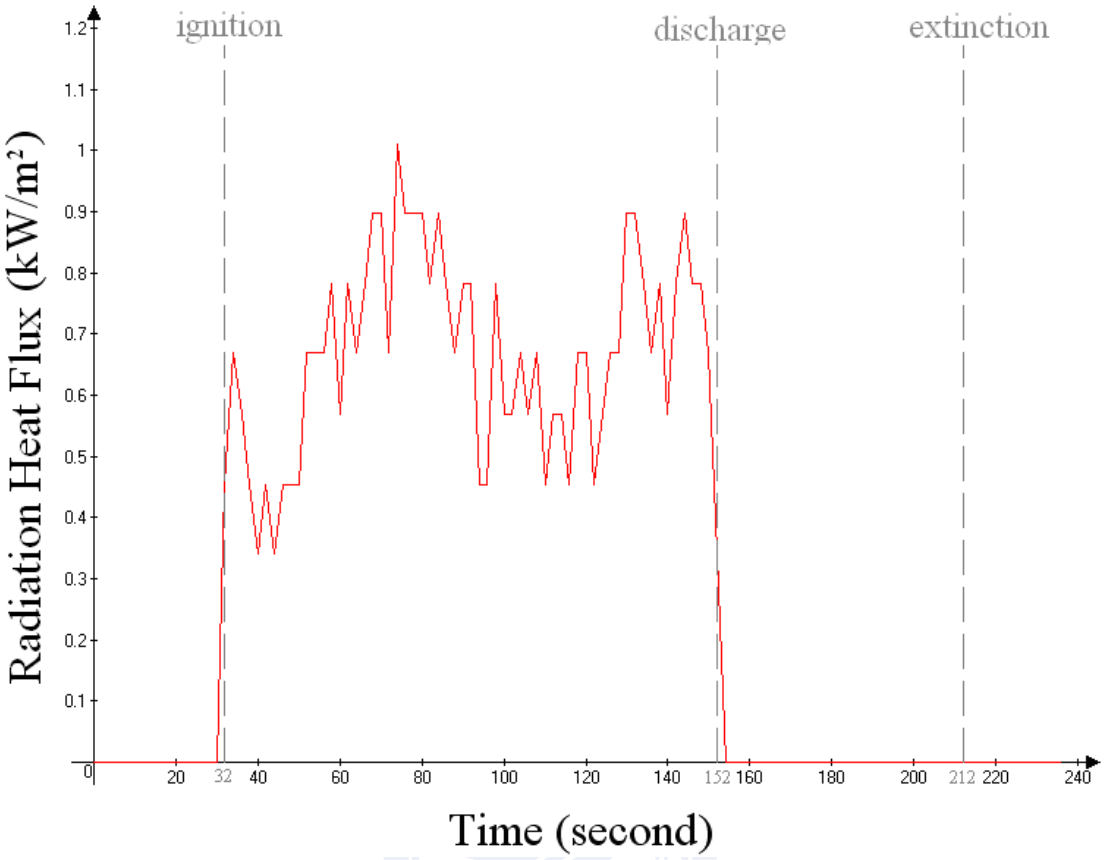

Fig. 4.8 The radiation heat flux history of fires with pure water at the nozzle discharge angle of 30° (a) Heptane (b) Gasoline (c) Diesel (Diameter of pan: 25*cm*, Amount of fuel: 250*ml*)

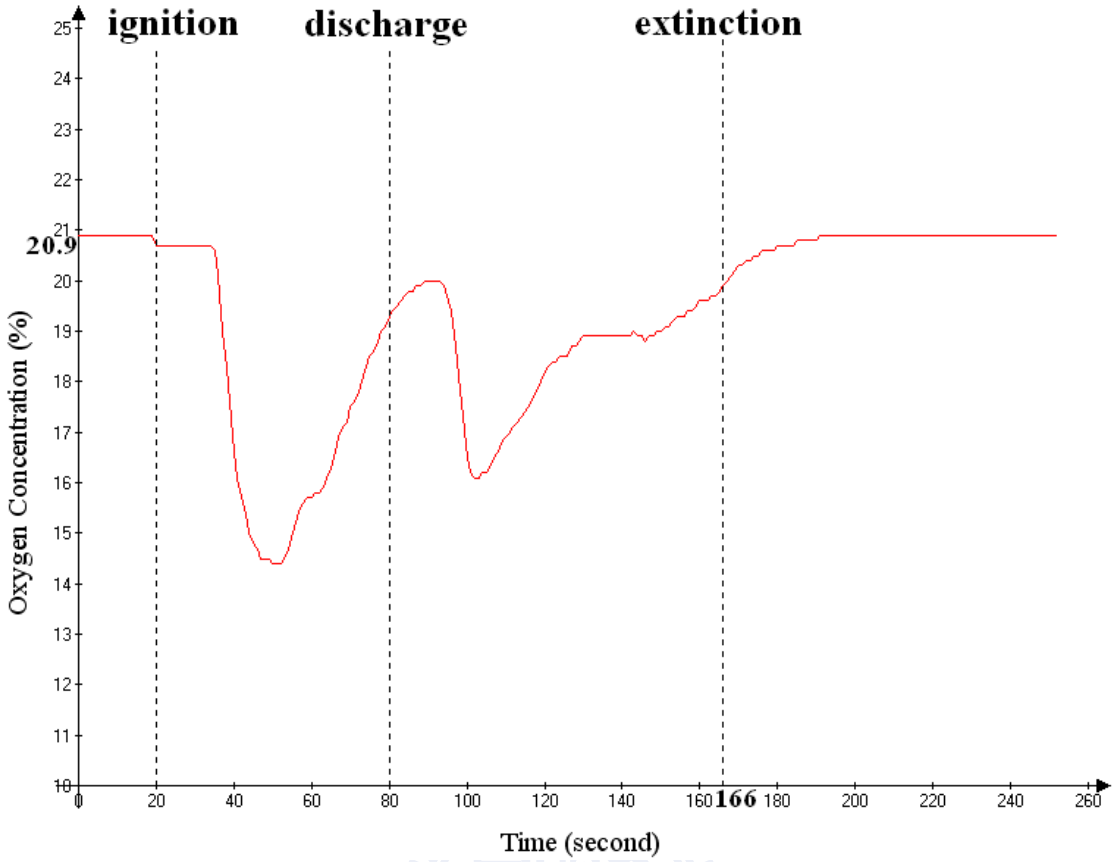

Fig. 4.9 Oxygen concentration variation history

(Diameter of pan: 25*cm*, Fuel type: gasoline, Amount of fuel: 250*ml*,

Nozzle discharge angle: 60°,Additive: 0%)

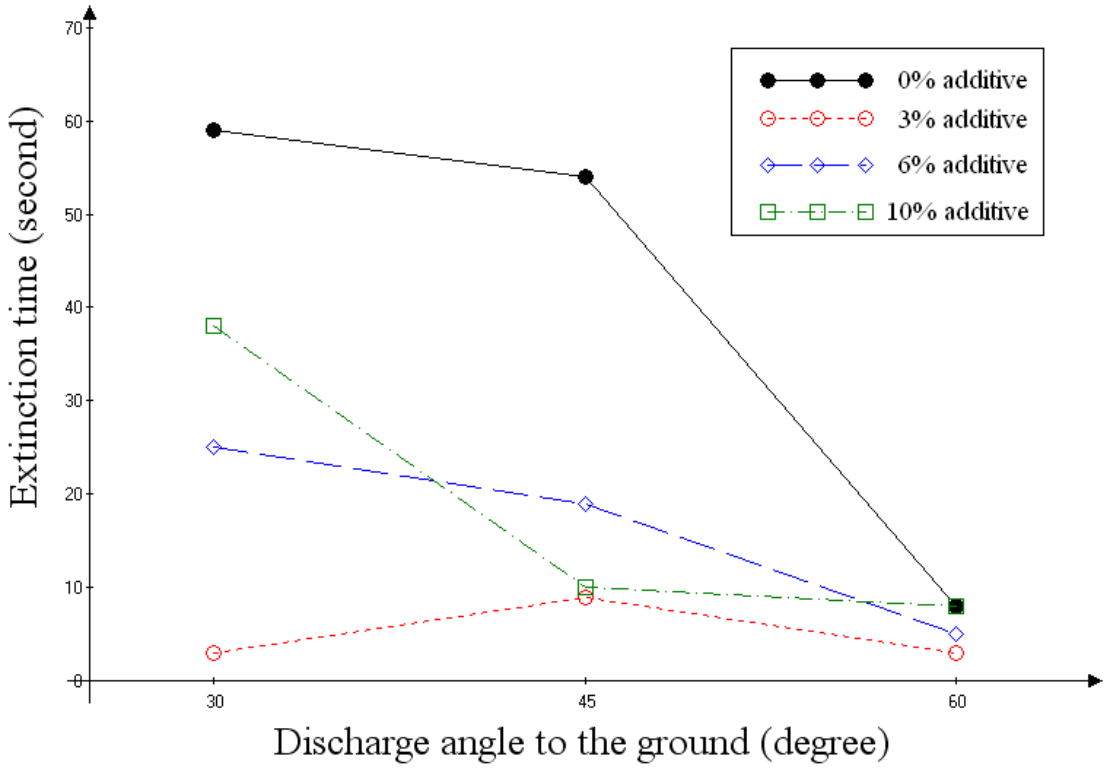

Fig. 4.10 Extinguishing time for diesel fire with different nozzle discharge angles and additive solution volumes
(Diameter of pan: 25*cm*, Amount of fuel: 250*ml*)

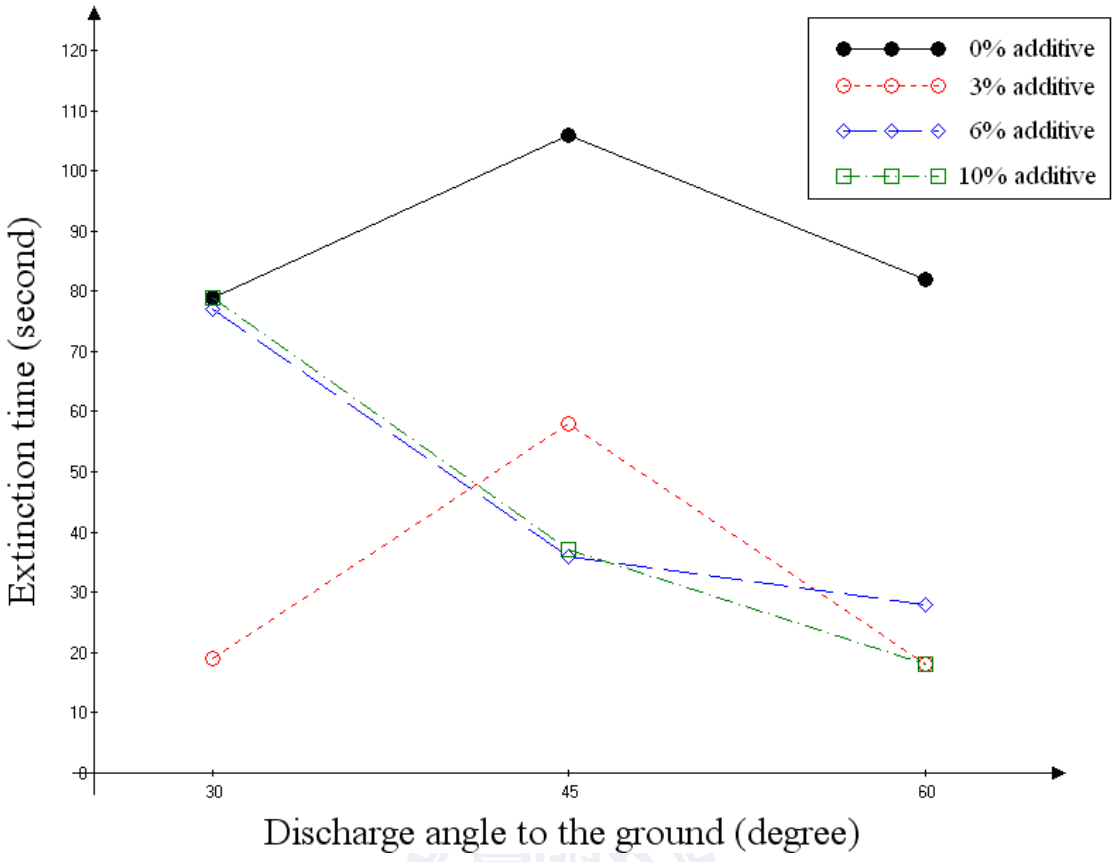

Fig. 4.11 Extinguishing time for heptanel fire with different nozzle discharge angles and additive solution volumes
(Diameter of pan: 25*cm*, Amount of fuel: 250*ml*)

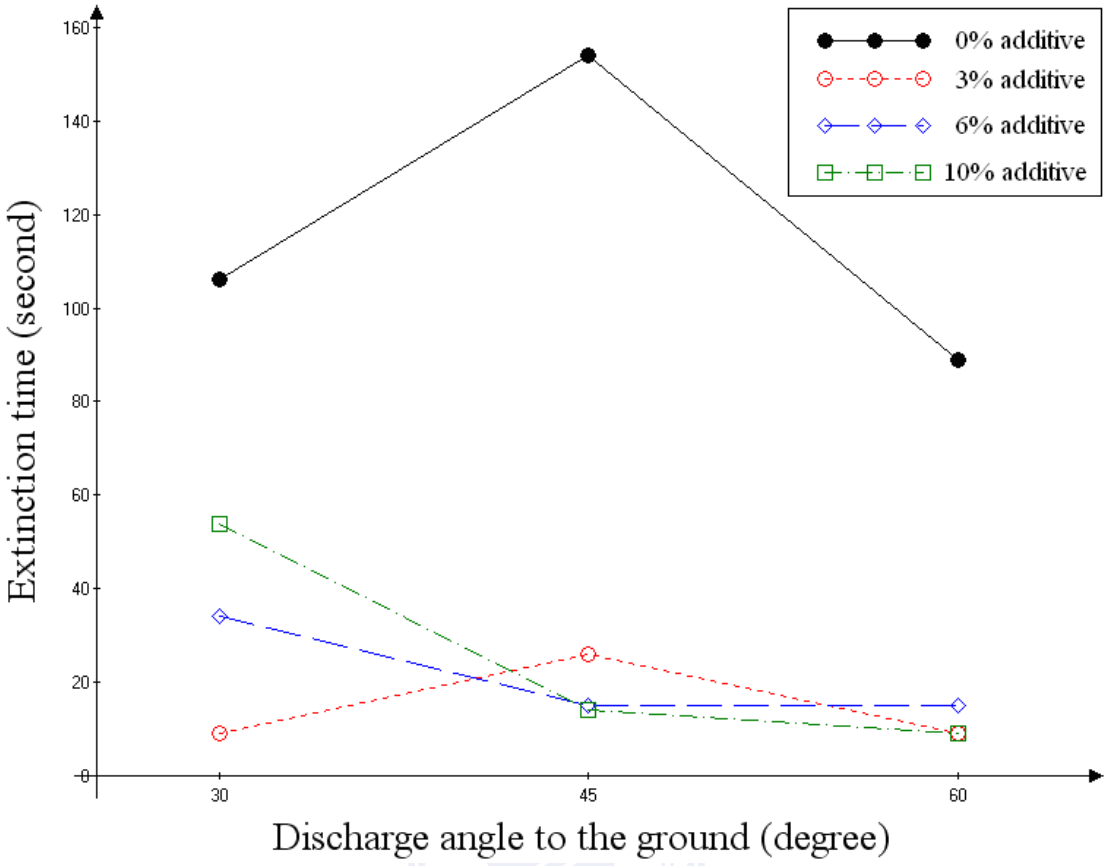

Fig. 4.12 Extinguishing time for gasoline fire with different nozzle discharge angles and additive solution volumes (Diameter of pan: 25*cm*, Amount of fuel: 250*ml*)

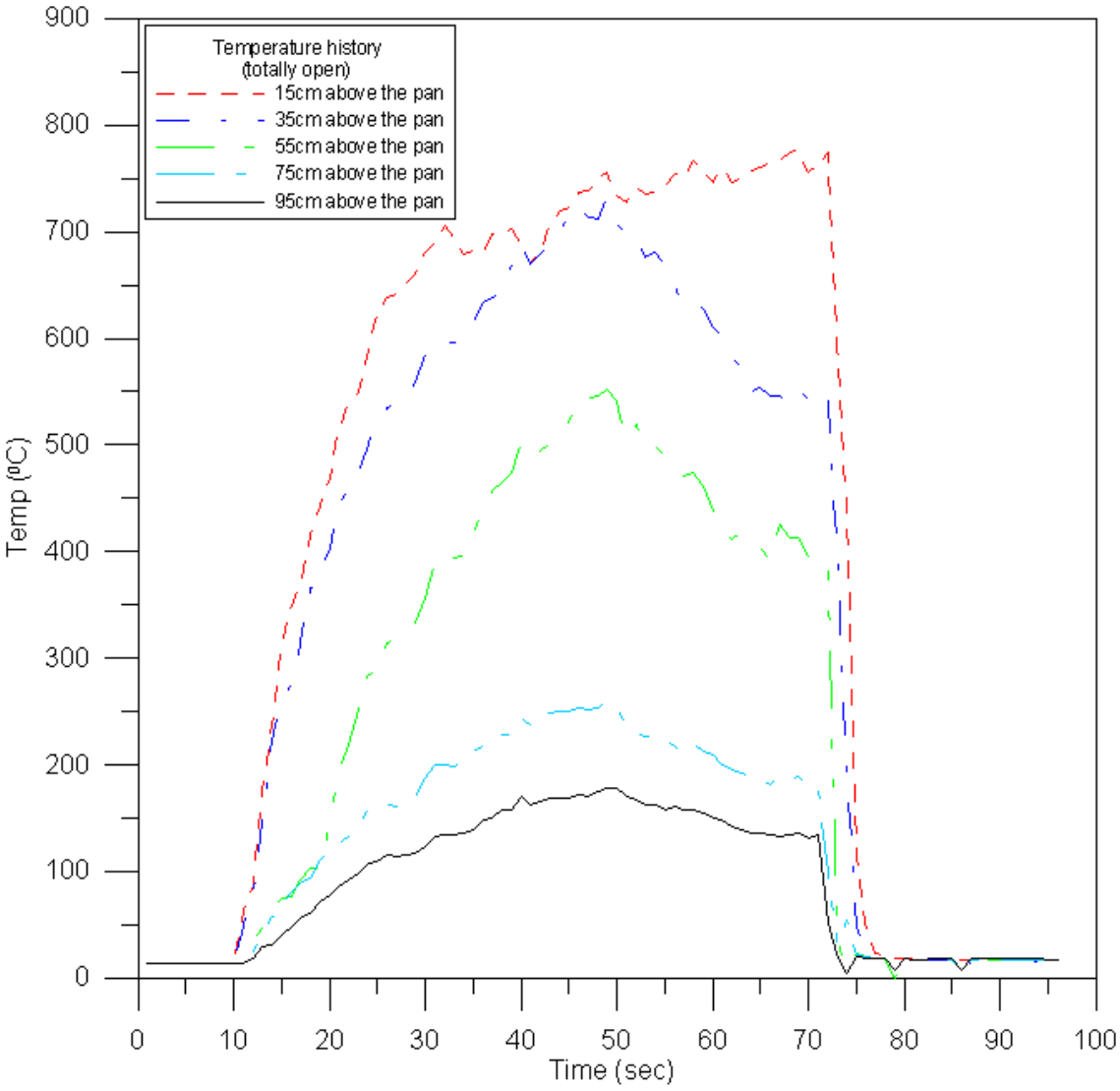

Fig. 4.13 Temperature history of totally open door tests

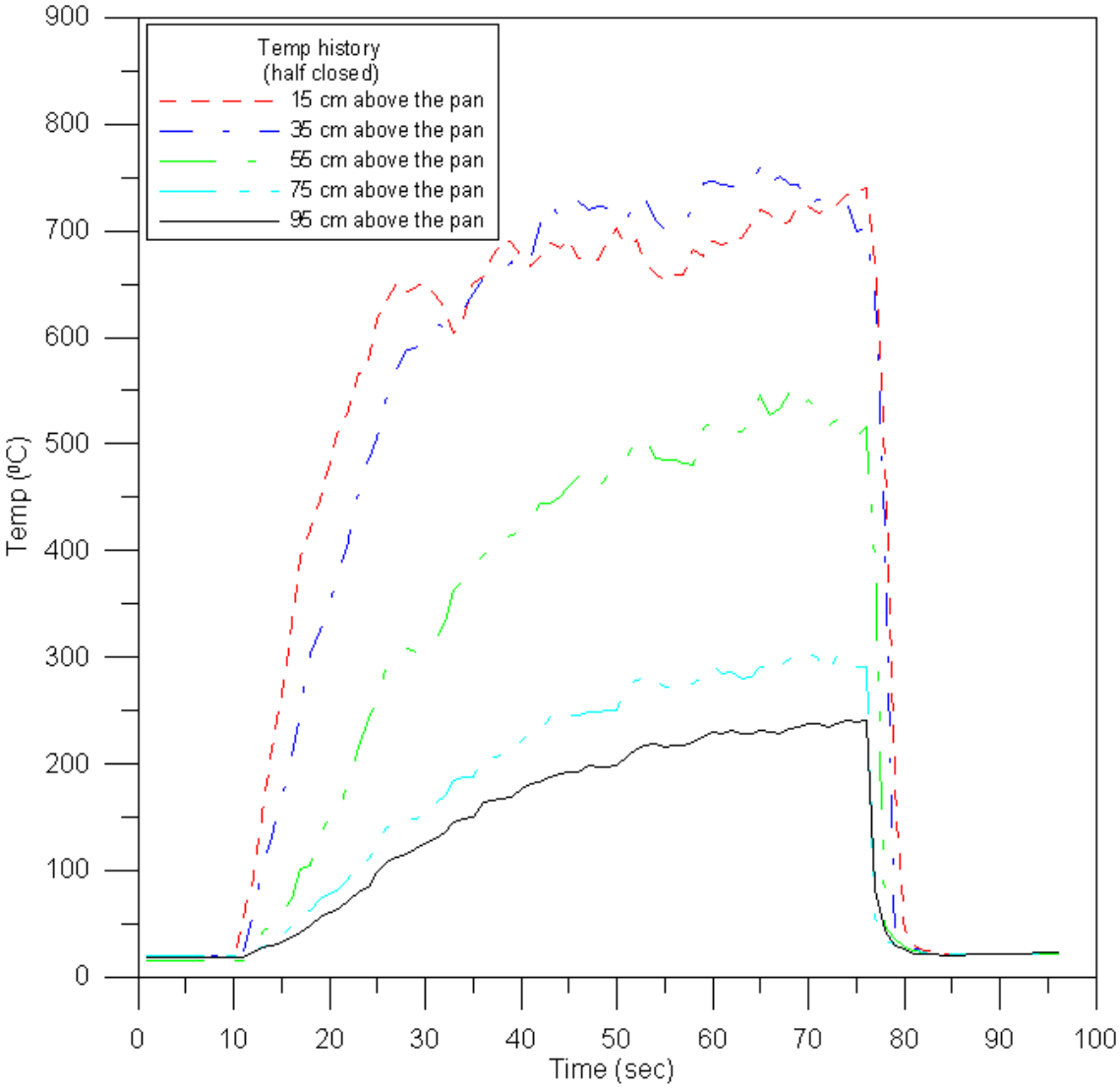

Fig. 4.14 Temperature history of half closed door tests

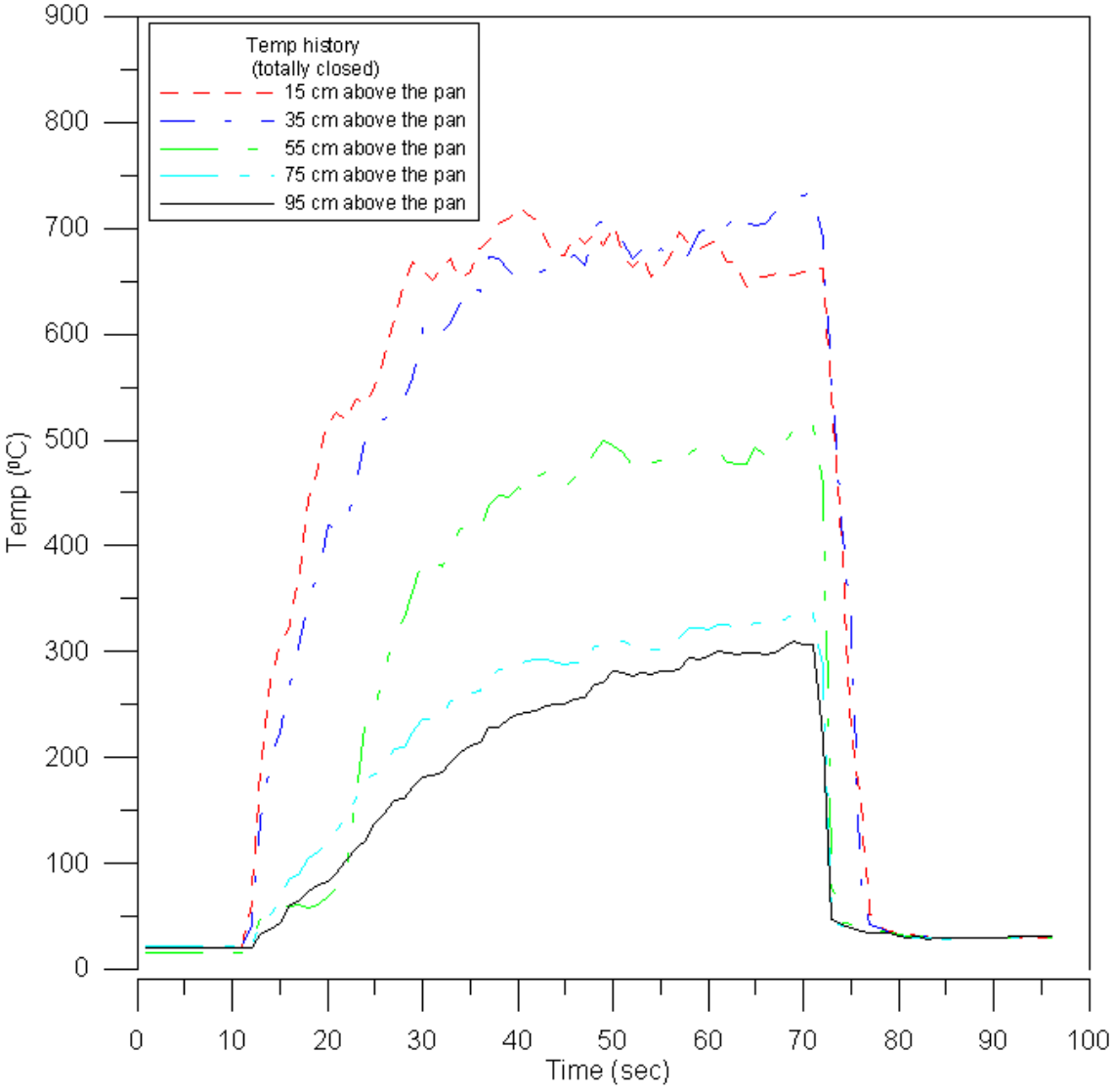

Fig. 4.15 Temperature history of totally closed door tests

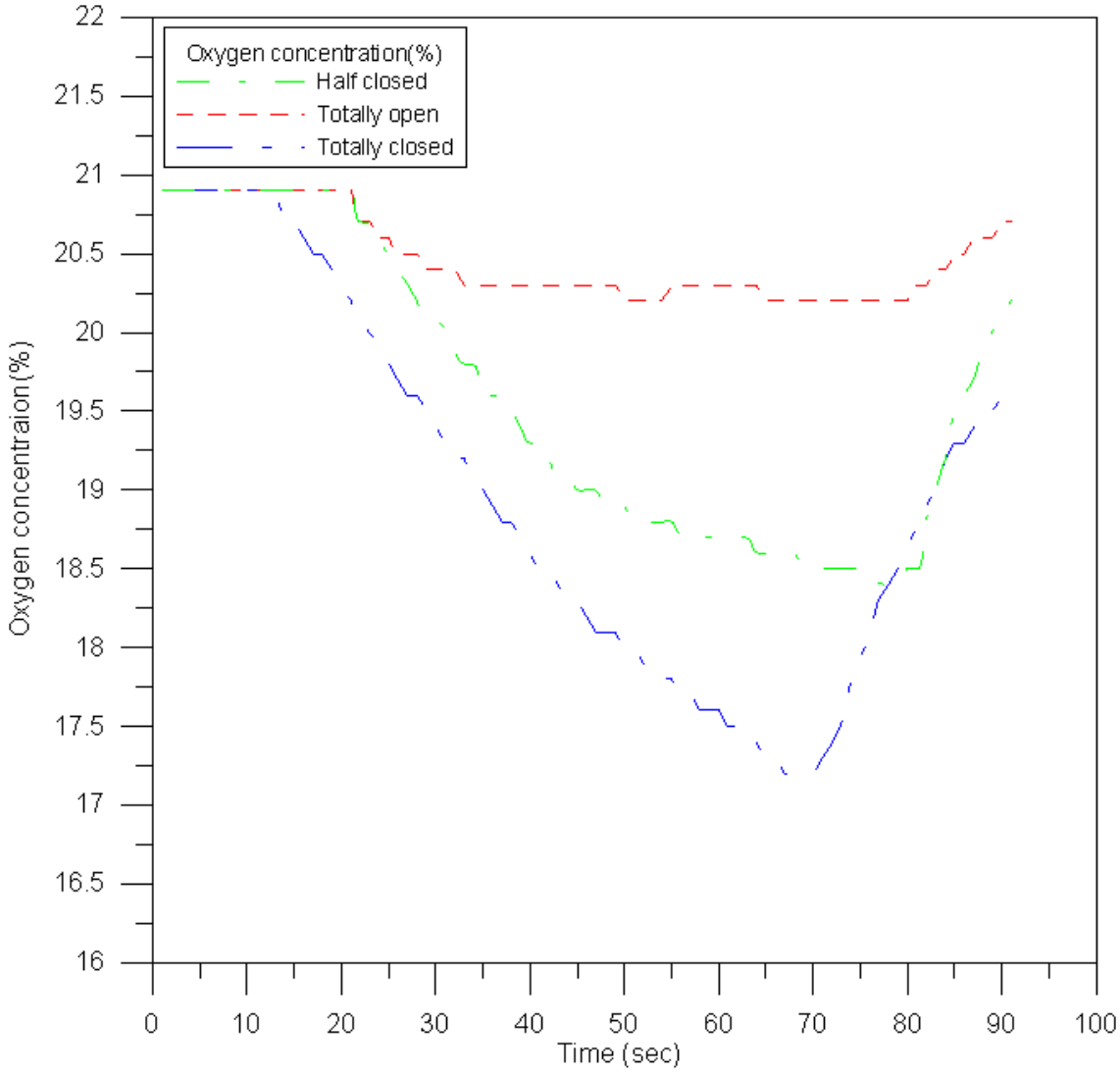

Fig. 4.16 Oxygen concentration history for different door closure degree

Fig 4.17 The relation between average diameter and pressure for different position.

Fig 4.18 The relation between SMD and pressure for different position.

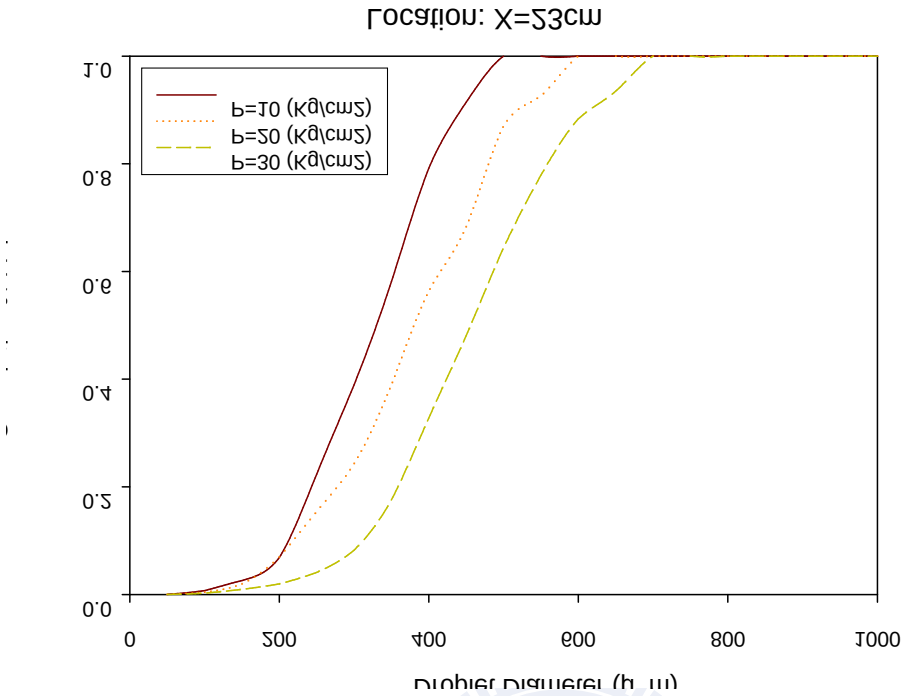

Fig. 4.19 The NFPA750 standard form for droplet diameter v.s. cumulative % volume at x=23cm.

Fig. 4.20 The NFPA750 standard form for droplet diameter v.s. cumulative % volume at x=40cm.

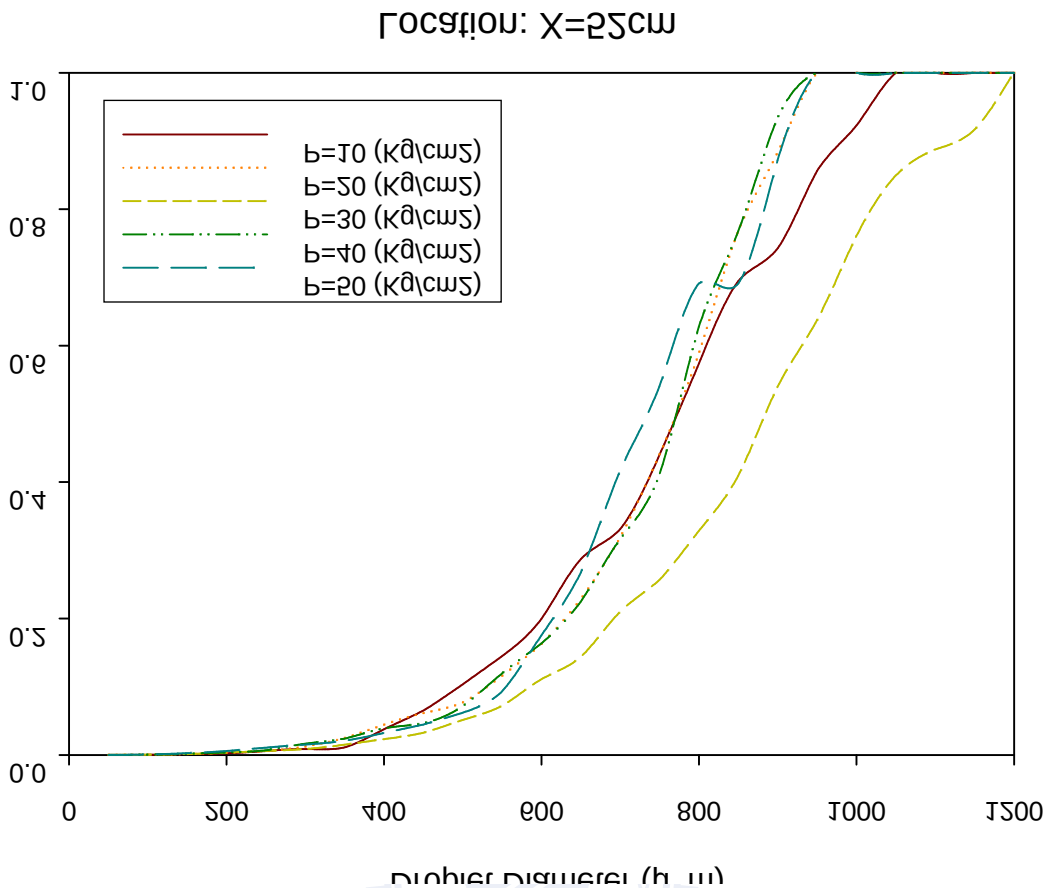

Fig. 4.21 The NFPA750 standard form for droplet diameter v.s. cumulative % volume at x=52cm.

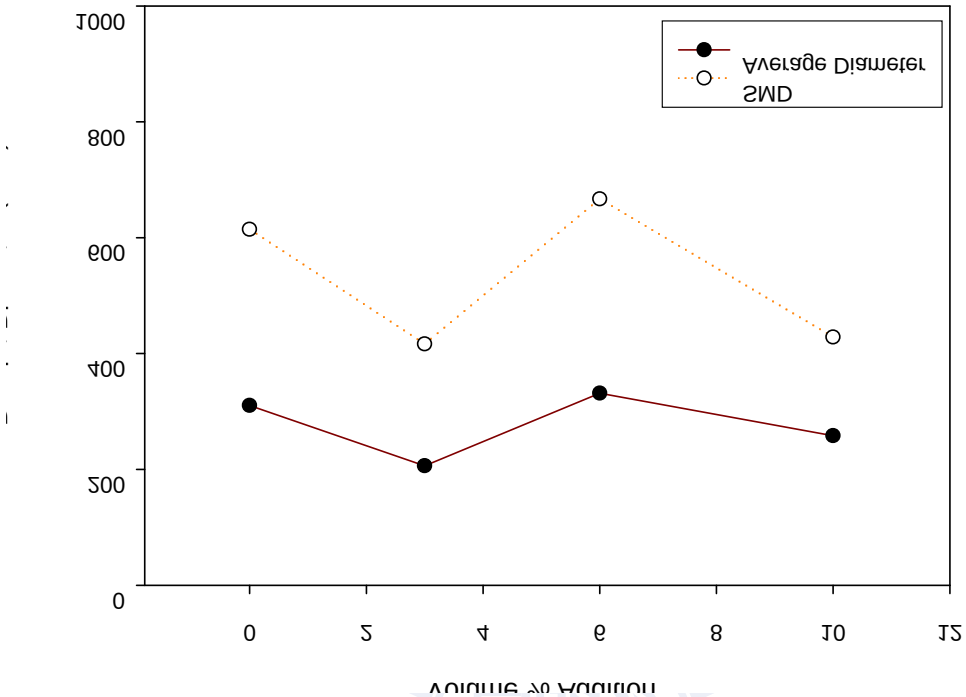

Fig 4.22 The relation between volume % addition and droplet diameter

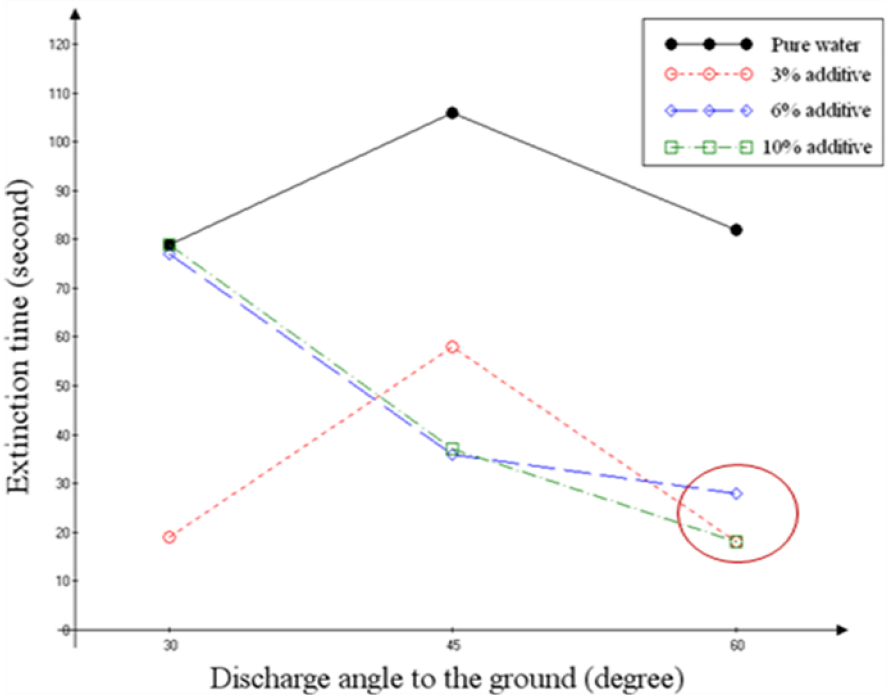

Fig. 4.23 Extinguishing time for heptanel fire with different nozzle discharge angles and additive solution volumes

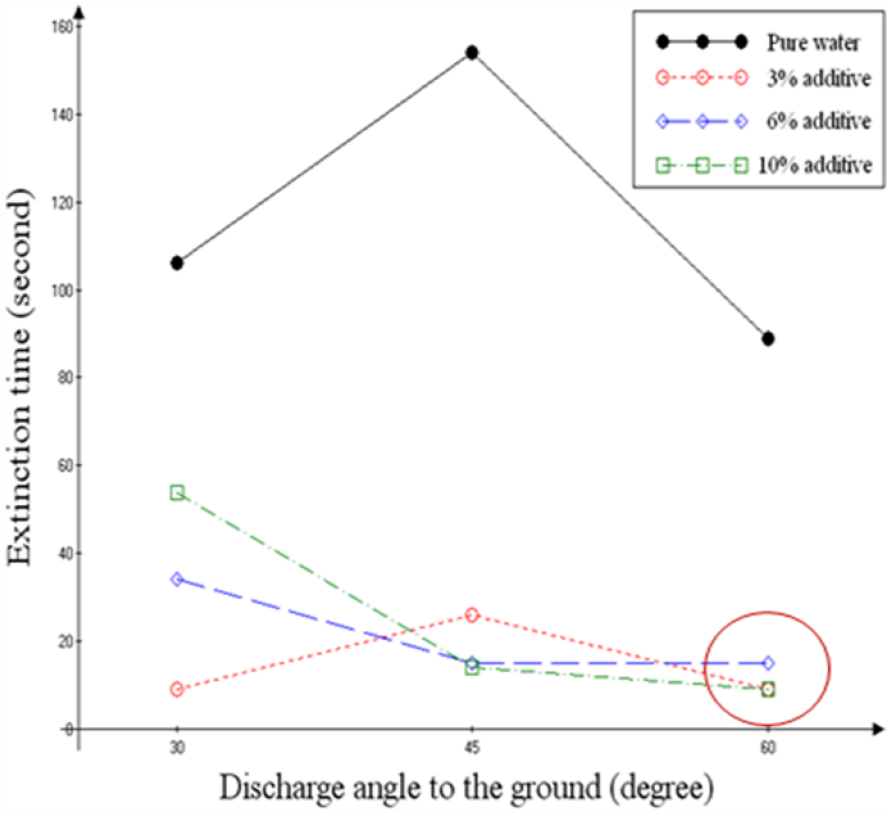

Fig. 4.24 Extinguishing time for gasoline fire with different nozzle discharge angles and additive solution volumes

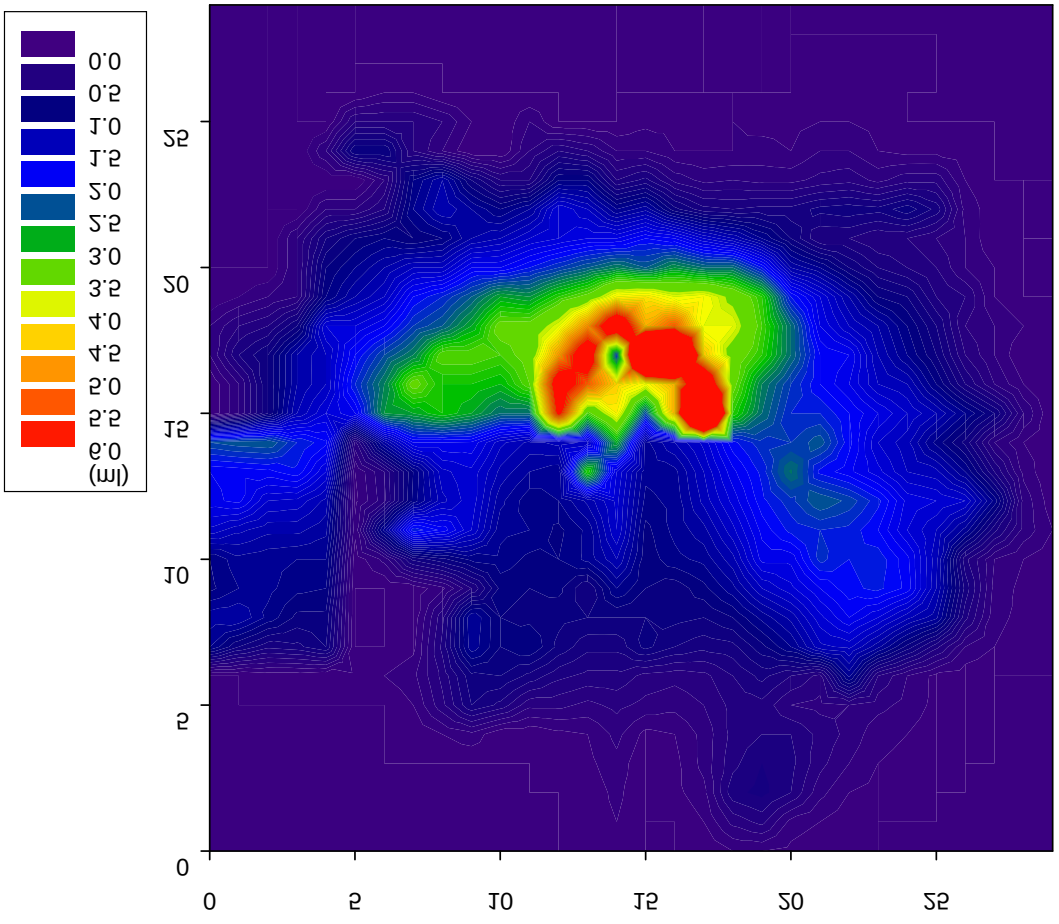

Fig. 4.25 Water mist density distribution measured by experiment.

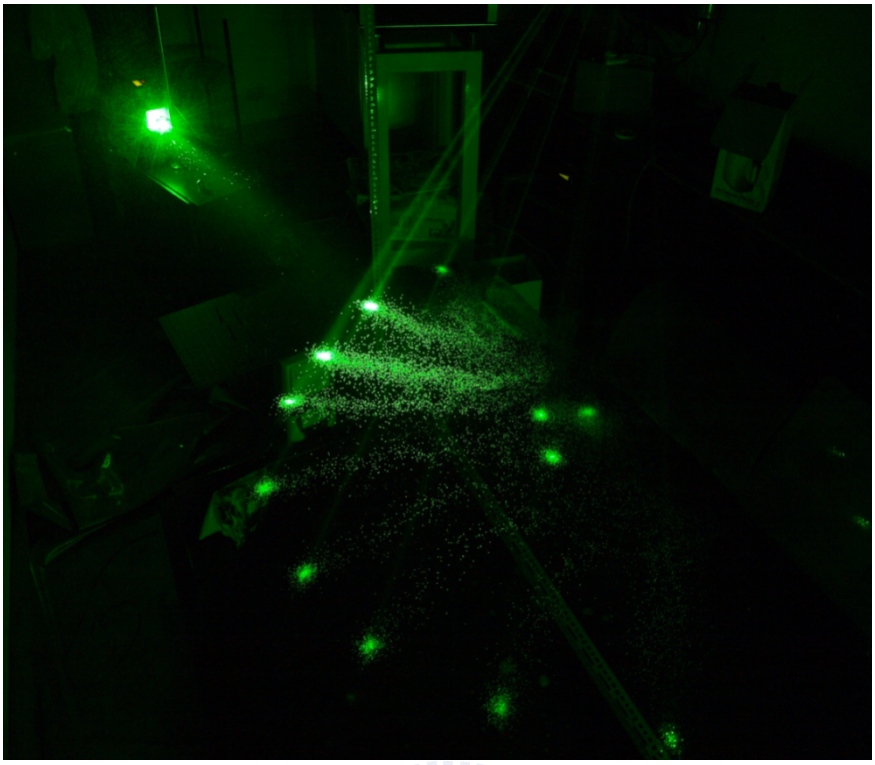

Fig. 4.26 Water mist distribution picture for P=10 Kg/cm2.

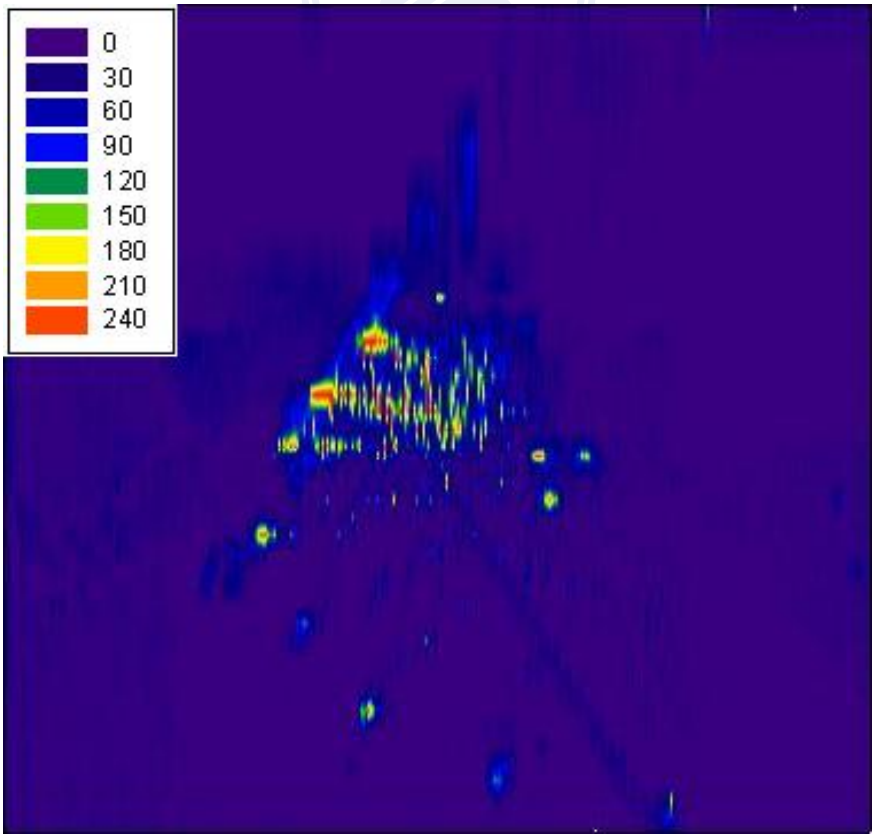

Fig. 4.27 Grey level for image captured at P=10 Kg/cm2.

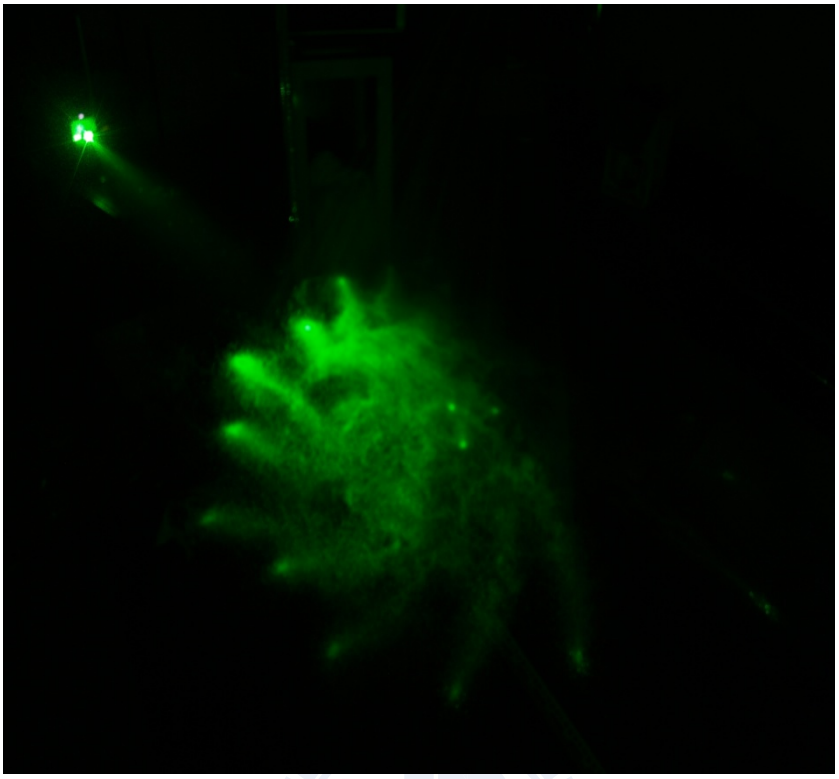

Fig. 4.28 Water mist distribution picture for P=20 Kg/cm2.

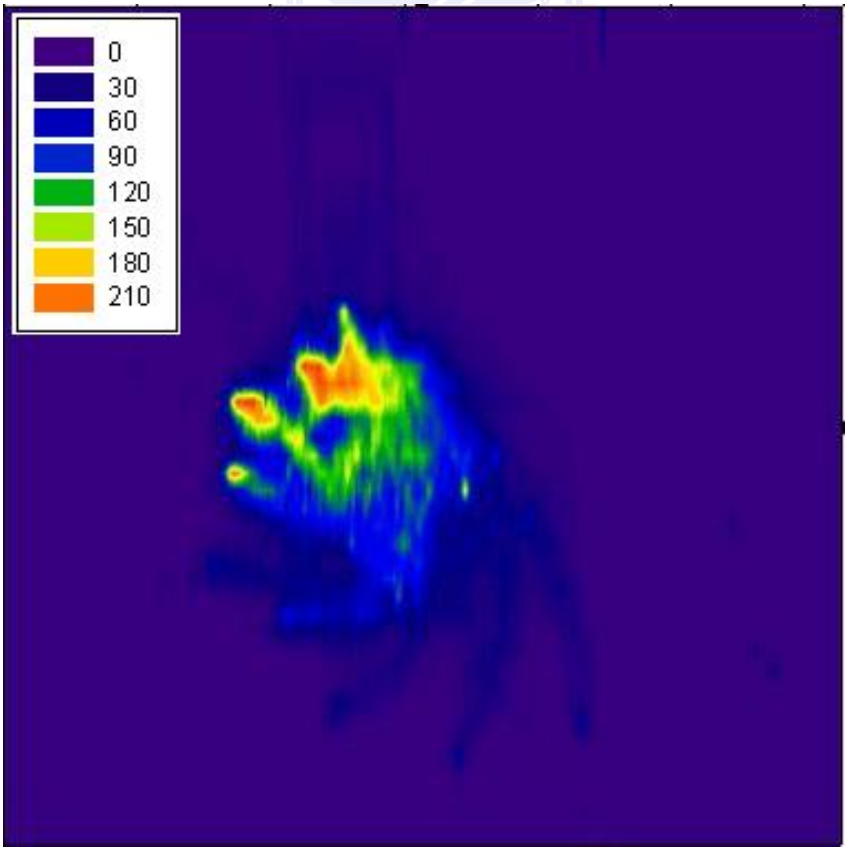

Fig. 4.29 Grey level for image captured at P=20 Kg/cm2.

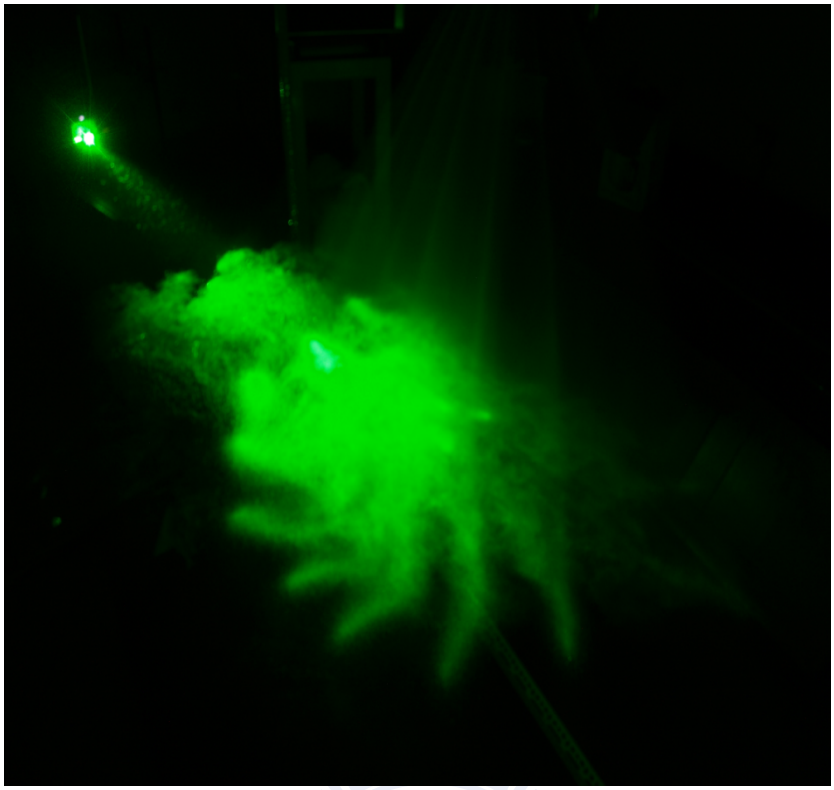

Fig. 4.30 Water mist distribution picture for P=30 Kg/cm2.

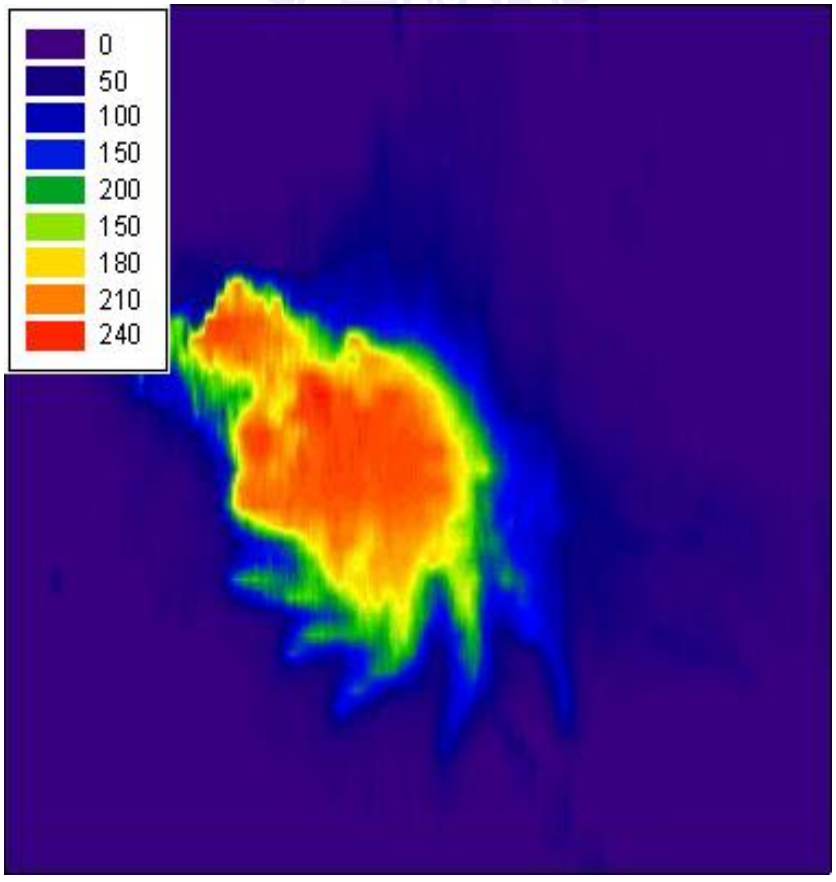

Fig. 4.31 Grey level for image captured at P=30 Kg/cm2.

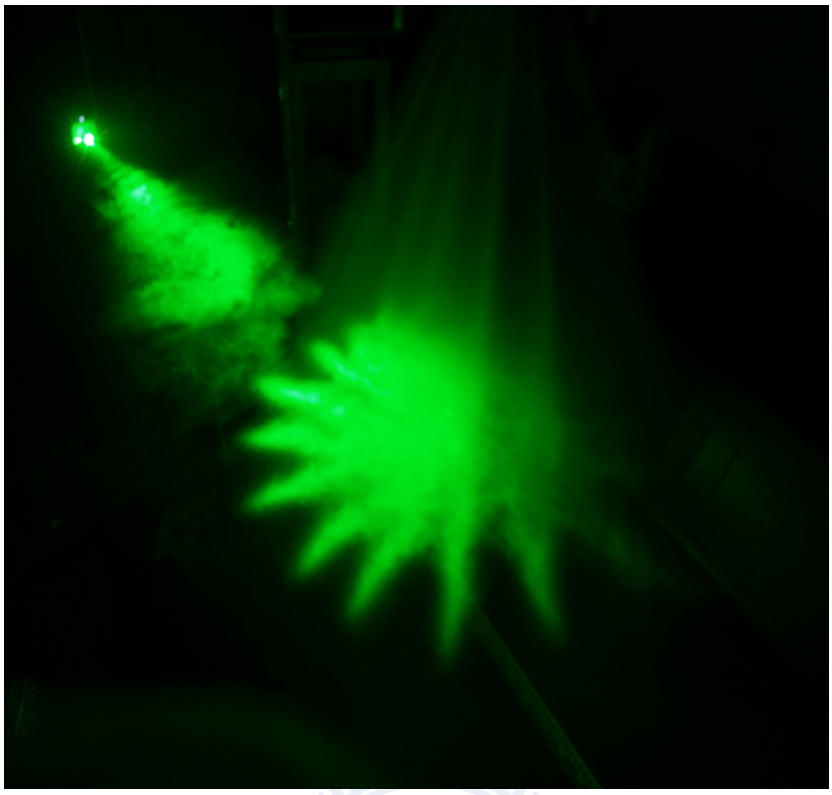

Fig. 4.32 Water mist distribution picture for P=40 Kg/cm2.

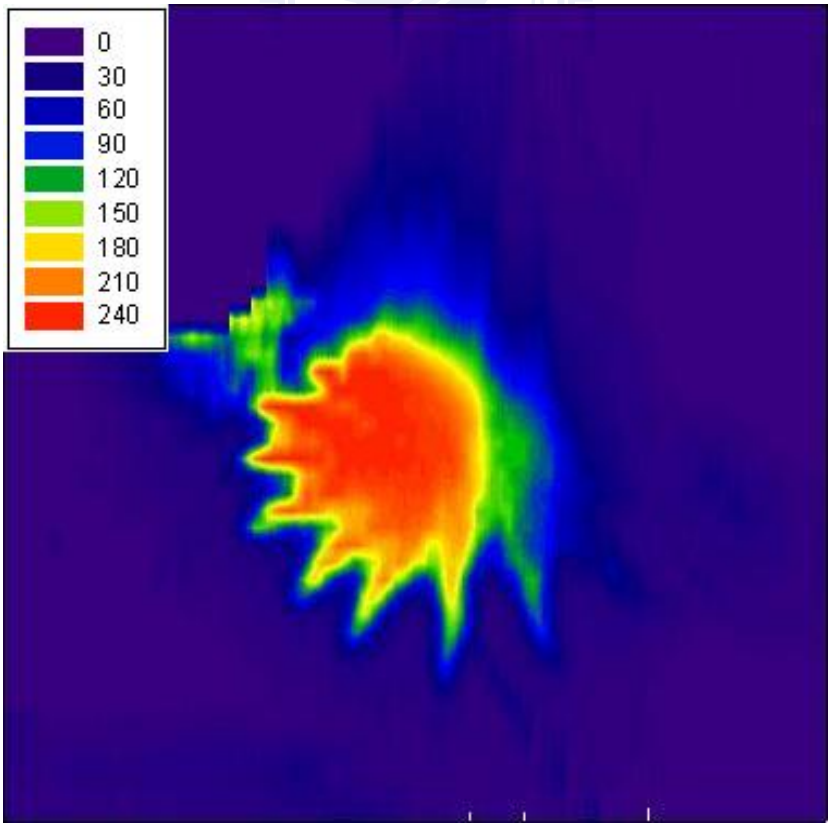

Fig. 4.33 Grey level for image captured at P=40 Kg/cm2.

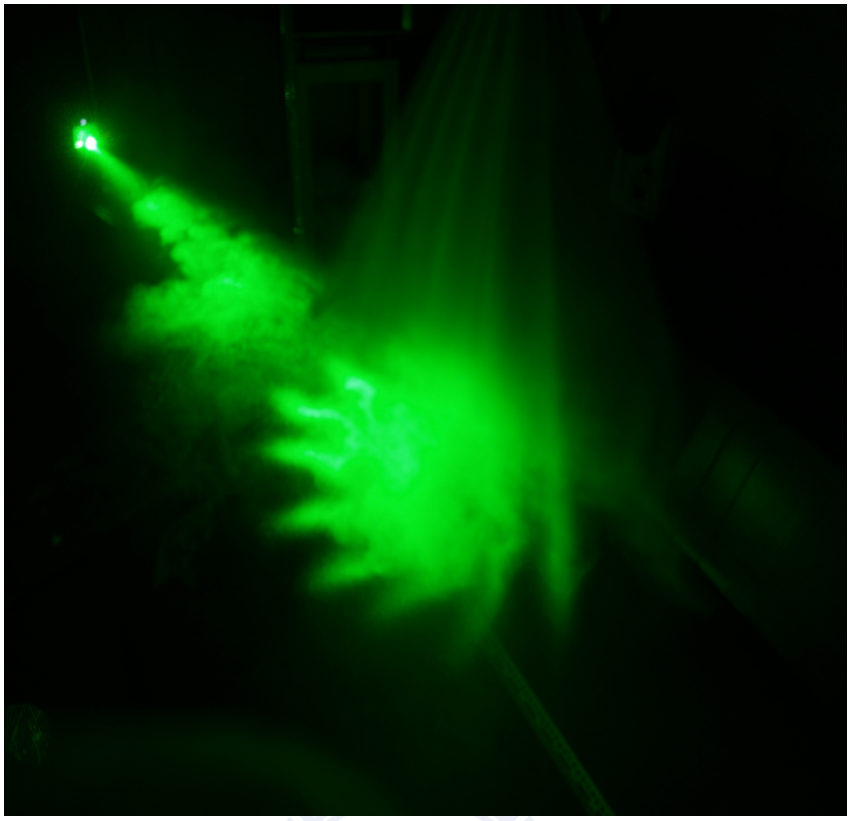

Fig. 4.34 Water mist distribution picture for P=50 Kg/cm2.

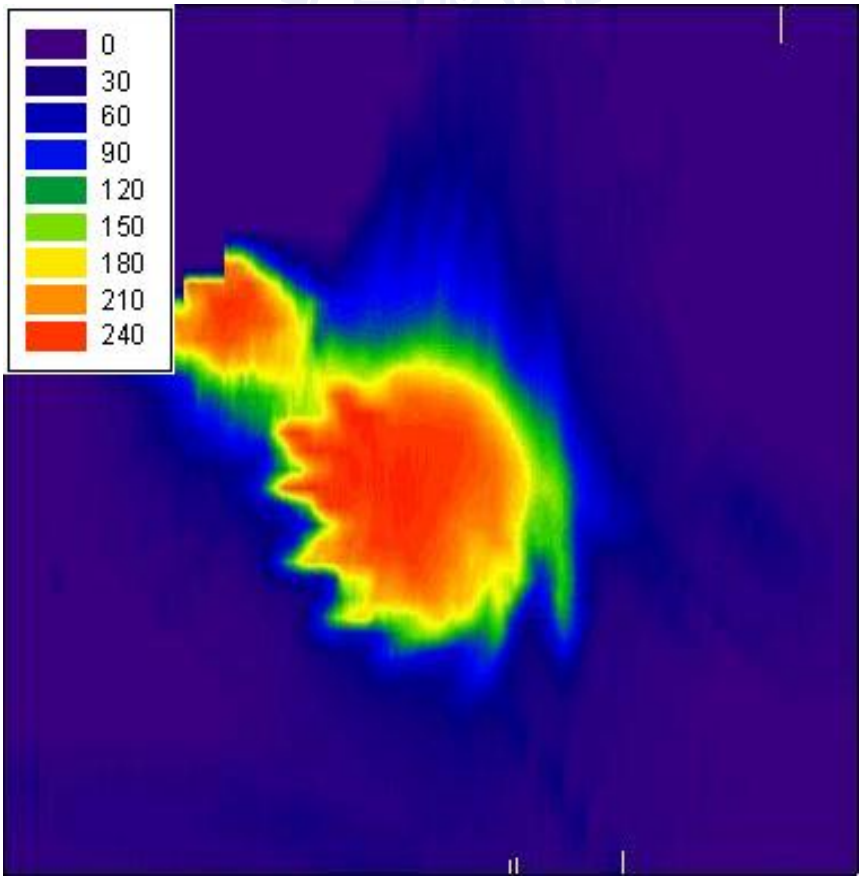

Fig. 4.35 Grey level for image captured at P=50 Kg/cm2.

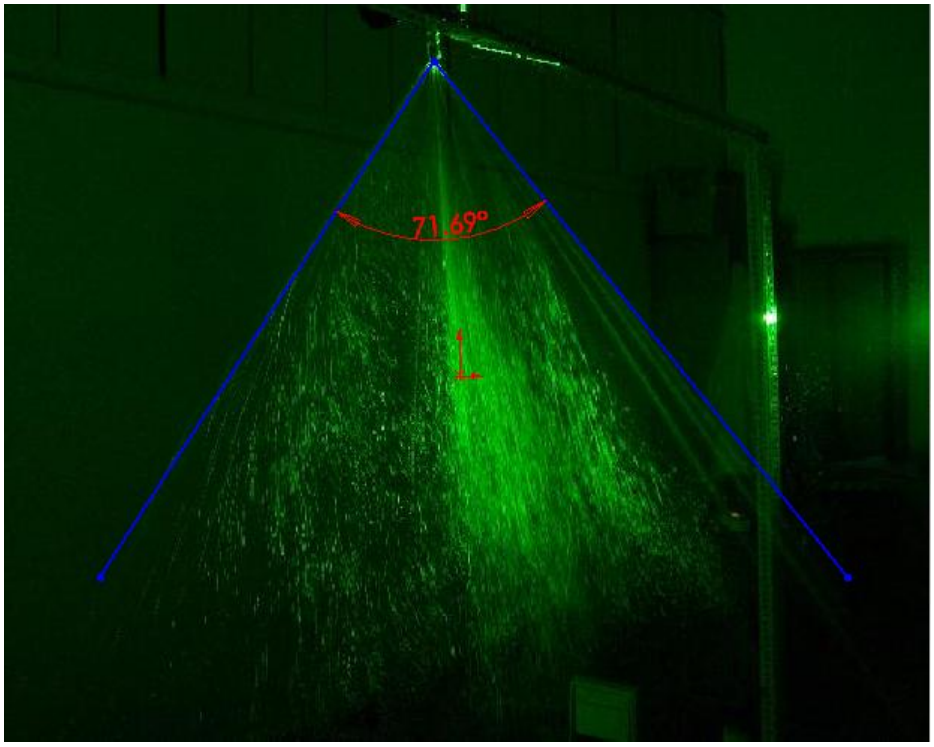

Fig. 4.36 Spray angle for P=10 Kg/cm2.

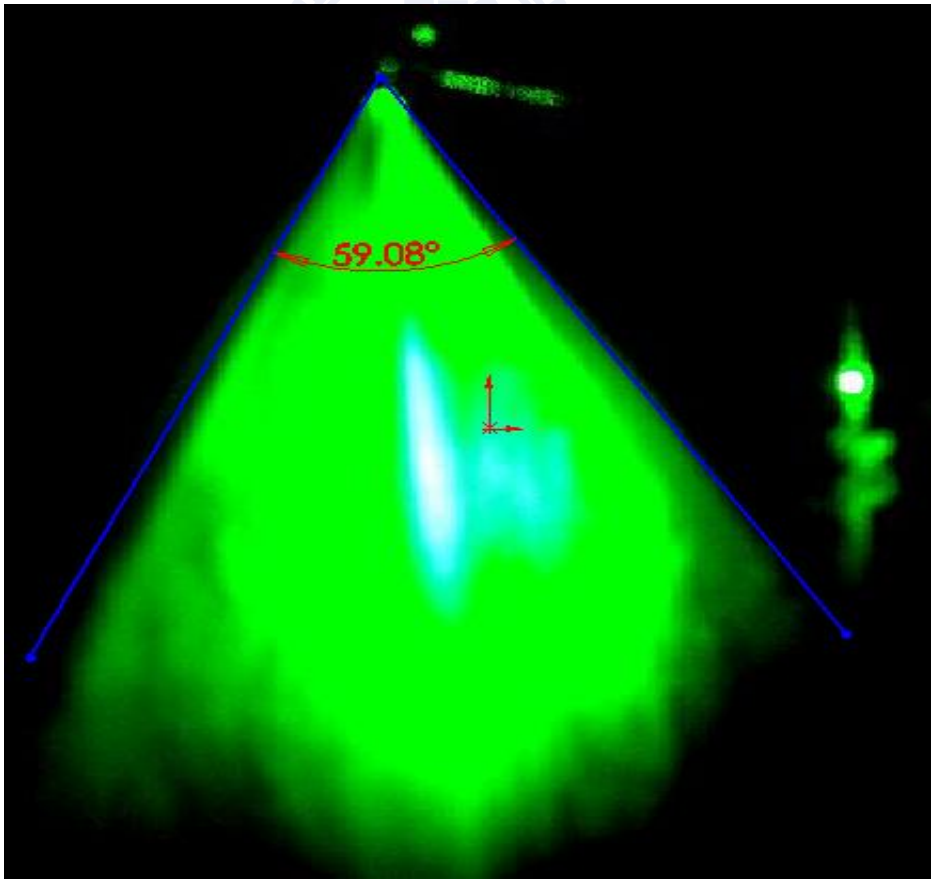

Fig. 4.37 Spray angle for P=20 Kg/cm2.

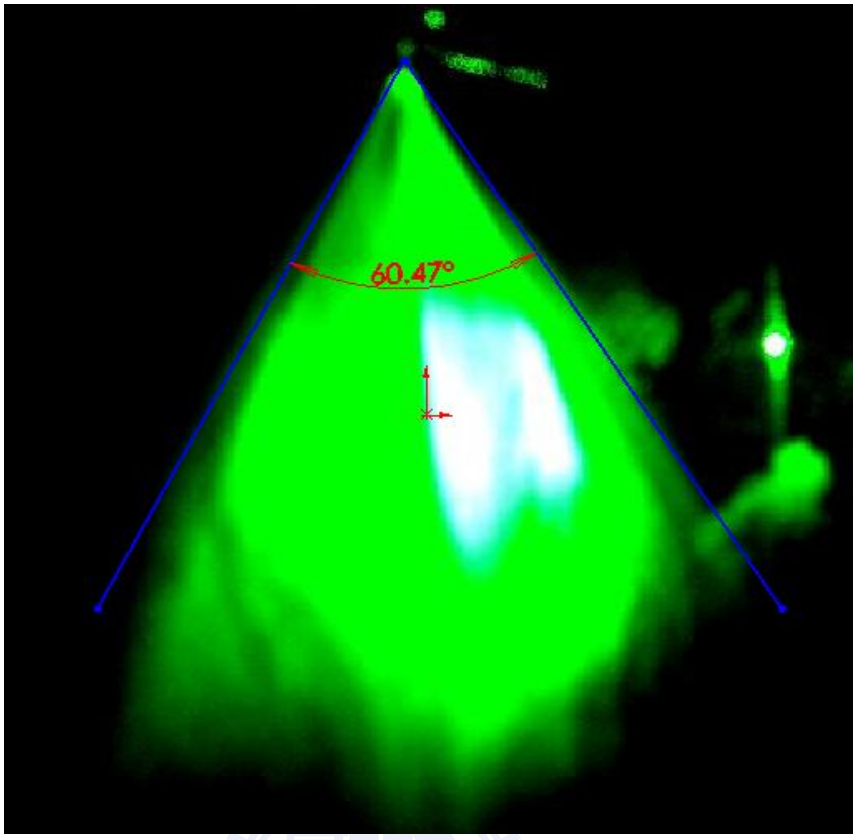

Fig. 4.38 Spray angle for P=30 Kg/cm2.

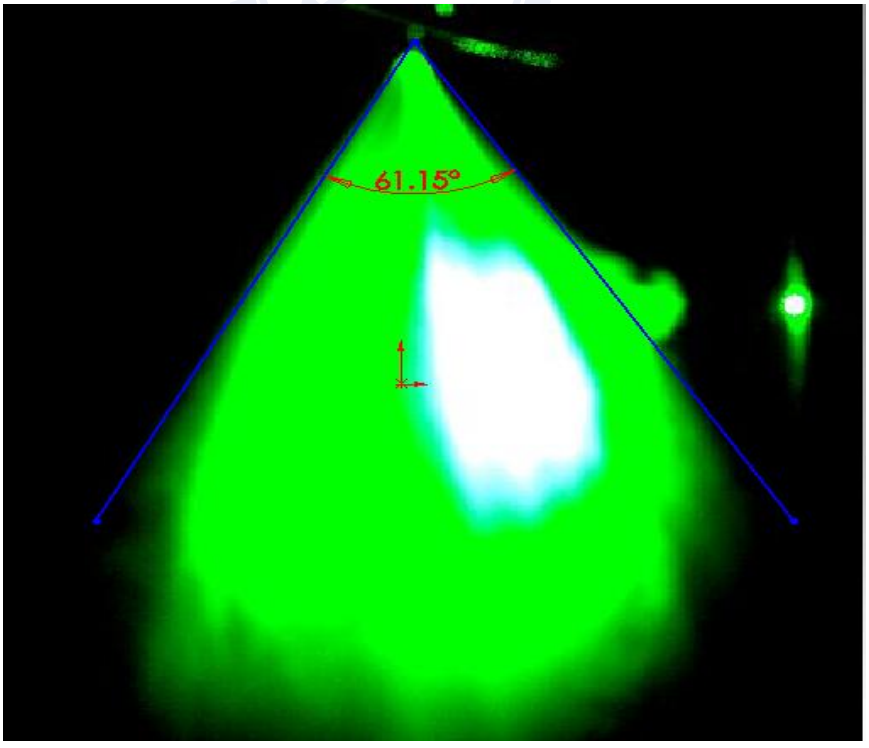

Fig. 4.39 Spray angle for P=40 Kg/cm2.

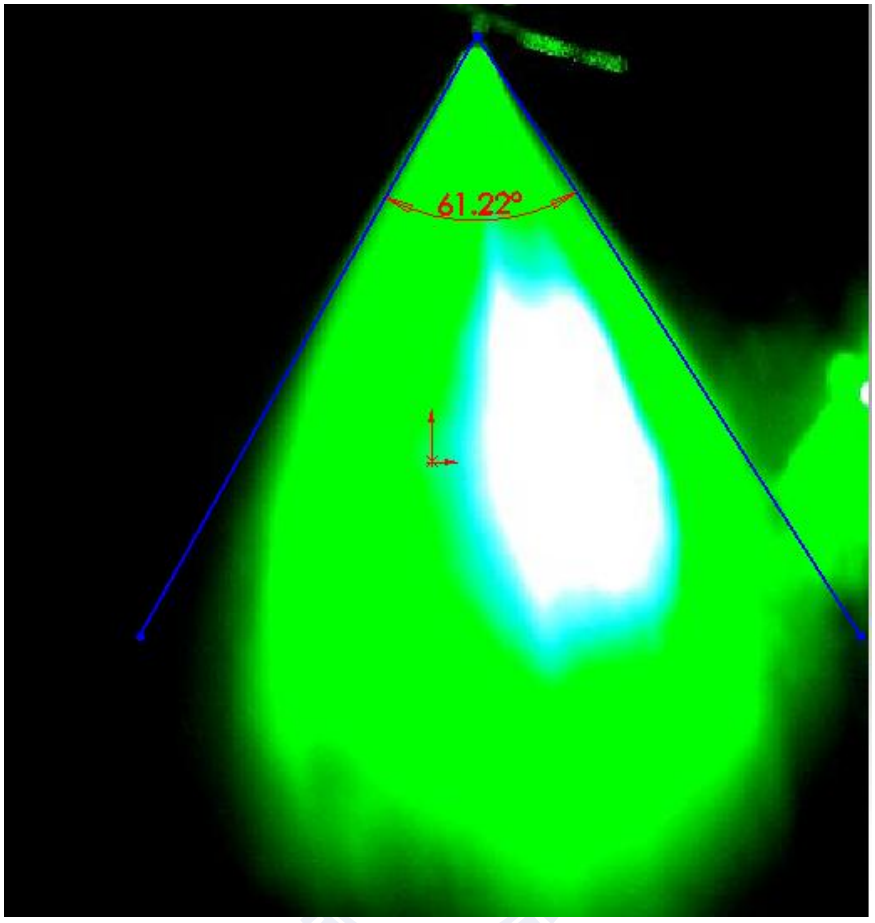

Fig. 4.40 Spray angle for P=50 Kg/cm2.